DEVELOPMENT AND TESTING OF A TISSUE ENGINEERED CARDIAC CONSTRUCT FOR TREATMENT OF CHRONIC HEART FAILURE

by

Jordan J. Lancaster

A Dissertation Submitted to the Faculty of the

GRADUATE INTERDISCIPLINCARY PROGRAM
IN PHYSIOLOGICAL SCIENCES

In Partial Fulfillment of the Requirements

For the Degree of

DOCTOR OF PHILOSOPHY

In the Graduate College

THE UNIVERSITY OF ARIZONA

2016

THE UNIVERSITY OF ARIZONA
GRADUATE COLLEGE

As members of the Dissertation Committee, we certify that we have read the dissertation prepared by Jordan Lancaster, titled Development and Testing of a Tissue Engineered Cardiac Construct for Treatment of Chronic Heart Failure and recommend that it be accepted as fulfilling the dissertation requirement for the Degree of Doctor of Philosophy.

_____ Date: 06/08/2016
Steven Goldman, M.D.

_____ Date: 06/08/2016
Karl Kern, M.D.

_____ Date: 06/08/2016
Betsy Dokken, Ph.D.

_____ Date: 06/08/2016
Paul McDonagh, Ph.D.

Final approval and acceptance of this dissertation is contingent upon the candidate's submission of the final copies of the dissertation to the Graduate College.

I hereby certify that I have read this dissertation prepared under my direction and recommend that it be accepted as fulfilling the dissertation requirement.

_____ Date: 06/08/2016
Dissertation Director: Steven Goldman, M.D.

STATEMENT BY AUTHOR

This dissertation has been submitted in partial fulfillment of the requirements for an advanced degree at the University of Arizona and is deposited in the University Library to be made available to borrowers under rules of the Library.

SIGNED: Jordan J. Lancaster

Acknowledgments

I would like to start by acknowledging and thanking the members of my scientific committee: Dr. Steven Goldman, M.D., Dr. Karl Kern, M.D., Dr. Betsy Dokken, Ph.D., and Dr. Paul McDonagh, Ph.D. You have each played a significant role in developing my scientific knowledge and insight. For that I am truly grateful. I look forward to continuing the conversation.

Thank you to Dr. Goldman for the numerous life lessons, guidance and above all opportunities. It is with your stern voice as guidance that every project had a light at the end of the tunnel, and that I learned it is not sufficient to communicate to be understood…you must communicate such that there is no chance you can be misunderstood.

To my other scientific committee members, Dr. McDonagh for our lengthy science chats. Your final years in the laboratory helped shape my first. To Dr. Dokken and Dr. Kern for their kindness, support and guidance, it has been invaluable.

In addition, I would like to thank the Physiological Sciences Graduate Program for the opportunity to be part of their program. Thank you.

Along the way, there have been numerous tremendous people that have supported and guided me in the laboratory. To Nicholle Johnson for helping me learn and develop my tissue culture skills and teaching me the ways of the laboratory from day one. I could not have asked for a better laboratory mentor. To Maribeth Stansifer and Sherry Daugherty, thank you both for your superb technical support.

Lastly, none of this would have been possible without the tremendous support of my family. To my Mom and Dad, THANK YOU. To my beautiful wife Teresa you have always pushed me to be better and to take the harder road. THANK YOU. To Little Bean, my daughter Samantha, “you are the best!”

Dedication

To my Mom and Dad

To my wife Teresa and daughter Samantha

THANK YOU!

Table of Contents

Abstract

There is a growing epidemic of chronic heart failure (CHF) in the developed world. The costs associated with providing care is profound and despite our best efforts, new, more effective treatments for CHF are needed; 50% of patients diagnosed with CHF are dead within 5 years. Current paradigms rely heavily on pharmacologic interventions, which merely help manage the disease. Surgical interventions may also be considered for late stage CHF patients such as heart transplant or left ventricular assist device (LVAD) but require burdensome and invasive surgical procedures. In addition they are costly, and require the need for life long immunosuppressive and anticoagulant therapies respectively. Despite our best intentions, the long-term prognosis for CHF patients remains poor.

With over a decade of clinical investigation taken place, data from cell-based therapy trials remains inconsistent. While demonstrating safety, limited efficacy has been reported and to date no stem cell therapy has been approved by the FDA. Despite these shortcomings important lessons have been learned that can be applied to future developments.

Retrospective analysis of early cell-based clinical trial data has suggested that variations in isolated cell number, viability, and potency from donor to donor in autologous preparations yielded wide discrepancies in functional outcomes. In addition, sub culturing adult stem cells, even for short periods of time in 2D polystyrene environments void of complementary cell populations and extra cellular matrix (ECM) protein interactions, may alter the therapeutic potential of a given cell. As a solution, allogeneic approaches where donor cell quality and potency can be assessed and optimized may help achieve functional benefits. Furthermore, co-dosing with multiple cell populations

or developing 3D sub-culture environments that more closely mimic the *in vivo* milieu may ultimately yield more potent therapeutic cell populations.

While these alterations may improve cell-based therapy outcomes, other solutions have been proposed such as tissue engineering. While the concept of tissue engineering is not new, advancements in biomaterials, bioreactor design and cell sources have greatly enhanced the reality of these preparations. Previously, one of the greatest limitations to tissue engineering is overcoming the cell requirements for developing and testing where millions if not billions of cells are required. Cell sourcing limitations appear to have been solved with the discovery and development of induced pluripotent stem cell (iPSC) derived cell populations. First reported in 2007, they have the ability to generate embryonic like pluripotent stem cells without the ethical concerns of embryonic stem cells. These iPSCs hold tremendous potential for drug toxicology / screening, personalized medicine and cell therapies.

The body of work described in this dissertation looks at developing and testing a tissue engineered (TE) cardiac patch to CHF. For which, an emphasis has been to provide 1) structural support for engrafted cells and 2) a rapidly inducible vascular supply once implanted *in vivo*. Biomaterials were sourced that facilitate infill by multiple cell populations in 3D culture and the establishment of ECM deposits. Together, these patches enhanced cellular development *in vitro* and result in long term functional improvements in small animal models for CHF. Additional feasibility work was performed in large animal models to permit up-scaling and development of surgical implantation techniques to demonstrate clinical applicability

Introduction

Cardiovascular Disease

Cardiovascular disease (CVD) results in more than 17M deaths worldwide per year, which is expected to increase to 23M by 2030. CVD claims more lives than all cancer deaths per year. In the US alone, more than 800,000 people died from CV related disease in 2013; 1 in 7 deaths are attributed to CVD. The cumulative cost of treating CVD and the lost economic productively CVD exceed more than $317B per year (Mozaffarian 2015).

Beyond genetic precursors and family history, the increase in prevalence and incidence of CVD is closely associated with poor health behaviors. Smoking, lack of physical activity and poor diet all greatly increase CVD risks through increased obesity, cholesterol, high blood pressure, diabetes all of which increased risk for atherosclerosis. Atherosclerosis is a build-up of fatty or calcified plaques that slowly develop over years to decades and is a manifestation of vessel inflammation and endothelial dysfunction (Libby 2013). These lesions are the leading cause of myocardial infarction (MI) and stroke.

Clinically, coronary atherosclerosis presents as either silent (asymptomatic) or as overt / active (symptomatic) (Fig. 1). Asymptomatic manifestations are denoted by lipid accumulation in the intima and atheroma formation. Subsequent macrophage and T-cell inflammatory infiltration increase the presence of foam cells and the development of a fatty streak significantly increasing lipid accumulation within the vessel intima (Libby 2013). Atheroma formation is associated with changes in vessel integrity as manifest through increased smooth muscle and collagen deposition, in addition to the establishment of the

plaque's lipid core and establishment of calcified layers. As these lesions progress, they may become symptomatic as a result of significant stenosis of the vessel or plaque rupture. Inflammation appears to be one of the critical components of plaque formation and rupture. Activated T cells play a role in inhibiting new interstitial collagen production, which is required to maintain the plaques fibrous cap. Furthermore, T cells can activate macrophages dwelling in the lesion, which activate an inflammatory cascade producing metalloproteinase (MMPs) and coagulants. Together, these MMPs catalyze collagen breakdown weakening the plaques fibrous cap making them prone to rupture (Libby 2013). In some cases, the plaque may stabilize (Fig. 2) and re-endothelialize through the generation of a thicker fibrous cap or plaque "healing." While this stabilizes the vessel it results in greater vessel stenosis and ablation of vasomotor regulation (Libby 2002).

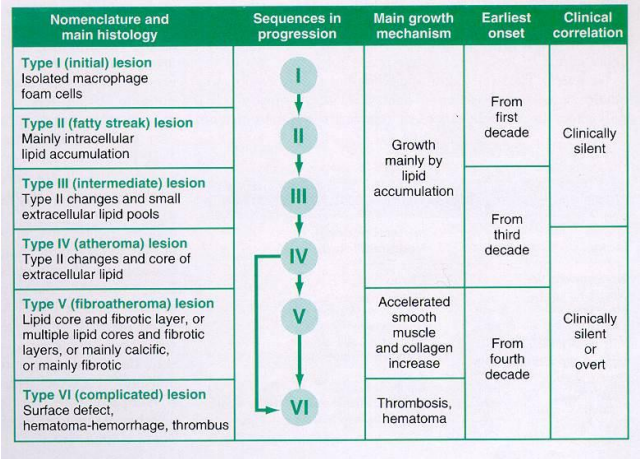

Figure 1. Describes atherosclerosis development from progression of lesion formation to plaque hemorrhage. Atherosclerosis develops over years to decades and begins with lipid accumulation in the vessel. Subsequent smooth muscle and collagen synthesis leads to vessel remodeling stenosis and an unstable fibrotic lesion. (Adapted from Libby 2002).

With respect to MI, atherosclerotic occlusion of the coronary vessels poses the greatest risk. Prolonged ischemic events lead to tissue infarction and cell/tissue necrosis. The site of the occlusion and duration of the occlusion leads to the size of the area in which myocyte death is eminent. Rapid percutaneous coronary intervention (PCI) is currently the only reasonable salvage for this tissue at risk.

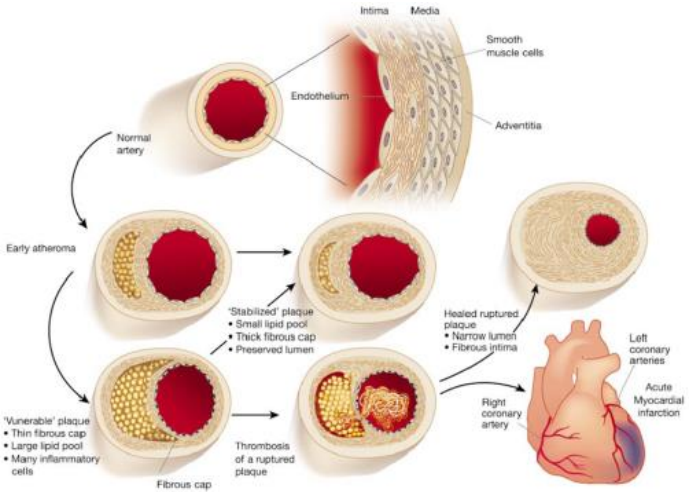

Figure 2: Plaque formation may progress into either a stabilized or vulnerable state. Vulnerable plaques progress and expand through inflammatory cell recruitment, lipid accumulation and fibrous cap development. These vulnerable plaques are susceptible to thrombotic rupture and acute myocardial infarction. Conversely, stabilization of plaque may occur, in which, the cell re-endothelializes. This is denoted by the development of a thick fibrous cap, small lipid pool and preservation of the lumen. This stabilized plaque is less susceptible to spontaneous rupture but carries with it, a stenosed lumen and a fibrotic intima potentially limiting vasomotor control (Adapted from Libby 2002.)

Acute MI and CHF

In the United States alone, there are over 450,000 acute MIs / year (Mozaffarian 2015). Of which, 95% of the insults are survived which is thought to be due to rapid cardiac catheterization and PCI.

As a result and in contrast, CHF is a growing epidemic. It is estimated that 50% of individuals that have an MI will go on to develop CHF within 5yrs (Pantilat 2004). Worldwide it is estimated that 23 million have CHF, 6 million of which preside in the US. Within the US more than 600,000 new cases present annually, and is the number one reason for hospital re-admissions, of which 50% will succumb to the disease within five years (Heidenreich 2013). Despite CHF's already almost epidemic presence in the developed world, there is projected to be an "epidemic" of CHF as more individuals survive acute MI yet have some level of myocardial injury (Jhund 2008). Furthermore, the economic consequences of CHF are staggering. Currently the US spends in excess of $30B on treating CHF, which is expected to explode to $70B by 2030 (Heidenreich 2013).

Acute MI sets off a cascade of signaling and inflammatory responses that initially attempt to salvage tissue but ultimately, leads to the development of CHF. Functionally, electrocardiographic changes (ST segment elevations), diastolic and systolic dysfunction, and elevated filling pressures (end diastolic pressure) manifest. On a cellular level an acute inflammatory response is initiated involving damage-associated molecular patters (DAMPs), which activate a cascade of other signaling including interleukin-1 (IL-1), C-reactive protein (CRP), and nuclear factor-kB (NF-kB). These signaling cascades initiate a number of cytokines, chemokines, and adhesion molecules, which recruit neutrophil, monocytes and mononuclear cells to the infarcted tissue (Frangogiannis 2014). After the inflammatory cascade and the development and stabilization of scar have occurred, the LV undergoes maladaptive remodeling in an effort to preserve stroke volume and cardiac output. This adverse ventricular remodeling is

denoted by increased LV chamber dimension, increased end diastolic pressure, and decreased ejection fraction (EF) (Mann 1999). This stabilization and cardiac remodeling are components of the development of CHF.

The myocardium consists of multiple cell populations, which include vascular and endothelial cells, cardiac fibroblasts and cardiomyocytes. Yet, as a percentage, cardiomyocytes account for only a relatively small percentage of the total cells, ~20% (Bergmann 2009). During an infarct, the high oxygen consuming cardiomyocytes are extremely susceptible to ischemic events. Within one gram of myocardium there are an estimated ~20million cardiomyocytes, of which ~4B reside in the LV (~200grams). An infarct affecting 25% of the ventricle would then affect about ~1B CMCs, thus, carrying potential significant consequences for the myocardium.

The heart carries limited regenerative capabilities and until recently was considered a post-mitotic organ, incapable of renewal. Elegant studies leveraging 14C from nuclear testing has calculated the rate of cardiomyocyte renewal in young versus old individuals. Individuals under the age of 20 demonstrate ~1% turnover, whereas by the age of 75, the turnover decreases to about 0.3%. In total, less than 50% of cardiomyocytes are replaced during and individual's life (Bergmann 2009). As a result, following even the shortest ischemic event previously healthy myocardium gives way to fibrotic collagen scar, which is limited in its contractile and filling properties (Bergmann 2009).

Current Therapeutic Approaches for MI and CHF

While PCI is the primary intervention for acute MI, the progressive and complex manifestations of CHF require alternative yet limited treatment strategies.

Current therapeutic paradigms rely heavily on medical management (ACE-inhibitors, angiotensin receptor blockers, beta-blockers, aldosterone antagonists, and diuretics) with the goal to prolong life, preventing further cardiac functional deterioration and to maintain quality of life through pharmacologically altering preload, afterload, and LV function. Only with late stage CHF are mechanical assist devices and heart transplantation considered. Both are limited by cost, surgical burden and the latter by donor supply (less than 2,500 heart transplants are performed in the US annually (US Department of Health and Human Services, Zammaretti 2004). While, LVADs have significantly improved in safety and outcomes providing a much-needed bridge to transplant option to patients (Wilson 2009, Kirklin 2013) LVAD success varies from individual to individual. In some cases, approval has been granted to use LVADs as destination therapy where the LVAD may remain as a long-term therapy solution. A small minority of patients demonstrates functional recovery resulting in complete removal of the device often the result of acute myocarditis. Meanwhile there remains a population of CHF patients that do not see functional improvements or are not granted LVAD as destination therapy ultimately require transplant at a future time (Wilson 2009, Kirklin 2013). Simply put, there is a need for the development of novel therapeutics to improve the quality of life for CHF patients with an emphasis on restoring cardiac function.

Next generation CHF regenerative therapies have the potential to alter the current medical paradigm by restoring cardiac function long-term. Recent scientific developments have advanced a number of promising therapies for CHF which include: in vivo cell reprogramming, gene therapy, whole organ printing / re-cellularization, injectable cell-based therapies in addition to implantable TE

solutions (Song 2012, Idea 2010, Tileman 2012, Ott 2008, Villar 2013, Kawamura 2012, Jiao 2014, Hirt 2014). While each demonstrates a significant scientific advancement, cell-based injectable or TE therapies may offer the least cumbersome approach to advance towards clinical utility, as they are not complicated by *in vivo* viral or gene administration. Furthermore, cell-based TE therapies are relatively better understood, developed, and feasible than whole organ printing / re-cellularization strategies. Specifically, the surgical burden and costs associated with whole organ printing /re-cellularization therapeutics may limit enthusiasm for widespread adoption.

Cell Therapies

Cell-based therapies for CHF carry tremendous potential as a regenerative solution for CHF capable of bridging the gap between pharmacological intervention and heart transplant / LVAD. To date a number of cell therapies have been evaluated in clinical trials (Fig. 3), which include sub populations of bone marrow such as mononuclear cells. Bone marrow mesenchymal stem cells, endothelial progenitors in addition to skeletal myoblasts, cardiac progenitors and cardiosphere derived cells (Traverse 2012, Perin 2003, Perin 20012, Karantalis 2014, Heldman 2014, Gnecchi 2005, Iso 2007, Mangi 2003, Murry 1996, Zeng 2007, Beltrami 2003, Doss 2004, He 2009, Smits 2005, Passier 2008, Murry 2005). To date, all studies evaluating cell-based therapies have relied on catheter based systems to inject the cells into the infarcted myocardium, coronary vascular or intravenously (Passier 2008, Murry 2005, Muller-Ehmsen 2002, Raynaud 2013, Dow 2005). Despite advances in injection mapping and specialized catheter injection tips to aid in cellular retention, these early studies have been plagued with high levels of transplanted cell loss, limited cellular

integration and lack of functional outcomes (Muller-Ehmsen 2002, Raynaud 2013, Dow 2005). However, with the exception of skeletal myoblasts all cell therapies have passed Phase I safety studies.

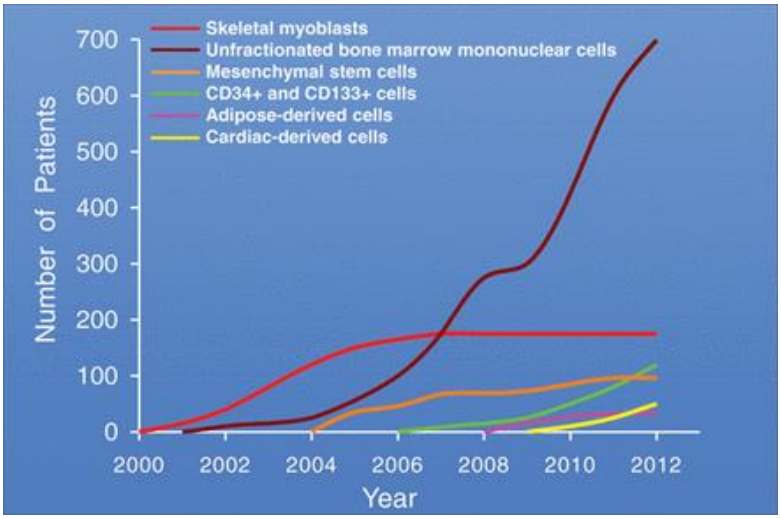

Figure 3: Overview of various types of cell-based therapies and number of patients enrolled per cell type in clinical trials. Adapted from Sanganalmath 2013.

To date the most promising injectable cell therapy evaluated consists of cardiosphere derived cell (CDC) populations. Data generated during the CADUCEUS trial suggest the ability of the CDCs to contain cardiogenic potentials superior to a single cell injectable. (Smith 2007, Makkar 2012). Furthermore, it has been recently suggested adjuvant therapy where a secondary cell population given in combination may enhance efficacy versus a single cell preparation (Williams 2013).

3D MicroTissues

One potential limitation to single cell-based therapeutics is that once cells are removed from their physiologic milieu for preparatory subculture in 2D polystyrene environments they lack important interactions with the ECM. Thus,

2D cultures do not precisely allow for mimicking of the physiologic environments. Cardiosphere derived cells may benefit from initial “microtissue” tissue cultures during which 3D spheroids are established in culture (Smith 2007, Makkar 2012). These 3D spheroids are cultured in microenvironments that enhance phenotype and gene expression profiles, develop enhanced cellular interactions and are capable of establishing an ECM and associated proteins which together may enhance engraftment and ultimately functional outcomes *in vivo* (Gunter 2016). In addition, 3D aggregates have superior size and organization as compared to single cell preparations with some level of ECM depositions, which may contribute to the reported functional benefits (Achilli 2012, Gattazzo 2014).

Induced Pluripotent Stem Cells

One of the greatest advancements in stem cell biology was the recent development and discovery of induced pluripotent stem cell (iPSCs), which were first reported in 2007. Previously, the gold standard multipotent / pluripotent stem cell lineage were of embryonic origins which were limited in use for ethical reasons. Successful de-differentiation of somatic dermal fibroblast into embryonic like iPSCs was achieved using only four transcription factors (Oct4, Sox2, Klf4, and c-Myc) that were known to drive pluripotency. These four factors are now commonly referred to as the Yamanaka factors (Takahashi 2007). This discovery carries tremendous potential for numerous areas of biologic study from drug development, toxicology, disease modeling and with respect to cell therapies. Early work aimed at nuclear reprogramming focused on somatic cell nuclear transfer (SCNT), altered nuclear transfer (ANT), or fusing methods, all of which required co-culture with embryonic cells yet laid the foundation and understanding for iPSC development (French 2008, Byrne 2007, Hurlbut 2007,

Meissner 2006, Cantz 2008, Cowan 2005). Comparatively, iPSCs maintain surprising consistent similarities to hES cells and carry similar differentiation profiles, with both capable of generating cell lineages from each of the three germ layers. With respect to iPSCs de-differentiation methods for cell therapies, early iPSC generation required integrating viral vectors such as retroviral or lentiviral vectors to drive Yamanaka gene expression in the targeted cells. Through these methods, exogenous DNA is incorporation into the host's genome and as such is not considered suitable for therapeutic use (Feng 2009, Stadtfeld 2009, Stadtfeld 2008, Page 2009). Subsequent episomal methods have been developed where exogenous DNA is removed during subsequent sub-culture propagation in the iPSC state (Yu 2011). With respect to cardiac cell therapies, numerous differentiated cell preparations are now available such as heterogeneous cardiomyocytes, ventricular pure cardiomyocytes, and early and late progenitors in addition to cardiac fibroblasts.

Autologous vs Allogenic

Ongoing discussions surrounding autologous vs allogeneic cellular preparations persevere with all cells preparations considered for cell therapy. This is also true of iPSCs. In theory, seeing that blood or dermal fibroblast biopsies can be acquired from an individual, reprogrammed and then administered back into the donor would be ideal, particularly from an immune tolerance perspective. As such, immunosuppressive drugs could be reduced or ultimately not required. Immune response however, despite its importance in iPSC adoption for cell therapy, is surprisingly void of study in the current literature (Okita 2011, Wang 2013, Lait 2014). With respect to allogeneic preparations there are currently three distinct proposed solutions to immune response 1) provide

immunosuppression, 2) HLA map the donor cells to the recipient, or 3) genetically ablate the HLA antigens creating a “universal cell” (Taylor 2012, Riolobos 2013).

This however is complicated and numerous factors play a determination in the ultimate preparation. For example, it is also known that increased donor age decreases reprogram efficiency and may untimely carry bioenergetics consequences limiting autologous reprogramming from older individuals (Reardon 2016). In addition, epigenetics may be a limiting factor for autologous iPSC generation as genetic deficiencies in the donor’s cells could progress through to subsequent population’s limiting therapeutic relevance (Kim 2010). Furthermore, teratoma formation needs to be considered. While it is not completely understood, it is suggested that somatic DNA mutations accumulated over time may manifest in one’s reprogrammed cells, again limiting enthusiasm of older donor populations in line with autologous preparations (Alessandro 2011).

To date only one clinical trial using iPSC-derived cells has been initiated for the repair of age related macular degeneration (Garber 2015). Interestingly, the study was halted after only one patient was treated due to mutations in the pre-implanted autologous cell preparations. It is important to note that in the treated individual, “no serious adverse effects” were observed (Garber 2015). The study’s sponsor, Healios, is currently repositioning, with a focus on re-starting the trial utilizing allogeneic opposed to autologous preparations.

Tissue Engineering

As previously mentioned, direct myocardial injection of therapeutic cells has been clinically tested with sparse success and limited long-term benefits (Gunter 2016) Potential barriers to success may be the injection modalities themselves and/or the ischemic and fibrotic milieu in which the cells are placed (Muller-Ehmsen 2002, Dow 2005). Observing the limitations with single cell injectable preparations, growing emphasis has been placed on the development of TE patches and matrixes for CHF as they provide the requisite structural to enhance cell survival, integration, and paracrine mechanisms to improve functional outcomes. These developments have utilized scaffold based, non-scaffold base, and even acellular preparations (Zhao 2014).

The ideal fundamentals of cardiac constructs have been previously described in that they should be: 1) contractile, 2) electrophysiologically stable, 3) mechanically robust yet flexible as to not impede contraction or relaxation, 4) vascularized, or at least quickly vascularized, after implantation, and 5) non-immunogenic (Leor 2005). However, TE constructs may be limited in application by: 1) burdensome surgical approaches for the patient, 2) ability to maintain construct integrity during surgical placement, and 3) overall scalability required for manufacture of the construct (Radisic 2006) which will all be discussed in more detail below.

Cellular Tissue Engineered Preparations

These types of constructs are capable of contraction, respond to electrical stimulus, generation of force, propagate an electrical signal, and can be described as biologically active, tissue like cellular patches. They can be engineered utilizing synthetic materials, natural materials or scaffold free without

any type of support structure and comprising solely of cells (Radisic 2006, Dvir 2009, Zimmermann 2002, Kawamura 2012, Kawamura 2013). Matrigel, alginagtes, polyethylene glycol, fibrin gets, polyglactin mesh, etc have been explored for delivery of cells to the heart (Reis 2012, Lancaster 2014, Lailiang 2011). Of importance in biomaterial selectivity is degradability, which is discussed in more detail below, and pore size. Adequate pore size is required for proper cellular infill during culture. Pores should be large enough to permit infill, transfer and exchange of nutrients and waste yet small enough for cells to proliferate across the pores. Scaffold based TE preparations with pores also pose challenges when incorporation of non-proliferative cell populations are desired or required as they will not effectively be capable of proliferating across the pores to generate intact cellular structures (Park 2011). While the short-term goals of the biomaterial are to provide structural support for TE implantation, it is considered favorable that the material breaks down over time. Biomaterials vary such that they can be 1) bioerosion – hydrolytic, 2) bioresportion – cellular activity, 3) biodegradation – enzymatic activity. Secondarily, the degradation time of the material is an important consideration (Reis 2016). Essentially, persistence of biomaterials will remain for the time course required but no longer.

Scaffold Free Engineered Preparations

While biomaterials can be used in TE patches, work evaluating the development and testing of biomaterial free patches has progressed. Examples of these include “cell sheet” technology which can be generated easily using variety of temperature sensitive poly(N-isopropylacrylamide)(PIPAAm) culture plates (Shimizu 2003). Once cellular monolayers are established, reduction of temperature from 37ºC to 25ºC initiates changes in the cell binding properties of

the culture plate. As a result, an intact cell sheet is dissociated which can be implanted onto the failing heart (Kawamura 2012). Yet, these patches are void of structural integrity, easily tear and are difficult to effectively handle during the implant process.

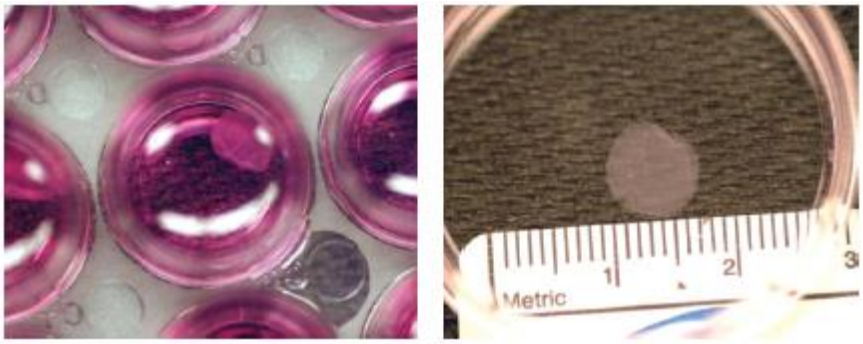

Figure 4: Bovine pulmonary artery endothelial cells (BPAEC) sheets harvested using 24-well PIPAAm temperature sensitive culture plates. Left, disassociated BPAEC cell sheet in culture well and media. Right, harvested BPAEC cell sheet harvested from original culture plate. Lancaster 2011.

Acellular Tissue Engineered Preparations

Acellular approaches include collagen, gelatin, alginate and decellularized extra cellular matrices. While they may be transplanted directly they may also be pre-loaded with varying growth factors such as VEGF to promote *in vivo* vascularization and endogenous cellular repopulation (Gaballa 2006, Schmuck 2014). Acellular approaches to treating the heart carry advantages compared to cellular based technologies. Among the benefits are reduced manufacturing costs and more streamlined FDA approvals. Downsides may include limited therapeutic benefits or the presence of only short-term functional benefits.

Cell Types and Sourcing for Tissue Engineered Preparations

Cell source has until recently been an issue limiting the development of TE therapeutics. While a number of cell populations have been examined for direct injectable cell therapies, with TE cardiac preparations, it is clear that cardiac lineage specific cells such as differentiated cardiomyocyte or cardiac progenitor cells would be ideal at repopulating the previously infarcted myocardium. Limitations to TE development have consistently been access to suitable cardiac cell preparations. Seeing that the adult cardiomyocyte is terminally differentiated and thus, has virtually no ability for *in vitro* expansion, other cardiac cell sources would be required to effectively develop a human TE therapeutic. While early adult stem cell trials, suggested that, *in vivo* differentiation into cardiomyocytes was possible, recent studies have shown otherwise (Orlic 2001, Murry 2004, Berlo 2014). Meanwhile, embryonic cells have been demonstrated to be capable of expansion into each of the three germ layers (ectoderm, mesoderm and endoderm). Yet, limited funding opportunities and ethical considerations have electively halted continued therapeutic work with hESs. A great hurdle in cell sourcing issues was solved with the discovery of iPSCs, which are capable of producing an unlimited supply of differentiated cells for TE preparations (Takahashi 2007).

Considerations for Handling and Implantation

One potential limitation to TE therapeutics is the modalities by which the therapies are effectively administered. As opposed to cell-based injectable technologies, typically surgical intervention is required for TE implantation. These surgeries may be *de novo* or given in combination to other surgical procedures such as coronary artery bypass grafting (CABG). Furthermore,

minimally invasive robotic delivery may be considered to reduce surgical burden and reduce recovery time for the patient. Despite the method of surgical implantation, sufficient TE structural integrity will be required for the surgeon to effectively handle, place and adhere the TE patch onto the heart. Challenges arise in biomaterial free cell sheet technology, even when multiple sheets are "plied" together they remain fragile, tear easily and are do not maintain an established shape. Excessive fragility increases the difficultly of implant, untimely increasing the time of the procedure and may limit clinical adoption. Yet it is important, as previously mentioned, to avoid implants that are too ridged, i.e., are restrictive and potentially impede ventricular filling (Leor 2005). In addition methods of securing the patches to the heart need to be considered that effectively permit placement and adherence to the heart without damaging the implant or interfering with cell-cell connectivity between the implant and the native tissue. Despite certain limitations with TE cell sheets, they may be superior in their ability to self-adhere to the host tissue (Shimizu 2003). During their creation in chilled preparations, adhesion molecules are preserved, allowing for rapid adherence through cellular mechanism.

Autologous versus Allogenic

As previously described, autologous vs allogenic approaches are still an open discussion. With respect to TE patches, it is important to denote the time course of culture in comparison to the timing requirement of therapy. While single cell preparations can be generated in the course of hours to days, typical TE patches require weeks to months to engineer. This time course may be a limitation for autologous preparations, which if derived of iPSC derived cells, may take 3-6 mo to effectively derive the cellular components (Takahashi 2007). Subsequent

tissue culture into 3D patches may take additional time on the order of weeks to months. Despite unknown yet potential issues with immune responses, it may be more advantageous to have allogeneic or partially matched TE patches prepared, cryopreserved and ready for use on demand, i.e., “off-the-shelf.”

Cryopreservation

In allogeneic preparations, TE products can be either shipped freshly prepared (25-37ºC), maintained in HypoTermosol (2-8ºC), or cryopreserved (-196ºC). Ultimately cryopreservation provides the greatest flexibility for post manufacture storage and shipping however limitation may be encountered. Numerous challenges need to be overcome which include identifying the optimal cryopreservation and thawing protocols (Mukherjee 2005, Gao 200). Chief among these issue include overcoming impaired diffusion of gases to the deeper section of the TE patch (Ma 2010), or compensating for higher metabolism cell populations such as cardiomyocytes. While challenges present with cryopreservation, Dermagraft™ (Organogenesis) is a dermal substitute comprised of human neonatal dermal fibroblasts and polyglactin mesh that is cryopreserved. In addition, umbilical cord can be effectively cryopreserved in intact 1cm x 1cm specimens for later use for isolating MSCs without issue (Choudhery 2013).

Significance and Research Plan

Chronic heart failure is the leading cause of morbidity and mortality worldwide (Mozaffarian 2015, Heidenreich 2013). Current medical treatments decrease mortality from CHF but they do not reverse the disease process or restore long-term cardiac function. As a result, new and novel treatment strategies are needed. One proposed

strategy is to use stem cells. Stem cells may prove useful as a regenerative therapeutic for CHF as they are multimodal, working through a number of mechanisms simultaneously. However, while enthusiasm for this work remains high through ongoing clinical trials, the results are generally confounding. The lack of success is thought to be due, in part, that the injected therapeutic cells do not survive transplantation via injection. It has been proposed that survival is limited due to three contributing factors 1) lack of matrix/structural support, 2) limited nutrient supply, and 3) loss of cells because of wash out through injection sites. This proposal seeks to develop and examine a new approach to cell-based therapy for CHF using tissue engineering (TE) to effectively deliver a multi-cellular construct to the infarcted myocardium. Tissue engineered constructs, provide structural/matrix support and nutrient supply for transplanted cells potentially enhancing survival and therapeutic outcomes to the recipient. Furthermore, construct generation with multiple cell populations may provide a multimodal response effectively enhancing outcomes as compared to singe cell administration. Our previous studies have evaluated functional outcomes of a three-dimensional fibroblasts construct (3DFC) when implanted in both acute myocardial (AMI) infarction and CHF. While 3DFC attenuates remodeling and preserves left ventricular (LV) function in AMI, in the clinic however patients with AMI receive optimal and effective care through cardiac catheterization, stent implantation, and reperfusion of the occluded vessel limiting marketability of stem cells in this setting. In CHF however, where clinical management is burdensome, the 3DFC does not restore maladaptive remodeling or improve LV function but it still promotes angiogenesis increasing myocardial blood flow. This endogenous angiogenic response may provide nutrient support to effectively enhance transplanted cell survival. In proof-of-concept studies the 3DFC has been explored as a platform for

cardiac cell seeding and co-culture. During co-culture, the cardiac 3DFC beats spontaneously in a synchronized fashion and can be electrically paced.

Specific Aims

Aim No 1

Develop a multicellular TE cardiac construct providing structural and nutrient support to engrafted cardiomyocytes capable of surgical implantation to effectively treat CHF.

Aim No. 1 Rational

Structural and nutrient supports are crucial for therapeutic delivery of cells. This aim seeks to develop a cell delivery platform in which, therapeutic cells of interest can be implanted onto the injured myocardium. Success of this aim will be enhanced though leveraging previous work with the 3DFC. The intent is to develop methods of seeding and co-culture that facilitate cellular adhesion, alignment, maturation, and electromechanical coupling *in vitro*.

Aim No. 1 Hypothesis

Co-culture of cardiomyocytes with dermal fibroblasts into synthetic woven Vicryl mesh provides requisite structural support facilitating myocyte maturation and electromechanical coupling *in vitro*.

Aim No. 2

Test feasibility, efficacy and mechanisms of action of a TE cardiac construct in a rat model of CHF.

Aim No. 2 Rational

Utilizing cell-based therapy as a treatment strategy for CHF holds great promise. While numerous therapeutic stem cells have been defined, a vast majority have demonstrated limited efficacy. A TE construct may enhance functional outcomes as they provide both structural and nutrient support to the transplanted cells. This aim focuses on testing the construct developed in Aim No. 1 in an established rodent model of CHF to define changes in myocardial blood flow, LV remodeling, electrical activation, and LV systolic/diastolic function at 3 weeks to 6 months after implantation.

Aim No. 2 Hypothesis

The embedded patch fibroblasts secrete growth factors increasing myocardial blood flow and provide a hospitable microenvironment enhancing transplanted cardiomyocyte cell survival, integration, electrical mechanical coupling with the native myocardium which facilitate improvements in LV function in CHF.

Aim No. 3

Confirm a large animal swine model of CHF for feasibility testing of a TE cardiac construct as a necessary prerequisite to initiating a clinical trial.

Rational

While rodent models are the gold standard for early *in vivo* testing, large animal models are required for advancement of therapeutics from bench to bedside; it is important to determine if the benefits seen in CHF rats occurs in a larger heart, close to the size of a human heart. The intent of this aim is to confirm clinically relevant modalities of infarct generation, time line of study duration pertinent to

infarct, CHF development and study endpoint, in addition to development of cardiac magnetic resonance imaging protocols, echocardiography, functional capacity testing, and develop and refine surgical approaches of cardiac patch implantation. After confirming and validating a swine model of CHF, the intention is to advance the cardiac construct into large animal CHF models to define changes in myocardial blood flow, LV remodeling and LV systolic/diastolic function after implantation.

Hypothesis

Embolization coils are capable of generating an effective, precise and re-producible method of MI in mini swine. Implantation of a TE cardiac construct will lay the foundation for efficacy studies and expansion into clinical trials.

Implantation of a Three Dimensional Fibroblast Matrix Improves Left Ventricular Function and Blood Flow after Acute Myocardial Infarction

Introduction

Cell-based therapy with direct injection of cells into the infarcted heart is currently being examined as a new treatment for heart failure. While a number of different cell types have been shown to improve left ventricular (LV) function in animal models of acute ischemic damage, the results of direct cell injection into the heart in clinical trials has been less dramatic (Assmus 2006, Balsam 2004, Bodo 2005, Chachques 2007, Cohen 2004, Fujimoto 2007). In part, this appears to be because few of the transplanted cells survive when injected into the infarcted heart (Muller-Ehmsen 2002, Dow 2005). While the explanation for this is not clear, it may be that injecting cells directly into injured myocardium or scar tissue

is a problem because this damaged tissue is not a supportive milieu (i.e., scar tissue has an inadequate blood supply with insufficient viable tissue or matrix support for new cells to attach, survive, and grow). Because of these drawbacks, we have developed a different approach to cell-based therapy for heart failure; we implant a matrix graft onto the infarcted heart to provide a support structure for new blood vessel growth (Gaballa 2006). This matrix provides a more hospitable environment for cell migration and growth into the damaged LV. In this report we provide data on 3DFC that is a matrix-embedded human construct of newborn dermal fibroblasts cultured in vitro onto a bio-absorbable mesh to produce a living, metabolically active tissue that has the potential to increase new blood vessel formation *in vivo* (Kellar 2001, Kellar 2005).

It is hypothesized that the 3DFC matrix or patch graft will improve LV function and increase myocardial blood flow when implanted onto an infarcted heart. To test this hypothesis, we created an anterior wall MI by ligating the left coronary artery of rats, implanted the 3DFC patch at the time of surgery and used solid-state micrormanometers to measure hemodynamics, two-dimensional echocardiography to measure LV regional wall motion, function, chamber size, immunohistochemistry for microvessel density analysis, and neutron-activated microspheres to measure myocardial blood flow. We treated a separate group of infarcted rats with a combination of the 3DFC patch and captopril in order to simulate the clinically relevant situation where a patient in heart failure after a MI is treated with an angiotensin converting enzyme inhibitor. The data show that the 3DFC patch improves blood flow, regional wall motion in the infarcted LV, EF, and partially reverses maladaptive LV remodeling after MI. We do not see these results when a nonviable patch alone is placed over the infarcted myocardium.

The addition of captopril to the 3DFC also lowers LV EDP and shifts the LV pressure–volume relationship toward the pressure axis. This study shows that placing a viable fibroblast matrix on the infarcted myocardium may be a new approach to cell-based therapy for heart failure after a MI.

Materials and Methods

Study Design and Treatment Groups

To test the efficacy of the 3DFC in the treatment of heart failure after MI, we had five treatment groups: sham (*N* = 14); MI (*N* = 18); MI + 3DFC (*N* = 11); MI + 3DFC (nonviable) (*N* = 12); MI + 3DFC + captopril (*N* = 8).

Coronary Artery Ligation Experimental MI

Heart failure is created in rats using standard techniques in our laboratory (Gaballa 2002, Gaballa 1995, Goldman 1995, Pennock 1993, Raya 1997). In brief, rats are anesthetized with ketamine and acepromazine and a left thoracotomy performed. The heart is expressed from the thorax and a ligature placed around the proximal left coronary artery. The heart is returned to the chest and the thorax closed. The rats are maintained on standard rat chow, water ad libitum, and pain medication postoperatively. The experimental protocols are approved by the animal use committees of the Southern Arizona VA Health Care System and the University of Arizona, guaranteeing that all animals have received human care in compliance with the Guide for the Care and Use of Laboratory Animals (www.nap.edu/catalog/5140.html). Infarcted rats undergoing this procedure have large MIs averaging 40% of the ventricle (Gaballa 2002,Goldman 1995). Myocardial infarction is confirmed by hemodynamics (LV end-diastolic pressure >16 mmHg) and presence of a scar. Prior to closing the

chest, the 3DFC patch is engrafted onto the injured myocardium with the chest open as described below. The lungs are inflated, the chest closed, and the rat allowed to recover. We treated two other separate groups of rats: MI and captopril (2 g/L drinking water) and MI + 3DFC patch and captopril (2 g/L drinking water) for 3 weeks.

The 3DFC Patch

The 3DFC patch is a cryopreserved human fibroblast-derived tissue composed of fibroblasts, ECM, and a bioabsorbable scaffold (Kellar 2001, Kellar 2005). Figure 1 is a scanning electron micrograph of the 3DFC showing that the Vicryl fibers are “tube-like” structures. The fibroblasts look like irregular structures with long appendages that span from one Vicryl fiber to another. The fibroblast cells are from a qualified cell bank, which has been extensively tested for animal viruses, retroviruses, cell morphology, karology, isoenzymes, and tumorgenicity. Reagents used in the manufacture of the 3DFC patch are tested and found free from viruses, retroviruses, endotoxins, and myocoplasma before use. One piece of approximately 2 × 3 in. (5 × 7.5 cm) in size is supplied frozen in a clear bag for a single-use application. The patch remains frozen at −75 ± 10°C continuously until ready for use when it is placed in a sterile bowl containing PBS (34–37°C). Using scanning electron microscopy, the Vicryl fibers of the 3DFC appear as “tube-like” structures (Fig. 5). The fibroblasts look like irregular structures with long appendages that span from one Vicryl fiber to another. The patch is handled gently by the edges to limit cellular damage and applied to the heart within 60 minutes of being removed from its container (Fig. 6). The 3DFC patch was provided Theregen, Inc. (San Francisco, CA). To separate the effects of the cells from physical effects of the Vicryl we examined the effects of nonviable 3DFC.

The nonviable 3DFC is the standard 3DFC that is rendered nonviable by storage for 9 or more days at −20°C. The nonviable 3DFC consists of the same biodegradable Vicryl mesh with fibroblasts and extracellular matrix with matrix-bound growth factors and cytokines. The fibroblasts are killed with the higher temperature freeze phase (−20°C), leaving behind the standard ECM (tissue) and matrix-bound proteins as well as the cellular debris. However, the nonviable 3DFC no longer contains viable, living cells. The viable 3DFC does not generate an immune response. Developmental work on 3DFC includes experiments in dogs treated with 3DFC showing no immune response (Investigators' brochure ITT-101, Theregen). The work reported here is the first in an immune-competent animal showing that the benefits of the 3DFC are not related to the immune status of the recipient. The low immunoginecity of allogeneic fibroblasts grown on a scaffold is thought to be due to the fact that the majority of these fibroblasts show little induction of CD40 and HLADR in response to γ-interferon (Kern 2001). The 3DFC patch is FDA approved for wound healing; it has been used in over 20,000 patients mostly as a skin graft for diabetic foot ulcers with no untoward complications. There is no activation of the immune system in patients treated with this patch for diabetic foot ulcers, other skin repair, and oropharyngeal palate repair.

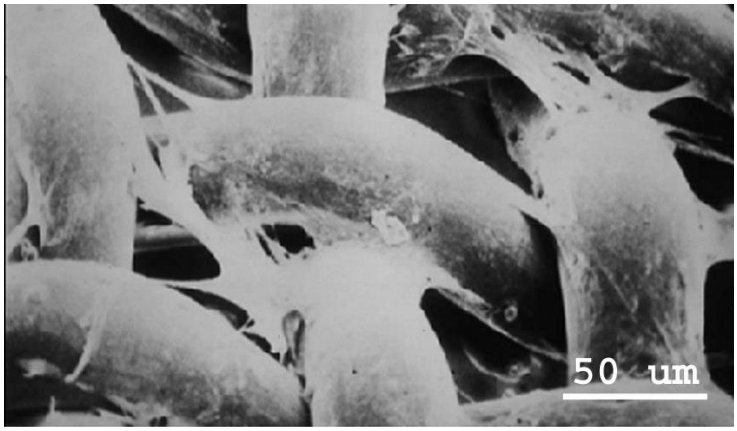

Figure 5: Scanning electron micrograph of the 3DFC patch. The Vicryl fibers are “tube-like” structures.The fibroblasts look like irregular structures with long appendages that span from one Vicryl fiber to another.

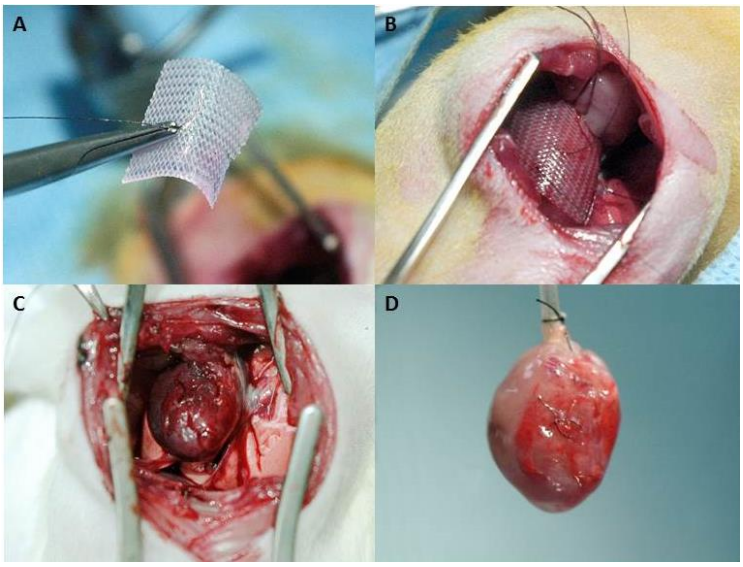

Figure 6: Three-dimensional fibroblast culture (3DFC) prior to implantation (A); the suture in the middle of the patch is used to attach the 3DFC to the LV. (B) 3DFC at the time of implantation on the infarcted LV. (C) 3DFC at 3 weeks after MI. Note that the 3DFC is well integrated and attached to the infarcted wall. (D) 3DFC in a perfused heart preparation at 3 weeks after MI. As noted above, the 3DFC is well integrated into the infarcted wall and the suture is easily visible.

Hemodynamic Measurements

We measure hemodynamics using methods reported previously by our laboratory (Gaballa 2002, Gaballa 1995, Goldman 1995, Pennock 1993, Raya 1997). In brief, rats are anesthetized with inactin (100 mg/kg IP injection) and placed on a specially equipped operating table with a heating pad to maintain constant body temperature. Following endotracheal intubation and placement on a rodent ventilator, a 2F solid state micromanometer tipped catheter with two pressure sensors (Millar) is inserted via the right femoral artery, with one sensor located in the LV and another in the ascending aorta. The pressure sensor is equilibrated in 37°C saline prior to obtaining baseline pressure measurements. After a period of stabilization, LV and aortic pressures, and heart rate are recorded and digitized at a rate of 1000 Hz using a PC equipped with an analog-digital converter and customized software. From these data, LV dP/dt is calculated.

LV Pressure-Volume Relationships

The LV pressure–volume relationship is measured as outlined in our previous work (Gaballa 2002, Goldman 1995). In brief, the heart is arrested with potassium chloride, and a catheter consisting of PE-90 tubing with telescoped PE-10 tubing inside is inserted into the LV via the aortic root. One end of the double-lumen LV catheter is connected to a volume infusion pump (Harvard Apparatus) while the other end is connected to a pressure transducer zeroed at the level of the heart. The right ventricle is partially incised to prevent loading on the LV. The LV is filled (1.0 ml/min) to 60–100 mmHg and unfilled while pressure

is recorded onto a physiologic recorder (Gould). Ischemic time is limited to 10 min. Volume infused is a function of filling rate.

Echocardiography

We perform closed chest transthoracic echocardiography at baseline prior to the MI, immediately after MI, and at 3 weeks after MI using methods previously developed in our laboratory (Thai 2006). We use a Vingmed, Vivid 7 system echo machine (GE Ultrasound) with EchoPac (GE Ultrasound) programming software with a 10 MHz multiplane transducer with views in the parasternal short axis and long axis, to specifically evaluate the anterior, lateral, anterolateral, inferior, and posterior walls. Two-dimensional (2D) and M-mode measurements of myocardial wall thickness and LV dimensions are obtained throughout the cardiac cycle and are used for calculation of systolic displacement of the anterior wall, EF, and regional fractional shortening. Systolic displacement is a measure of focal LV wall thickening. Using M-mode through the anterior wall of the LV, the LV wall thickness is measured at diastole and systole; the difference in the thickness between the two measurements is the systolic displacement. This is a useful measurement to quantify focal LV wall systolic function.

Myocardial Perfusion

We use neutron activated microspheres (BioPal Inc, Worcester MA) to measure myocardial blood flow. The isotopes are injected, a tissue sample obtained, and at a later time activated with the emitted radiation measured with high-resolution detection equipment (Fukuda 2004, Lei 2004, Reinhardt 2001). With this system, BioPal, Inc. provides the isotopes and tissue containers. Three separate isotopes (lutetium, gold, and samarium) are injected in each rat: one at baseline prior to coronary ligation, one immediately after ligation, and one at the endpoint of the

study. Because different rats are used for each group we are able to obtain end point data after different treatments (MI at 3 weeks, MI at 3 weeks + 3DFC). For each measurement 750,000 nonradioactive elementally labeled 15-μm microspheres (V = 300 μl) from Biopal, Inc. are injected into the LV transapically with a 1-cc syringe and 27-gauge needle. At the terminal study point, the tissues are harvested, oven dried, and collected for analysis. At the time of microsphere injection we perform a transthoracic echocardiogram to measure stroke volume. By knowing the heart rate, we calculate cardiac output as stroke volume × heart rate. Assuming 4% of the cardiac output perfuses the coronary arteries (Reinhardt 2001), we know the total myocardial blood flow; the number of microspheres deposited in the anterior wall is percentage of blood flow down the left coronary artery to the anterior wall at each time point.

Histopathology

Hearts were formalin fixed (10%) prior to paraffin embedding. HIER antigen retrieval of 3-μm-thick sections was performed in citrate-based Diva buffer (pH 6.2) for 1 min at 125°C using a “Decloaker” pressure cooker (Biocare Medical Concord, CA). We used single immunohistochemical staining for anti-rabbit factor VIII (Dako) (1:1000) to perform nhistological analysis of microvessel density.

Vessel Density

We defined vessel density by light microscopy at 40× magnification. The number of cross section vessels per field was counted by two persons blinded to treatment. Average measurements from six different fields were recorded for each value. Knowing the area of the optical field, data are reported as number of vessels/μm^2.

Results

In Vivo Hemodynamics

Rats with MI had a fourfold increase in LV EDP, a 22% reduction in LV systolic blood pressure, a 24% reduction in mean arterial blood pressure, a 37% reduction in LV dP/dt, and a 21% prolongation of the time constant of LV relaxation or tau (Table 1). The baseline data are consistent with our previous reports using this model showing that ligation of the left coronary artery results in a large anterior wall MI and CHF with a decrease in LV systolic function, an elevation of LV EDP, and a prolongation of tau (Gaballa 2002, Gaballa 1995, Goldman 1995, Pennock 1993, Raya 1997). The 3DFC lowered ($p < 0.05$) mean arterial pressure and increased ($p < 0.05$) peak developed pressure or PDP (126 ± 4 to 146 ± 8 mmHg).

Table 1. Hemodynamics for 3DFC patch/captopril after MI

	MAP (mmHg)	HR (bpm)	LV SP (mmHg)	LVEDP (mmHg)	LV dP/dt (mmHg/sec)	PDP (mmHg)	Tau (msec)
Sham	106±5	287±15	124±5	7±1	7360±379	192±18	19±1.3
MI	90±2*	269±13	103±3*	25±2*	4542±215*	126±4	24.2±1.8*
MI +captopril	72±3*	283±15	88±3**α**	14±2**	4398±315*	118±7*	21.8±1.8*
MI+3DFC (viable)	84±3**	248±10	100±5*	23±2**α***	4242±156*	146±8**∞	29.7±3.5*
MI+3DFC (nonviable)	88±4*	270±7	102±4*	24±2*	4502±179*	118±4	26±3*
MI+3DFC (viable) + captopril	83±4**	265±23	100±6*	13±3**	4502±179*	123±5∞	25.8±2.8*

Table 1: *P < 0.05 versus Sham. ** P < 0.05 versus Sham and MI. α P < 0.05 vs MI+3DFC/Captopril. ∞ P < 0.05 versus Sham and MI+3DFC. Values are mean±SE; Sham, N=14; MI, N=18; MI+3DFC, N=11; MI+3DFC+Capopril, N=8. Abbreviations: mean arterial pressure, MAP; myocardial infarction, MI; left ventricular, LV; LV end-diastolic pressure, LV EDP; PDP, peak developed pressure; Tau, time constant of LV relaxation; 3-dimensional fibroblast construct, 3DFC.

Captopril Treated

Treatment with captopril after MI lowered ($p < 0.05$) MAP, LV SP, and LV EDP; these changes are similar to what we and other investigators have previously shown (26). The addition of captopril in the 3DFC rats lowered LV EDP from 23 ± 2 to 13 ± 3 mmHg and PDP from 146 ± 8 to 123 ± 5 mmHg ($p < 0.05$); all other hemodynamic parameters were unchanged (Table 1). Vascular resistance increased ($p < 0.05$) with acute MI from 2.3 ± 3.7 to 9.1 ± 1.9 mmHg/ ml/min; compared to acute MI, vascular resistance in CHF was unchanged at 7.7 ± 0.92 mmHg/ml/min. The 3DFC decreased ($p < 0.05$) vascular resistance to 3.9 ± 0.86; the addition of captopril further decreased ($p < 0.05$) vascular resistance to 0.41 ± 0.03 mmHg/ ml/min.

Echocardiographic Changes in LV Function and PV Loops

The data on global and regional changes in LV function are seen in Figure 7, Figure 8, Figure 9, and Figure 10. There was a decrease ($p < 0.05$) in LV EF (75 ± 4% to 37 ± 3%) with the acute MI and a subsequent increase ($p < 0.05$) with the 3DFC patch (53 ± 4%). The EF did not increase with the nonviable 3DFC (31 ± 2%); the addition of captopril to the 3DFC did not change the EF compared to 3DFC alone (48 ± 3%). The changes in regional LV function, defined as systolic displacement calculated from parasternal short axis M-mode echocardiography, were similar. With the coronary ligation, there was a decrease ($p < 0.05$) in systolic displacement of the anterior infarcted wall (0.15 ± 0.03 to 0.05 ± 0.02 cm) with a return toward normal with the placement of the 3DFC patch (0.11 ± 0.04 cm). The nonviable 3DFC did not alter EF or systolic displacement. The LV end-diastolic diameter increased ($p < 0.05$) from 4.6 ± 0.4 to 8.1 ± 0.3 mm and the LV end-systolic diameter increased ($p < 0.05$) from 1.2 ± 0.2 to 4.1 ± 0.7 mm 3 weeks after MI (Fig. 9). The 3FDC patch decreased ($p < 0.05$) LV end-diastolic diameter to 6.6 ± 0.4 mm and end-systolic diameter to 1.8 ± 0.08 mm. The PV relationship shows dilatation of the ventricle with the MI but no shift when the 3DFC patch was added (Fig. 10). The addition of captopril to the 3DFC shifted the PV loop to the left toward the pressure axis and deceased the operating LV end-diastolic volume from 0.57 ± 0.05 to 0.34 ± 0.03 ml ($p < 0.05$). The nonviable 3DFC did not alter end-diastolic or end-systolic diameter.

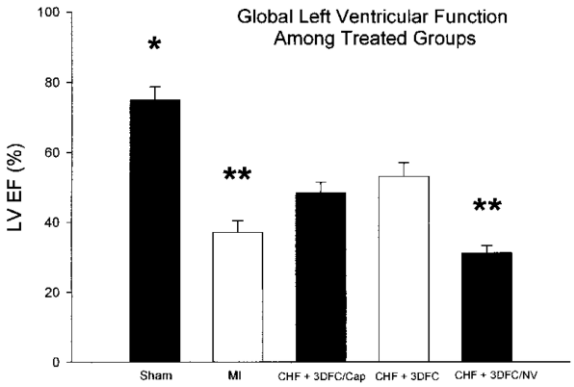

Figure 7. Echocardiographic measured EF in sham, myocardial infarction (MI), MI + 3DFC, MI + 3DFC/Cap (captopril), and MI + 3DFC/NV (nonviable). Note that the viable 3DFC increased the EF. The EF remained increased with the addition of captopril to the viable 3DFC; the nonviable 3DFC did not improve EF. Values are mean ± SE. Sham (*N* = 5); MI (*N* = 8); MI + 3DFC/cap (*N* = 10); MI + 3DFC (*N* = 14); MI + 3DFC (nonviable) (*N* = 5). **p*< 0.05 sham versus all groups; ***p* < 0.05 MI and MI + 3DFC/NV versus MI + 3DFC/cap and MI + 3DFC.

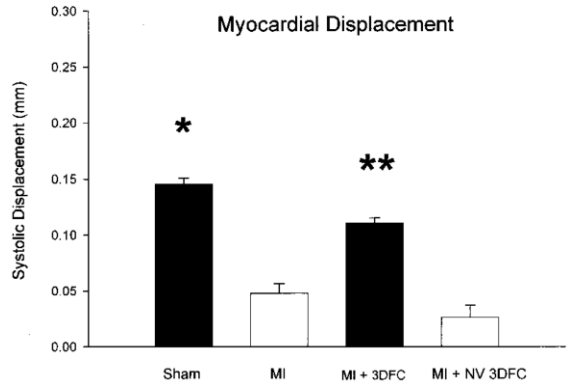

Figure 8. Echocardiographic measured systolic displacement of the infarcted anterior wall in sham, myocardial infarction (MI), and MI + 3DFC. Note that the 3DFC improved EF back toward the normal value. Values are mean ± SE. Sham (*N* = 6); MI (*N* = 12); MI + 3DFC (*N* = 15); MI + NV 3DFC (*N* = 12). **p* < 0.05 versus MI; ***p* < 0.05 versus MI.

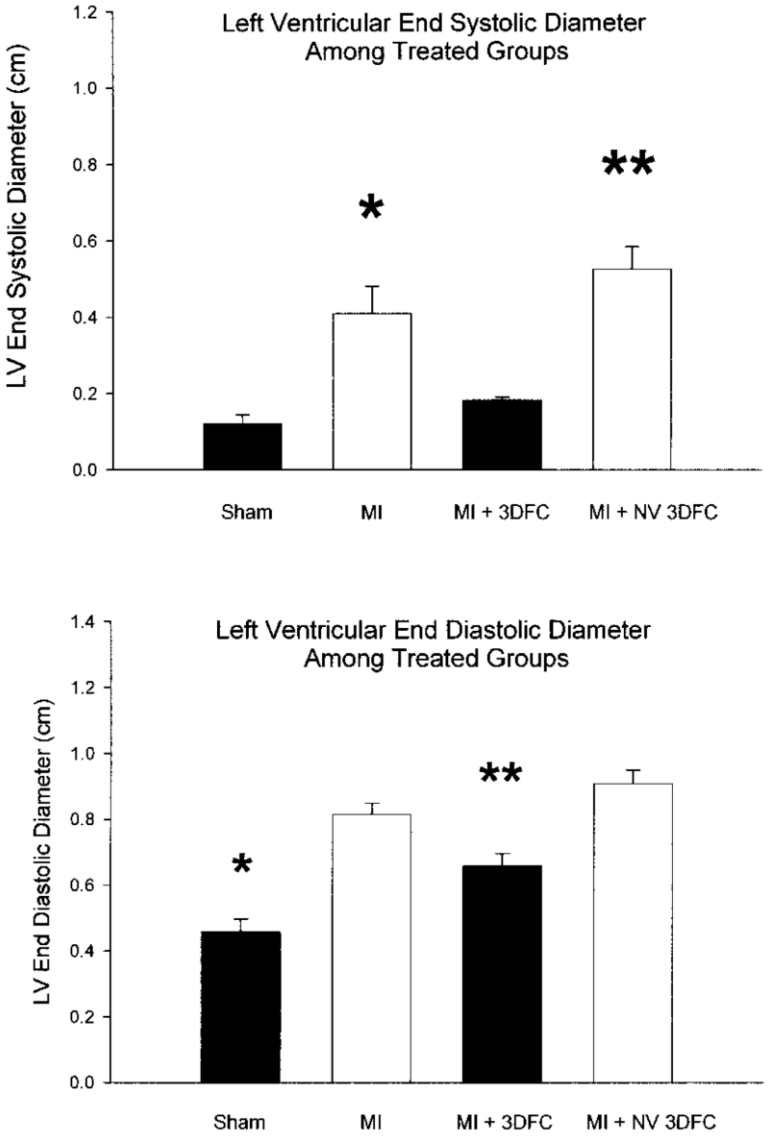

Figure 9: Echocardiographic measured LV end-diastolic and end-systolic diameters in sham, myocardial infarction (MI), and MI + 3DFC. Note that both the LV end-diastolic diameter and end-systolic diameters decrease with the 3 DFC. Values are mean ± SE. Sham (N=6); MI (N=12); MI + 3DFC (N=15); MI + NV 3DFC, (N=12). *$p < 0.05$ versus sham; **$p < 0.05$ versus MI.

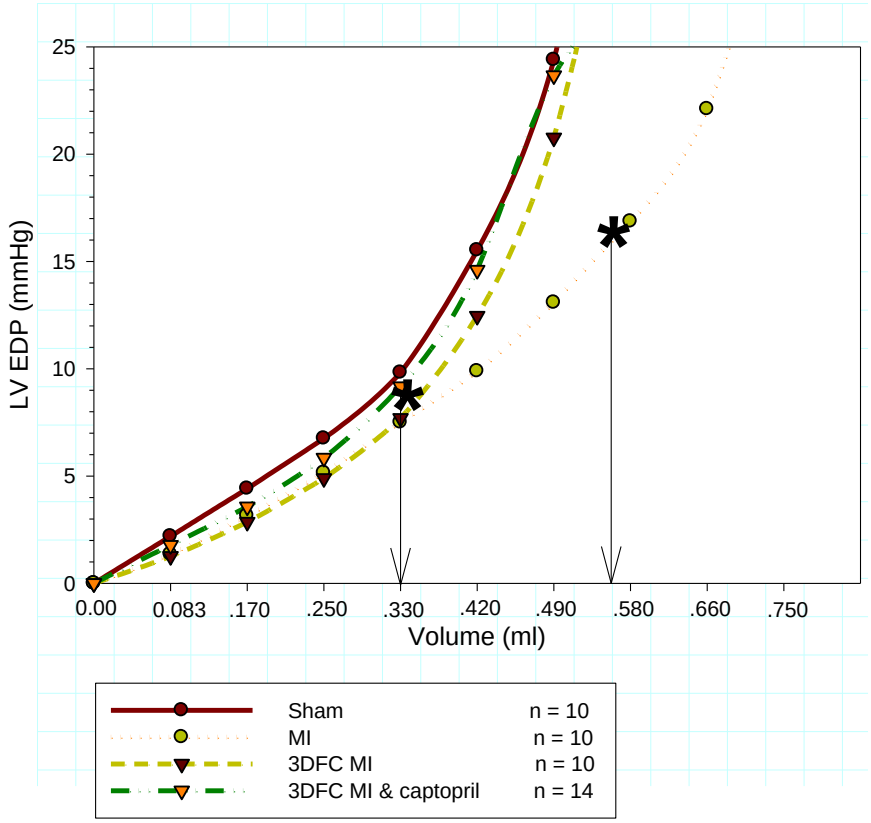

Figure 10: Pressure–volume loops in sham, MI, MI + 3DFC, and MI + 3DFC/captopril. Note that the major shift in the PV loop was with the addition of captopril where the operating LV end-diastolic volume decreased.

Increased Blood Vessels and Myocardial Blood Flow

With acute MI, there was an approximately 80% decrease in blood flow to the infarcted wall, which was not altered at 3 weeks. With the 3DFC, the blood flow increased to about 70% of baseline (Fig. 11). The increase in blood flow was a result of new blood vessel formation with the 3DFC (Fig. 12 & Fig 13).

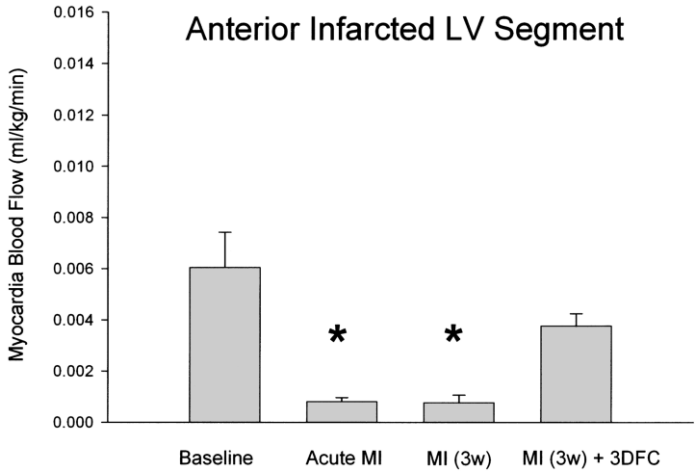

Figure 11: Anterior wall myocardial blood flow in sham (*N* = 11), at the time of MI. MI (*N* = 7), MI at 3 weeks (*N* = 4), and MI at 3 weeks with 3DFC (*N* = 4). Note that the 3DFC improved blood flow in the infarcted wall. Values are mean ± SE; **p* < 0.05 versus baseline and MI (3w) + 3DFC.

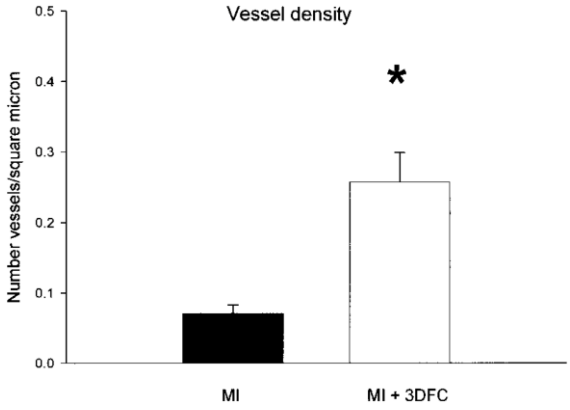

Figure 12: Vessel density defined by Factor VIII staining. Note the increase in vessel density in the area with the 3DFC compared to the untreated MI. MI (*N* = 9), MI + 3DFC (N=9). Values are mean ± SE. **p*< 0.05 versus MI.

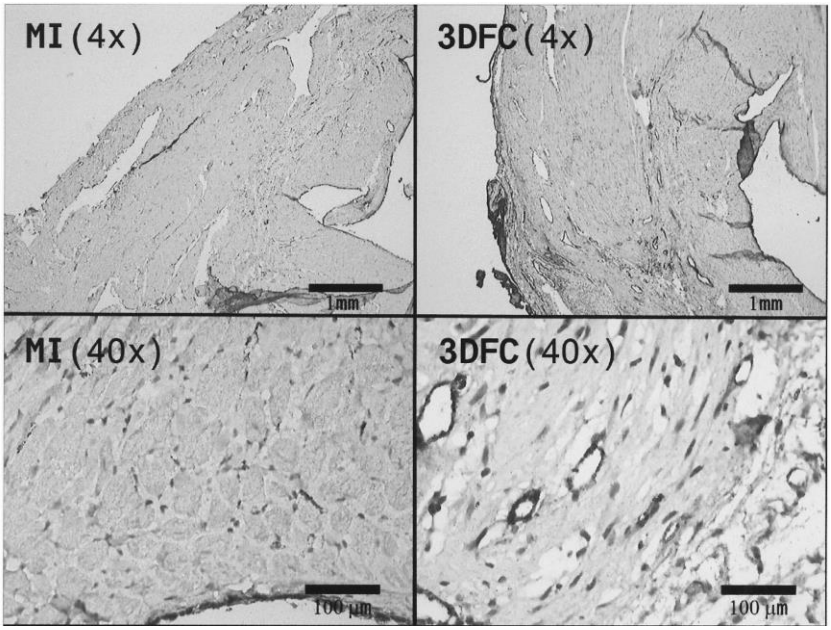

Figure 13: Histopathology sections of Factor VIII staining in MI + 3DFC (A–C) and MI alone (4× and 40×). Note the increased in Factor VIII staining and vessel density with the 3DFC.

Discussion

The important findings in this study are that this 3DFC increases myocardial blood flow in the damaged region of the LV and increases systolic displacement in the anterior infarcted wall after an acute MI. The 3DFC reverses maladaptive LV remodeling, by increasing EF and decreasing LV end-diastolic and end-systolic diameters. The addition of captopril lowers LV EDP and decreases the operating LV end-diastolic volume. These data support our hypothesis that this viable fibroblast patch provides a supporting structure for the damaged heart and may be an alternative to direct cell injection for cell-based therapy for heart failure after MI.

Cell-Based Therapy for Heart Failure

While the original animal data with cell-based therapy for CHF were very encouraging, the results from the most recent clinical trials with direct cell injection into the heart and/or coronary arteries have been disappointing. Clinical trials such as the BOOST, TOPCARE, the IACT, the REPAIR-MI, the ASTAMI Trial, and a bone marrow transplant study from Belgium of intracoronary delivery of autologous bone marrow cells in patients after MI with PCI show only modest improvement in LV function, mostly in patients with preserved EFs with some questions about delivery techniques (Strauer 2005, Schachinger 2004, Schachinger 2006a, Schachinger 2006b). The most positive results are a subset analysis of the REPAIR-MI trial showing that at 1 year, bone marrow cell injection with a higher percentage of CD34+ cells decreases re-infarctions and revascularization procedures with revascularizations driving an improved composite end-point of revascularizations, MI, and death (Schachinger 2006b). We believe that this general lack of positive results with direct cell injection is due in part to the observation that most of these newly injected cells do not survive chronically in the infarcted heart and do not transdifferentiate into cardiac myocytes (Murry 2004, Waggers 2002). Investigators are now injecting cardiac stem cells into the heart in an attempt to obviate the need for stem cells to transdifferentiate (Patel 2007).

Three-Dimensional Fibroblast Patch

Our hypothesis is that the lack of survival of new cells directly injected into the heart is related, in part, to an inadequate blood supply and inadequate matrix support for the new cells. The injected cells are fragile, resulting in cell aggregation due to lack of physical support for the cells to attach to the tissue

ECM. This 3DFC offers a potential solution to the problem of an inadequate support structure. While injection of passive materials has been proposed to improve EF potentially by decreasing wall stress (Gaudette 2006, Wall 2006), the 3DFC provides a viable cell matrix that supports new blood vessel growth (Kellar 2001, Kellar 2005). This viable cellular matrix is important because in addition to providing a new support structure for the damaged heart, we also need to create a mature blood supply such that new viable cardiac muscle can be organized in parallel forming physical and neural connections that will conduct electrical signals and create synchronized contractions. Investigators have proposed that the ideal scaffold structure for the heart would consist mainly of highly interconnected pores with a diameter of at least 200 μm, the average size of a capillary, to permit blood vessel penetration and cell interactions (Cohen 2004).

The 3DFC is a viable construct composed of a matrix embedded with human newborn dermal fibroblasts cultured in vitro onto a bioabsorbable mesh to produce living, metabolically active tissue (Kellar 2001, Kellar 2005) (Fig. 5 & Fig 6). As the fibroblasts proliferate across the mesh, they secrete human dermal collagen, fibronectin, and glycosaminoglycans (GAGs), embedding themselves in a self-produced dermal matrix. The fibroblast cells produce angiogenic growth factors: vascular endothelial growth factor (VEGF), hepatocyte growth factor (HGF), basic fibroblast growth factor (bFGF), and angiopoietin-1. The construct is grown in medium supplemented with serum and ascorbate; at harvest, the medium is replaced with a 10% DMSO-based cryoprotectant, the tissue is frozen and stored at −70°C. This cryopreservation and rewarming technique has been extensively studied to ensure viability of the patch. Although the mechanisms of

action of the 3DFC are not completely understood, new blood vessel growth has been documented previously in SCID mice (Kellar 2001).

Previous work using the 3DFC as a patch for the infarcted heart in SCID mice showed histological evidence of new blood vessel growth and improvements in global LV function using a conductance catheter (Kellar 2005). Our data show increases in myocardial blood flow in the infarcted heart, confirming that these blood vessels are functional and that they connect to the native myocardium. We used echocardiography to document improvements in global and regional LV function. The improvements in regional LV function are important because recent work suggests that the injection of passive materials alone may be enough to reduce wall stress and increase global EF (Wall 2006). In order to prove that cell-based therapy is affecting more than a passive response, the point has been made that it is necessary to be able to define regional changes in the area of the infarcted myocardium (Gaudette 2006). We have done this using echocardiography to document that the 3DFC increases systolic displacement of the infarcted regional anterior wall (Fig. 9). Although the mechanism of action of the 3DFC has not been completely delineated, the viable fibroblasts secrete a number of growth factors, thus providing a paracrine effect to stimulate new blood vessel growth. The Vicryl mesh is biodegradable such that, with dissolution, the new blood vessel growth is in the previously damaged myocardium. The most likely explanation for the improvements in regional systolic displacement of the anterior wall is that the increases in myocardial blood flow in the border zone results in recruitment of hibernating or stunned cardiac myocytes.

The fact that the 3DFC is viable with fibroblasts implanted on a mesh is important. There are data showing that inert biodegradable patches are beneficial in treating CHF. In our laboratory we have shown that an inert biodegradable collagen patch placed on the rat heart after a nontransmural MI improves LV function and prevents adverse LV remodeling (Gaballa 2006). There are clinical trials with a collagen type 1 matrix seeded with autologous bone marrow cells in patients undergoing coronary artery bypass surgery (Chachques 2007). The best-known implanted mechanical constraint device is the Acorn Corp Cap device; it decreases LV size but does not cause constrictive physiology (Oz 2003). There are no blood flow studies with the Acorn device. There is a recent report using an inert biodegradable polyester urethane cardiac patch applied to rats 2 weeks after coronary ligation where the LV cavity size does not change but fractional area change increases and compliance improves; there are no blood flow data in this report (Fujimoto 2007).

Application of a Patch as an Alternative to Direct Cell Injection

The use of a biodegradable patch that provides a support structure allowing new cells to attach and grow in a damaged heart is a possible alternative to the current approach of direct cell injection for cell-based therapy. Not only are the results from current clinical trials of cell- based therapy disappointing, the approach used in these trials is cumbersome, requiring harvesting bone marrow and a repeat cardiac catheterization with infarct artery re-occlusion to re-inject purified autologous mononuclear cells into the coronary arteries. Another problem is the recent report that intracoronary delivery of bone marrow cells results in damage to the coronary artery with luminal loss in the infarct related

artery (Mansour 2006). These data suggest that we need new options for cell-based therapy for CHF.

The translational aspect of this work is important; there is potential for clinical application of this 3DFC patch. At present there are two ongoing phase I clinical trials using the 3DFC; the first is a pilot trial in patients applying the 3DFC patch at the time of coronary artery bypass surgery when the surgeon cannot place a graft to a area of viable myocardium. This trial is designed to determine if the 3DFC increases myocardial perfusion to an area that the surgeon could not graft. While in this clinical study the 3DFC patch is placed with the chest open, two cases have been done with a minimally invasive approach using a modified video-assisted thorascopic surgery VATS procedure. The second trial is in patients getting a left ventricular assist device (LVAD). The 3DFC is applied at the time of LVAD placement and, upon LVAD removal, histology is done on the area of 3DFC placement in order to examine for evidence of angiogenesis.

Viable Fibroblast Matrix Patch Induces Angiogenesis and Increases Myocardial Blood Flow in Heart Failure after Myocardial Infarction

Introduction

Cell-based regenerative therapies have been explored recently as a treatment for MI with mixed results (Schachinger 2004, Wollert 2004, Strauer 2005). Basic laboratory work shows dramatic increases in LV function and survival. Meanwhile, clinical trials demonstrate that intracoronary delivery of cells is safe, well tolerated, and results in modest improvements in LV function (Assmus 2006, Janssens 2006, Lunde 2006, Schachinger 2006, Abdel-Latif 2007, Lipinski 2007,

Menasche 2008). However, few studies focus on CHF, which affects nearly 5 million Americans with an estimated 500,000 new diagnoses annually. Fewer than 50% of patients found to have CHF survive more than 5 years (Mozaffarian 2015, Heidenreich 2013). Current clinical treatments focus on stabilizing CHF and preventing further deterioration; they neither stimulate angiogenesis nor regenerate myocytes or restore the lost functional and structural elements of the heart (Yoon 2005, Bearzi 2007, Wagers 2002). Studies evaluating cell-based therapies in CHF are generally non-conclusive showing 2%-3% increases in EF including studies of skeletal myoblast injections in patients with ischemia undergoing CABG that show no improvement in LV function (Balsam 2004).

While enthusiasm for cell-based therapy for heart failure remains high, the limited clinical beneficial effects may be because most transplanted cells do not survive when injected into the infarcted heart (Chein 2004, Murry 2004, Kajstura 2005). Alternatively, new cell-based delivery techniques using bioengineered patches are evolving (Gaballa 2006, Kellar 2001, Kellar 2005). Previously, our laboratory (Gaballa 1995) evaluated a biodegradable 3DFC composed of a matrix-embedded human newborn dermal fibroblasts cultured onto a Vicryl mesh to produce a living, metabolically active tissue. The 3DFC secretes angiogenic growth factors, including hepatocyte growth factor (HGF), vascular endothelial growth factor (VEGF), and basic fibroblast growth factor (bFGF) (Table 4), which have been shown to increase new blood vessel formation in vivo (Goldman 1995, Gaballa 2002, Pennock 1992).

In this study, the 3DFC was evaluated in a rat CHF model. Echocardiography was employed for evaluation of EF, systolic displacement, and LV end systolic and diastolic diameter. We used solid-state micromanometers to obtain

hemodynamic data. Structural improvements were verified using histological methods. Extensive investigation evaluated both the *in vivo* and *in vitro* angiogenic properties of the 3DFC. Lastly, the 3DFC's proinflammatory markers were evaluated in strained versus static culture conditions *in vitro*.

Materials and Methods

Experimental Design and Treatment Groups

Normal adult male Sprague-Dawley rats underwent left coronary artery ligation and were randomized to sham or 3DFC placement 3 weeks after surgery with three treatment groups: Sham, CHF, and CHF + 3DFC. The experiments were performed in an Association for Assessment and Accreditation of Laboratory Animal Care International (AAALAC) accredited facility with approval from animal use committees of Southern Arizona Veterans Administration Health Care System (SAVAHCS) and the University of Arizona.

Coronary Artery Ligation Experimental MI

The rat coronary artery ligation model is standard in our laboratory (Gaballa 1995, raya 1989, Raya 1997, Thai 2006, Thai 2009). Rats were anesthetized with ketamine and acepromazine, a left thoracotomy was performed, and the heart expressed from the thorax, and a ligature was placed around the proximal left coronary artery. The rats were maintained on standard rat chow, water ad libitum, and pain medication postoperatively.

The 3DFC Patch

The 3DFC is a cryopreserved human fibroblast, extracellular matrix, on a bioabsorbable scaffold (Thai 2009, Kellar 2001, Kellar 2005, Kern 2001) (Fig. 14). The fibroblast cells are tested for animal viruses, retroviruses, cell

morphology, karology, isoenzymes, and tumorgenicity and free from viruses, retroviruses, endotoxins, and mycoplasma. The 3DFC was provided by Theregen, Inc., and is frozen (-75±10C) in pieces 5x7.5 cm with an average thickness of 200 micrometers. The 3DFC was thawed in phosphate buffered saline (34-37C), handled gently by the edges to limit cellular damage, and applied to the heart within 60 minutes of being removed from its container (Fig. 15). The 3DFC does not generate an immune response in previous work (Kellar 2001, Kellar 2005, Kern 2001) (Investigators' brochure ITT-101; Theregen), or in current clinical studies (data not published). The low immunogenicity of allogeneic fibroblasts may be because these fibroblasts show little induction of cluster of differentiation (CD) 40 and human leukocyte antigen-DR (HLA-DR) in response to g-interferon (Gaudette 2006).

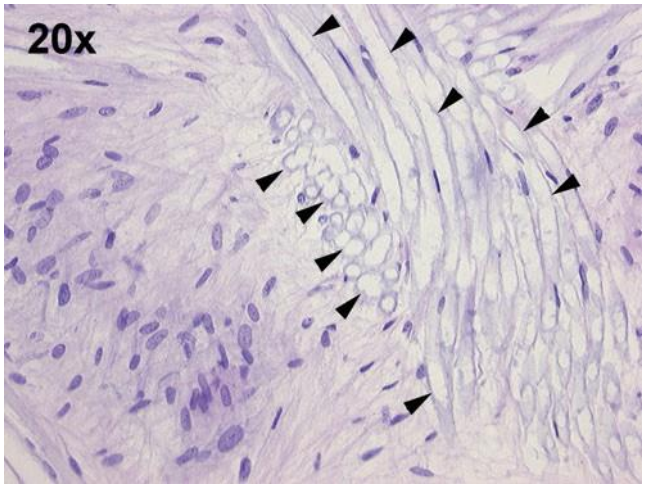

Figure 14: Hematoxylin and eosin stain of the three-dimensional fibroblast construct (3DFC) at 20min after thawing from -75C. Arrowheads denote Vicryl mesh construct of the 3DFC that provide structural support for resident fibroblast growth and proliferation.

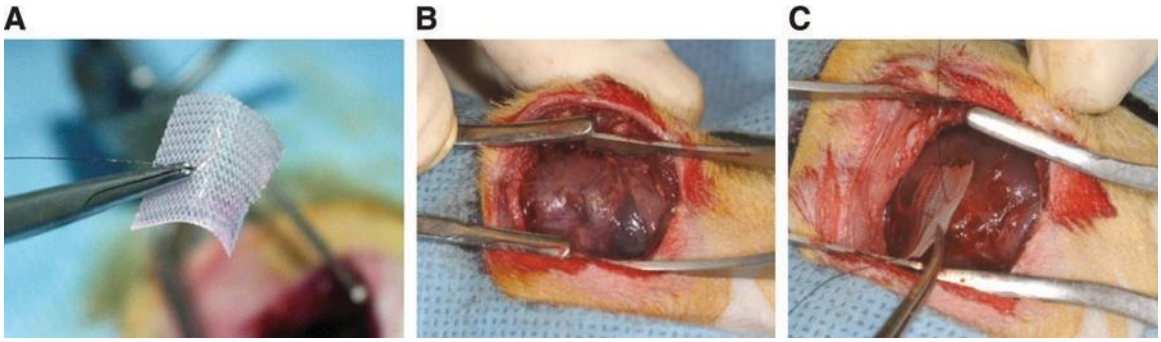

Figure 15: The 3DFC before implantation (A), chest open with infarcted dilated heart 3 weeks after coronary artery ligation (B), and 3DFC placed on the dilated infarcted heart (C).

Hemodynamic Measurements In Vivo

Using standard techniques developed in our laboratory, rats were anesthetized with inactin (100 mg/kg intraperitoneal injection), placed on a specially equipped

operating table with a heating pad, intubated, and placed on a rodent ventilator with a 2F solid state micromanometer tipped catheter with two pressure sensors (Millar Instruments, Inc.) inserted via the right femoral artery, with one sensor located in the LV and another in the ascending aorta. The pressure sensor is equilibrated in 37C saline, and LV and aortic pressures/heart rate were recorded, digitized at a rate of 1000 Hz to calculate LV dP/dt and the time constant of LV relaxation or tau (Gaballa 1995, raya 1989, Raya 1997, Thai 2006, Thai 2009).

LV Pressure-Volume Relationships In Vitro

We measured LV pressure-volume (PV) relations with the heart arrested with potassium chloride, and a PE-90 catheter with telescoped PE-10 tubing inside, inserted into the LV via the aortic root. One end of the double-lumen LV catheter was connected to a volume infusion pump (Harvard Apparatus), whereas the other end was connected to a pressure transducer zeroed at the level of the heart. The right ventricle was partially incised to prevent loading on the LV. The LV was filled (1.0mL/min) to 60-100 mmHg and unfilled while pressure was recorded onto a physiologic recorder (Gould Electronics); ischemic time from euthanasia to the PV curves was limited to 10 min; the volume infused is a function of filling rate (Gaballa 1995, Raya 1997, Thai 2006).

From the pressure-volume data recorded in vivo, the stiffness constants [K_0], [K_1], [K_2], [K_3], and [K_4] are determined by methods described previously by our laboratory (Fukuda 2004). In brief, pairs of simultaneous pressure-volume points (15 pairs for each pressure interval) were obtained. The stiffness constants were calculated with the following analysis: the pressure-volume data are fitted to the exponential equation $P = [P_0][e^{KV}]$ (pressure is assumed to be equal to P_0 when volume is zero). Thus, $\ln P = \ln [P_0] + KV$, and when lnP was plotted versus V, K

is the slope of this relation. The overall stiffness constant was [K_0] = (2.5-30 mmHg), [K_1] = (0-3 mmHg), [K_2] = (3-10 mmHg), [K_3] = (10-20 mmHg), and [K_4] = (20-30 mmHg) were derived.

Echocardiography

We performed closed chest transthoracic echocardiography using a Vingmed, Vivid 7 system echo machine (GE Ultrasound) with EchoPac (GE Ultrasound) programming software with a 10 MHz multiplane transducer with views in the parasternal short axis and long axis, to evaluate the anterior, lateral, antero-lateral, inferior, and posterior walls. Systolic displacement of the anterior wall and EF were obtained from 2D and M-mode measurements of myocardial wall thickness and LV dimensions. Systolic displacement is a measure of focal LV wall thickening; from the M mode through the anterior wall, the difference in the thickness between systole and diastole is the systolic displacement. This was used to quantify focal LV wall systolic function with particular reference to this study where we measure systolic displacement of the anterior infarcted wall (Gaballa 1995, Reinhardt 2001).

Myocardial Perfusion

We used neutron-activated microspheres (BioPal, Inc.) to measure myocardial blood flow. The isotopes were injected, and a tissue sample was obtained, and at a later time activated with the emitted radiation measured with high resolution detection equipment (Gaballa 1995, Reinhardt 2001). Three separate isotopes (lutetium, gold, and samarium) were injected: one at baseline before coronary ligation, one immediately after ligation at the time of the acute MI, and one at 6 weeks in separate groups of rats with CHF, and with CHF + 3DFC. For each measurement 750,000 nonradioactive elementally labeled 15 mm microspheres

(V = 300 µL) from Biopal, Inc., were injected into the LV transapically with a 1 cc syringe and 27-gauge needle. At the terminal study point, tissues were harvested, oven-dried, and collected for analysis. At the time of microsphere injection we performed a transthoracic echocardiogram to measure stroke volume and calculate cardiac output as stroke volume x heart rate. Assuming that 4% of the cardiac output perfuses the coronary arteries, (Oz 2003) we know the total myocardial blood flow. The microspheres deposited in the anterior wall represent the percentage of blood flow down the left coronary artery to the anterior wall at each time point (Gaballa 1995).

Microvessel Histopathology

Hearts were formalin fixed (10%) before paraffin embedding. Heat-induced epitope retrieval of 3-mm-thick sections was performed in citrate-based Diva buffer (pH 6.2) for 1 min at 125C using a Decloaker pressure cooker (Biocare Medical). We used single immunohistochemical staining for anti-rabbit factor VIII (Dako) (1:1000) to perform histological analysis of microvessel density defined by light microscopy at 40 x magnification. The number of cross-sectional vessels per field was counted by two people blinded to treatment, and average measurements from six different fields were recorded for each value. Knowing the area of the optical field, data were reported as number of vessels/μm_2.

Fibroblast Identification Histopathology

Rodent heart samples were processed and embedded into paraffin for subsequent 5 mm sectioning. Vimentin antibody was purchased from Santa Cruz Biotechnology (cat# sc32322) and used at a 1:100 dilution in blocking solution. Heat antigen retrieval using citrate buffer was applied before blocking incubation. Primary antibody was incubated overnight. An ABC system from Vector

Laboratories was used to amplify the signal with subsequent peroxidase 3,3'-diaminobenzidine (DAB) treatment. Light methyl green was used as a background counterstain.

Trichrome Staining

Cut sections were deparaffinized and incubated in potassium dichromate-hydrochloric acid solution, stained with acid fuchsin, fixed with phosphomolybdic acid solution, and stained with orange G. Lastly, sections were treated with aqueous acetic acid, aniline blue, and acetic acid; rinsed with EtOH; and dehydrated in absolute alcohol.

Left Ventricle Measurements

We injected 40 meq/mL potassium chloride into the right ventricle to arrest the heart in diastole. A bolus of 1 mL per 100 g of body weight was rapidly injected into the right ventricle, effecting arrest. Images of trichrome-stained heart sections were captured around the entire circumference of a mid-LV cross-sectional slice. Calibrated, scaled, individual images were stitched together using imaging processing software (Adobe Photoshop Elements). Measurements of each heart were taken using image analysis software (NIH Image J 1.39u), again calibrated from images with a standardized micrometer. The average of three measurements for each heart was taken to represent the wall thickness and LV cavity area value for each heart. Five animals were evaluated from each treatment group (CHF vs. CHF+3DFC).

Biomechanical Strain Induced Cytokine Secretion

The 3DFC were attached to BioFlex collagen-coated membranes using a waterproof adhesive and incubated in a medium containing 2% fetal bovine

serum for 24 h. The 3DFC were equilaxially strained using a flexercell apparatus at 10% 1 Hz for 48 h to model an in vivo cardiac cycle. Conditioned medium samples were collected, and secreted peptides were identified and quantified via protein microarrays (RayBiotech Inc.). Fibroblast proliferation was assayed via dsDNA and total cellular protein concentration was assayed calorimetrically. Peptides were normalized in pg/mL per dsDNA concentration.

Statistical Analysis

Data were expressed as mean ± standard error. For the physiologic and echocardiographic measurements, the Student t-test was used for single comparison of sham versus other study groups. Interactions were tested using two-way analysis of variance; intergroup differences were evaluated using the Student-Newman-Keuls test for statistical significance ($p \leq 0.05$). Pressure-volume relations were evaluated using multiple linear and polynominal regression analysis. The correlation of statistical difference was based on the Durbin Watson statistic, F-statistic, p-value, and variance coefficients.

Results

The rat coronary artery ligation model results in about a 40%-50% operative mortality to produce large infarcts with LV end-diastolic pressures >20 mmHg (Fukuda 2004, Lei 2004). Figure 15 shows the 3DFC before implantation (A), with the chest reopened in a rat with an infarcted dilated heart 3 weeks after left coronary artery ligation (B), and the 3DFC implanted on this infarcted heart 3 weeks after MI (C).

LV Dimensions

Echocardiography and immunohistochemistry were employed to detect functional and structural improvements in CHF groups treated with 3DFC. In a rat model of CHF, classically, there is a decrease ($p < 0.05$) in LV EF (75% ± 2% to 35% ± 3%) with CHF; placement of the 3DFC does not restore EF (35% ± 5%) at 6 weeks (Fig. 16a). In addition, regional LV function, defined as systolic displacement of the infarcted anterior wall, does not increase with the 3DFC (Fig. 16b).

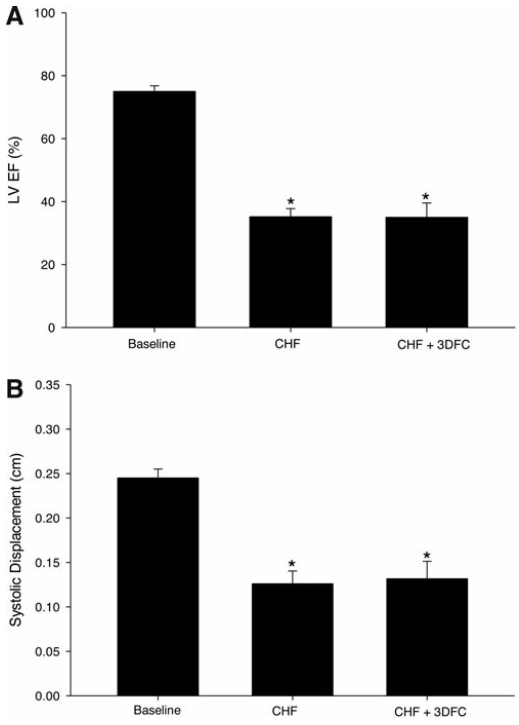

Figure 16: (A) Ejection fraction in CHF after 3DFC. Values are mean ± standard error (SE); sham, *n* = 10; CHF, *n* = 6; CHF 3DFC, *n* = 6. **p* < 0.05 versus sham. (B) Systolic displacement of the infarcted wall in CHF with 3DFC. Values are mean SE; sham, *n* = 10; CHF, *n* = 6; CHF+3DFC, n= 6. **p* < 0.05 versus sham.

The LV end-systolic and end-diastolic diameters increase almost twofold ($p < 0.05$) in CHF from 0.39 ± 0.03 to 0.66 ± 0.10 cm and from 0.64 ± 0.04 to 0.93 ± 0.05 cm in CHF, respectively (Fig. 17). Placement of the 3DFC in CHF rats does not change the end-systolic (0.77 ± 0.04cm) or end-diastolic dimension (0.90 ± 0.04 cm). Histological assessment reveals an increase in anterior wall thickness (Fig. 18, Fig. 19) with implantation of the 3DFC from 0.53 + 0.02 to 1.02 + 0.17mm (Fig. 1 A, B) but does not decrease LV cavity area (37.89 + 3.72 to 38.46 + 5.17mm2). Human-specific vimentin staining demonstrated resident fibroblasts from the 3DFC were present within the epicardial section of LV 3 weeks after implantation (Fig. 20).

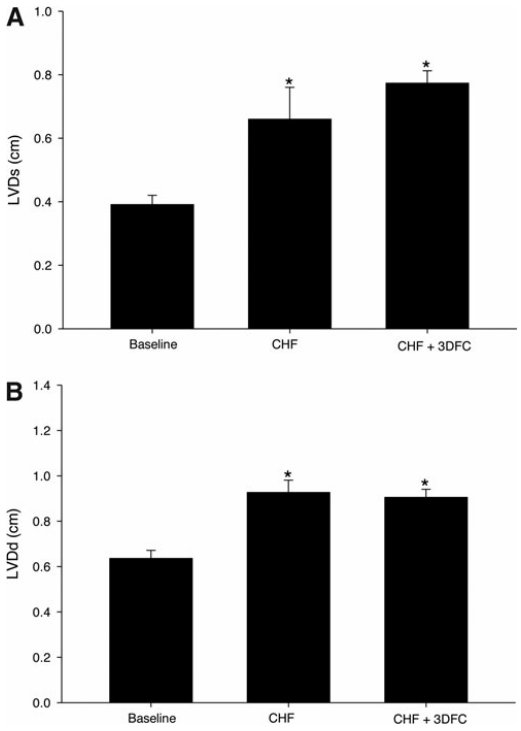

Figure 17: (A) Left ventricular end systolic diameter (LVDs) with 3DFC in CHF. Values are mean ± SE; sham, $n = 10$; CHF, $n = 6$; CHF+3DFC, $n = 6$. $^*p < 0.05$ versus sham. (B) LV end-diastolic diameter (LVDd) with 3DFC in CHF. Values are mean ± SE; sham, $n = 10$; CHF, $n = 6$; CHF+3DFC, $n = 6$. $^*p < 0.05$ versus sham.

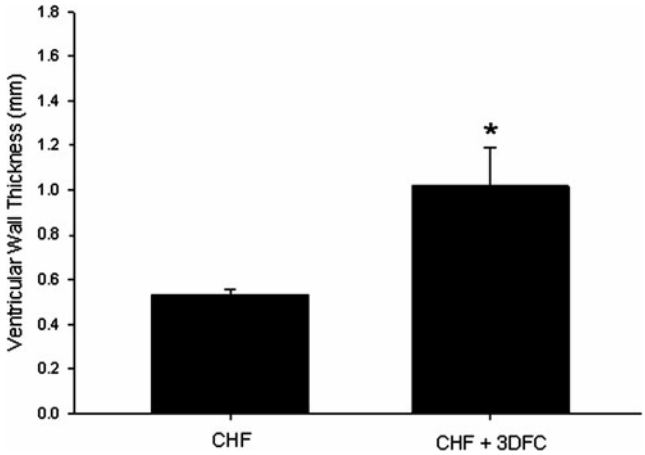

Figure 18: Ventricular wall thickness in rats with CHF versus 3DFC-treated hearts. Implantation of the 3DFC in rats with CHF increases LV wall thickness. *Statistical significance ($p < 0.05$). Values are mean ± SE; CHF, $n = 5$; CHF+3DF, $n = 5$.

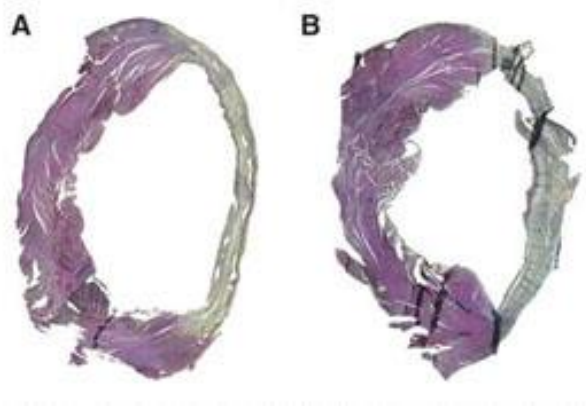

Figure 19: Trichrome-stained LV sections of (A) CHF versus (B) 3DFC-treated CHF hearts. The 3DFC increases LV wall thickness in treated versus untreated hearts.

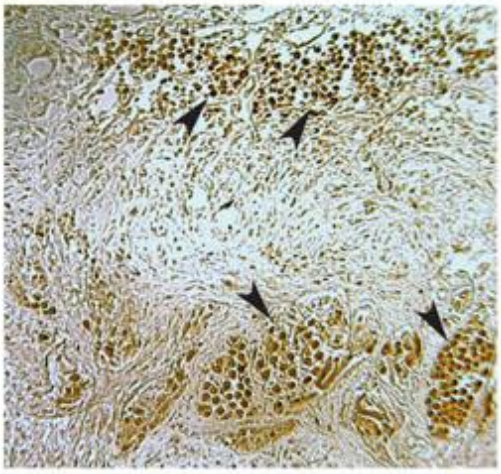

Figure 20: Positive human-specific vimentin antibody staining demonstrates presence of the 3DFC's resident fibroblasts 3 weeks after implantation into a rat CHF model. Arrows illustrate positive human fibroblast staining. Scale bar = 100μm.

LV Hemodynamics

Solid-state micromanometer catheters were placed in the LV and ascending aorta to evaluate LV hemodynamic changes. These data show what we and other laboratories have shown: rats with CHF, 6 weeks after left coronary artery ligation with a threefold increase in LV end diastolic pressure, a 23% reduction in LV systolic blood pressure, a 22% reduction in mean arterial blood pressure, a 36% reduction in positive LV dP/dt, a 50% reduction in negative LV dP/dt, a 40% decrease in peak developed pressure, and a 60% increase in tau ($p < 0.05$), the time constant of LV relaxation (Table 2). Implanting the 3DFC does not significantly ($p < 0.05$) change any hemodynamic parameters described above. There is an increase ($p < 0.05$) in right ventricular weight in the CHF rats (Table 3). Thus, implanting the nonviable 3DFC has no effect on any hemodynamic parameter.

Table 2: Endpoint hemodynamics of three dimensional fibroblast treated rats with CHF.

	MAP (mmHg)	*Tau (ms)*	*HR (bpm)*	*L V SP (mmHg)*	*LVEDP (mmHg)*	*+LV dP/dt (mmHg/s)*	*-LV dP/dt (mmHg/s)*	*PDP (mmHg)*
Sham	135± 7	19.8± 3.6	297± 24	152 ± 12	5.6 ± 1.8	8091± 1050	6396 ± 1237	198± 19
CHF	105± 6α	31.2 ± 5 α	270 ± 33	116 ± 7α	23.4 ± 2α	5153± 590α	3111± 651α	121± 7α
CHF +3DFC	95± 19α	30.6 ± 8 α	270 ± 28	113± 24 α	22.3± 7α	4961± 1127α	3035± 763α	132 ± 26α

Table 2: Values are mean ± SD; Sham, n =5*;* CHF, n = 5; CHF+3DFC, n = 10.$^{\alpha}p$ <0.05 versus sham. Abbreviations: CHF, chronic heart failure; 3DFC, three-dimensional fibroblast construct; LV, left ventricle; MAP, mean arterial pressure; .HR, heart rate; LVSP, left ventricular systolic pressure; LVEDP, left ventricular end diastolic pressure;+/-LV dP*/*dt, left ventricular derivative pressure/ derivative time; PDP, peak developed pressure.

Table 3: Heart weights of three dimensional fibroblast treated rats with CHF.

	Body Weight (g)	*Right Ventricle (g)*	*Left Ventricle (g)*	*Heart weight to Body weight ratio*
Sham	351±222	0.21±0.03	0.82±0.17	0.23±0.04
CHF	353±35	0.38±0.13α	0.83±0.12	0.24±0.03
CHF+3DFC	342±26	0.28±0.08	0.81±0.11	0.24±0.04

Table 3: Values are mean ± SD; Sham, n = 5; CHF, n = 5; CHF+3DFC, n = 10.$^{\alpha}p$ <0.05 versus sham.

Pressure-Volume Loops

The PV relationship shows dilatation of the LV in CHF; the 3DFC patch attenuates this dilatation with a shift to the left ($p < 0.05$) toward the pressure axis (Fig. 21). The overall LV chamber stiffness constant (K_0) decreases ($p < 0.05$, Table 4) with CHF and returns toward sham with 3DFC (Table 4).

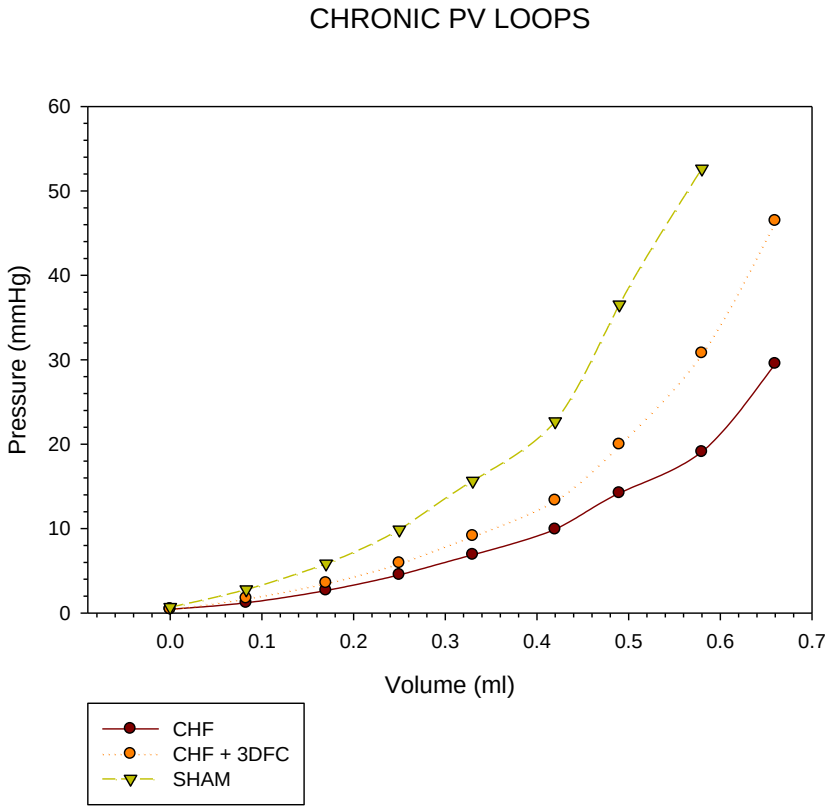

Figure 21: Pressure-volume (PV) relations in sham, CHF, and CHF+3DFC. Note that the 3DFC shifts the CHF PV curve to the left toward the pressure axis. Sham, N=5. CHF, N=7, CHF+3DFC, N=8.

Table 4. Left ventricular chamber stiffness constants in sham, CHF, and CHF+3DFC rats

	SHAM	CHF	CHF+3DFC
K_0 (2.5-30 mmHg)	5.86±0.37	4.78±0.31*	5.24±0.48
K_1 (0-3 mmHg)	7.57±0.78	5.95±0.86	7.10±0.86
K_2 (3-10 mmHg)	5.08±0.62	4.53±0.27	5.16±0.86
K_3 (10-20 mmHg)	5.7±0.64	5.03±0.31	5.07±0.64
K_4 (20-30 mmHg)	5.82±1.02		4.78±0.76

Table 4: Values are mean±SE; Sham N = 5; CHF N = 5; CHF/3DFC N = 10. There are not enough points to calculate K_4 for CHF. *P < 0.05 versus Sham.

Myocardial Blood Flow and Vessel Density

To determine if the 3DFC revascularized ischemic tissue, myocardial blood flow was evaluated using neutron-activated microspheres. Myocardial blood flow to the anterior infarcted wall decreases ($p < 0.05$) in CHF; the 3DFC increases ($p < 0.05$) myocardial blood flow in 3DFC-treated groups (Fig. 22). Additionally, using immunohistochemistry, we evaluated microvessel density formation within the epicardial infarct and peri-infarct zones. Factor VIII staining (Fig. 23) reveled an increase ($p < 0.05$) in microvessel density in groups treated with 3DFC (Fig. 24).

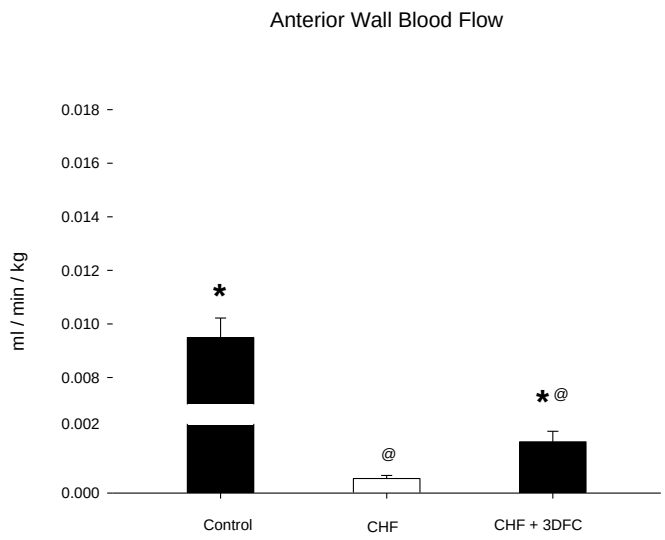

Figure 22. Anterior wall myocardial blood flow in treated (3DFC) vs control groups. Data are mean±SE. * denotes P≤0.05 as compared to 6wk CHF. @ denotes P≤0.05 compared to control. Note that the 3DFC improves blood flow in the infarcted wall in CHF+ 3DFC. N=12 (control), 8 (6wk CHF), 13 (6wk CHF + 3DFC).

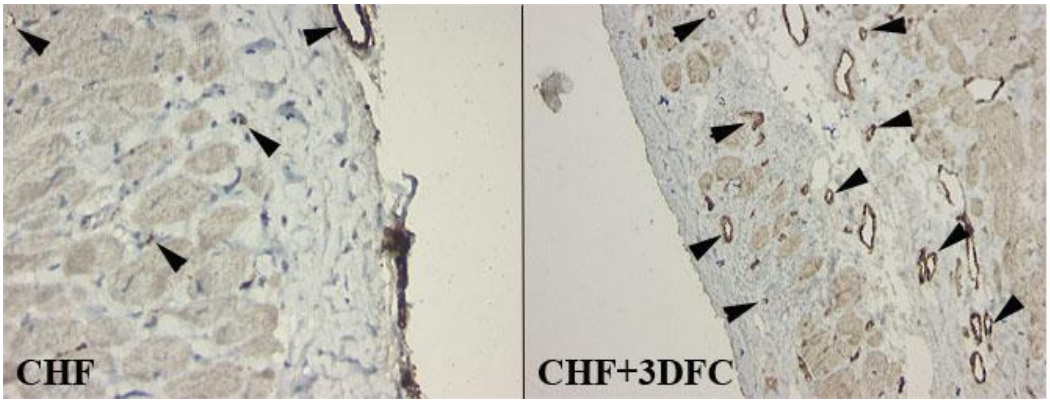

Figure 23. Factor VIII staining showing more staining, i.e., increased vessel density with the 3DFC in CHF rats. Arrows indicate positively stained (brown) microvessel (40X).

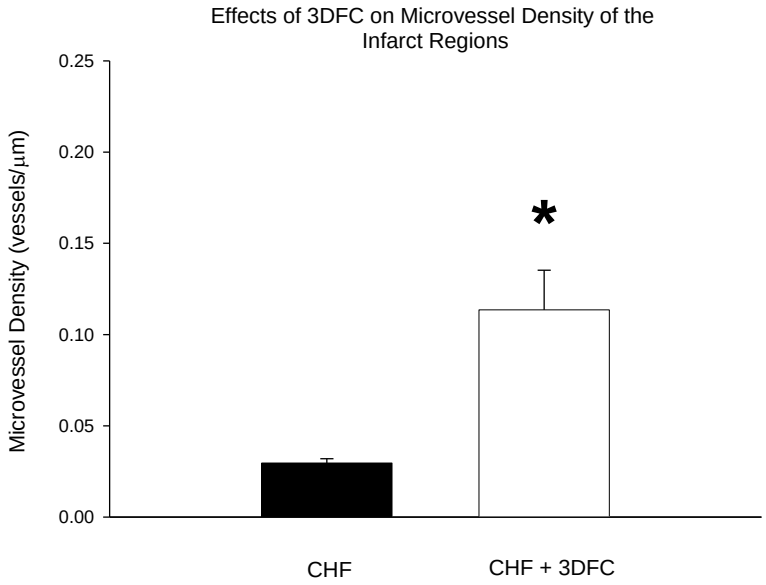

Figure 24. Microvessel density for 3DFC in CHF. The 3DFC significantly increases microvessel density in ischemic tissue. Values are mean ± SE, N=5 for CHF; N=9 for CHF+3DFC ***** P<0.05 versus CHF.

Strain Induced Cytokine Stimulation

In an effort to understand the cytokine production of the 3DFC, selected angiogenic cytokines were measured (in vitro) in control (static) versus strained settings. Measurable amounts of monocyte chemoattractant protein-1 (MCP-1), HGF, interleukin-8 (IL-8), interferon-[gamma], tumor necrosis factor-α, Angiogenin, VEGF, IL-1α, bFGF, Leptin, IL-1P, IL-4, IL-6, platelet-derived growth factor-BB, placental growth factor, and epidermal growth factor (EGF) were detected in conditioned medium samples from both control and strained 3DFC. Strain significantly ($p < 0.05$) decreased extracellular concentrations of interferon-γ, tumor necrosis factor-α, IL-1α, IL-1β, IL-4, and EGF. No appreciable angiopoietin-2 (Ang-2), heparin-binding EGF-like growth factor, IL-10, or IL-13 was detected in any samples (Table 5). In addition, equilbiaxial strain showed no

significant ($p < 0.05$) change in dsDNA concentration; however, total protein content was significantly ($p < 0.05$) elevated with strain 2.32 ± 0.3 versus 3.44 ± 0.3 mg/mL.

Discussion

Our work demonstrates that implanting a viable fibroblast matrix patch in rats with CHF increases LV wall thickness and induces angiogenesis with a resultant increase in myocardial blood flow in the area of previous infarction. In addition, the 3DFC improves passive filling of the LV but does not contribute to improvement in EF or attenuate LV remodeling. Although the mechanisms responsible for the increase in myocardial blood flow and capillary density are not clear, we do show that 3DFC induces selective paracrine activation in vitro that may explain part of its benefit.

Previous work by our laboratory shows that when 3DFC is implanted acutely after MI, the patch improves myocardial blood flow, LV function, and also partially reverses LV remodeling (Gaballa 1995). It is unclear why the 3DFC, when implanted in rats with CHF, does not restore LV function or reverse LV remodeling. Acute placement of the 3DFC results in significant revascularization and restored blood flow to potentially stunned myocardium, possibly preserving tissue viability. However, if the 3DFC is placed in CHF after infarct expansion and scar development has already occurred, although the 3DFC still induces angiogenesis, the adverse LV remodeling cannot be reversed, at least not in the 3-week time frame, that is effective in an acute MI (Gaballa 1995).

Ex Vivo Pressure Relationship Versus In Vivo Analysis

The 3DFC treatment shifts the PV relationship to the left, toward the pressure axis; however, the 3DFC had no change on LV end systolic or diastolic diameter. To explain this contradiction, echocardiography data were collected in vivo, while PV loop data were collected ex vivo. To measure the PV relation ex vivo, hearts were arrested in diastole using KCL, while left ventricular end diastolic diameter (LVEDD) was measured in vivo while the heart may not have been completely relaxed due to incomplete diastole and/or the presence of pericardium, which is typically removed during ex vivo preparation.

Paracrine Activation

The 3DFC is a viable construct composed of a matrix, embedded with human newborn dermal fibroblasts cultured in vitro onto a bio-absorbable mesh to produce a living, metabolically active tissue that secretes growth factors (Table 5) but engendering no immune response (Gaudette 2006). The fibroblasts proliferate across the mesh (Fig. 14) and secrete human dermal collagen, fibronectin, and glycosaminoglycans, embedded in a self-produced dermal matrix. Although the mechanisms of action of cell-based therapy are not clear, most investigators believe that paracrine stimulation from the cells themselves may be responsible for the beneficial effects. Paracrine stimulation has been shown to result in cardioprotection of the cardiomyocytes at the cellular level. (Gaballa 2006) The 3DFC releases a complex blend of cardioactive cytokines (Table 5) with well-documented roles in regulating ventricular function, blood flow, and vessel density. The functional dynamics of some cytokines are potentially stimulated by other active peptides as well as interpolated environmental conditions, as in the case with the peptide MCP-1 acting together

with IL-8 to enhance the metastatic migration of mural cells toward endothelial cells, promoting both the maturation of new blood vessels and arteriogenesis (Callegar 2007, Leor 2000, Landa 2008). In hyperemic flow conditions, but not at rest, MCP-1 and Leptin increase collateral blood flow (Landa 2008). We measured several potent angiogenic growth factors secreted from the 3DFC in high concentrations, including HGF, VEGF, angiogenin, and bFGF. The HGF induces powerful mitogenic activity on endothelial cells, and increases blood vessel number when introduced into infarcted canine myocardium (Goldman 1995). VEGF and bFGF bind to cell-surface-expressed receptors equipped with tyrosine kinase activity leading to improvements in LV remolding and myocyte hypertrophy (Gaballa 2002). VEGF also increases functional improvement of post-infarcted hearts (Gaballa 2002). Interestingly, our data show that the imbedded fibroblasts of the 3DFC response to biomechanical strain results in an increase in total protein, which may be due to upregulation of intracellular proteins such as actin, or an increase in extracellular matrix proteins such as collagen, elastin, and fibronectin, providing structural support and a scaffolding for cellular migration aiding in cardiac growth. In addition, these data show that strain decreased the fibroblasts' secretion of proinflammatory molecules (Table 5), and suggest the possibility that heart rate and force of contraction may modify the peptide secretory profile of 3DFC. Mechanotransduction of human fibroblasts in 3D constructs have been investigated by others and supports these findings (Ma 2007). This described paracrine effect does not occur with the nonviable 3DFC (data not shown) presumably because the nonviable 3DFC does not contain living fibroblasts. Previous work in rats and mice has shown that implanting the nonviable 3DFC does not improve myocardial blood flow or improve LV function (Kellar 2001, Kellar 2005). Thus, the benefits from the 3DFC

are due to more than just the physical presence and the restraining effects of the patch.

Table 5. Cytokine activation in static (control) versus strained 3DFC patches

Angiogenesis	Control (Static)	Strain
Angiogenin	1322 ± 769	383 ± 140
Angiopoientin-2	-71 ± 183	-180 ± 100
Basic Fibroblast Growth Factor	461 ± 290	38 ± 50
Endothelial Growth Factor	15 ± 0.7	5 ± 3
Heparin-Binding Endothelial Growth Factor	-226 ± 189	-172 ± 49
Hepatocyte Growth Factor	9725 ± 4307	9285 ± 5219
Leptin	-152 ± 3610	459 ± 1970
Platelet-Derived Growth Factor BB	38 ± 8	23 ± 4
Placental Growth Factor	11 ± 4	27 ± 14
Vascular Endothelial Growth Factor	324 ± 152	758 ± 392
Inflammation	**Control (Static)**	**Strain**
Interferon-gamma	3573 ± 258	2060 ± 153 **
Interleukin-1alpha	577 ± 23	212 ± 6 **
Interleukin-1beta	171 ± 27	36 ± 5 **
Interleukin-4	101 ± 16	36 ± 7 **
Interleukin-6	83 ± 33	36 ± 19
Interleukin-8	3937 ± 2192	2966 ± 1517
Interleukin-10	-20 ± 14	-48 ± 8
Interleukin-13	-77 ± 35	-137 ± 34
Monocyte Chemotactic Protein-1	11900 ± 5890	10830 ± 2847
Tumor Necrosis Factor-alpha	2183 ± 100	1277 ± 110 **

Table 5: Cytokine, chemokine, and growth factor stimulation of angiogenic and inflammatory markers in static (control) versus strained 3DFC patches in vivo over 48hr (10% 1Hz). Expression in pg cytokine / µg DNA, n=3. Adjusted for 2% fetal bovine serum media. $^{\alpha}p<0.05$.

Using the 3DFC as a Delivery System

Although this present report outlines the use of the 3DFC by itself, as treatment for CHF, the fibroblast patch could be used as an adjuvant delivery system for cell-based therapy. Because patients in heart failure present in the chronic phase of their disease, this could be an elective procedure where cells are harvested, grown in culture, seeded on the 3DFC, and re-implanted in the patient.

With direct cell injection into the heart, the majority of transplanted cells do not survive (Muller-Ehmsen 2002, Dow 2005). The lack of survival of these injected cells is related, in part, to an inadequate blood supply and inadequate matrix support for the new cells. The injected cells are fragile, resulting in cell aggregation due to lack of physical support for the cells to attach to the tissue extracellular matrix. This 3D scaffold offers a potential solution to the problem of an inadequate cellular support structure (Fig. 14). In addition, Figure 25 demonstrates the integration of the 3DFC into the infarcted tissue and remnants of the Vicryl mesh support structure 3 weeks after implantation.

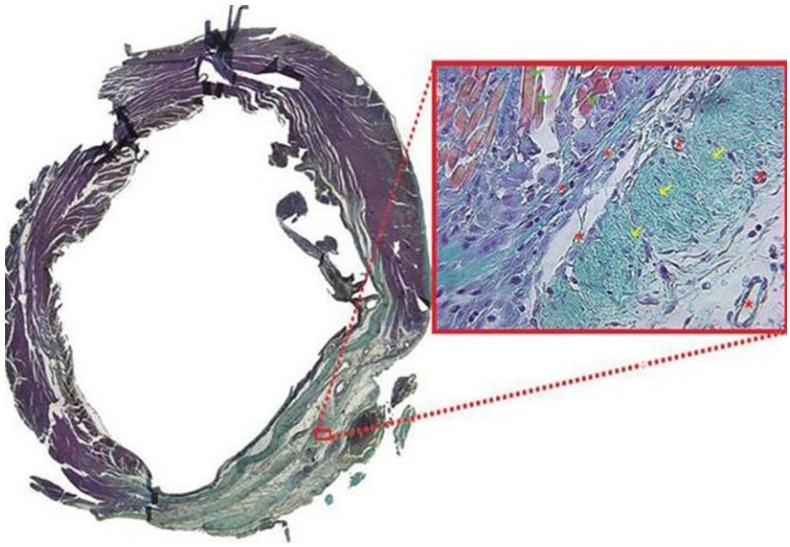

Figure 25: Trichrome-stained LV cross section of a 3DFC-treated CHF heart. Higher magnification image inset highlighted in red; green arrows indicate remnants of Vicryl mesh, yellow arrows indicate collagen fibers, and red asterisks indicate microvasculature. Within 3 weeks, the 3DFC Vicryl mesh fibers have incorporated into the anterior wall.

An Electrically Coupled Tissue Engineered Cardiomyocyte Scaffold Improves Cardiac Function in Rats with Chronic Heart Failure

Introduction

Chronic heart failure is the leading cause of morbidity and mortality worldwide. Although current medical therapeutics decrease mortality from CHF, they do not reverse the disease process or restore long-term cardiac function. Recently, a number of novel strategies have been proposed for improving functional and clinical outcomes of patients with CHF such as, cell-based therapies (Srivastava 2006), in vivo tissue reprogramming (Song 2012) and gene therapy (Tileman 2012). Each of these approaches may carry therapeutic potential, but cell-based therapies offer the least cumbersome approach and are not complicated by *in vivo* viral or gene administration.

Evaluation of cell-based therapies for CHF has progressed through a number of clinical trials (Schachinger 2004, Wollert 2004, Strauer 2005, Assmus 2006, Janssens 2006, Lunde 2006, Schachinger 2006). Although questions remain regarding the most effective cell type and dosing strategies, the major limitation to success may be the development of an effective cell-delivery system. Current delivery techniques, for the most part, use direct injection by catheter-based systems that result in limited cellular survival and minimal retention of cells in the target area (Muller-Ehmsen 2002, Dow 2005). As a result, new cell-delivery strategies, such as TE constructs, are being developed that provide structural support facilitating implanted cell survival and integration into the underlying myocardium (Zimmerman 2006, Seikine 2008, Madden 2010).

Previous studies by our laboratory, and others, have tested a 3-dimensional fibroblast construct (3DFC) consisting of viable human dermal fibroblasts embedded onto a bioabsorbable polymeric Vicryl mesh (Ethicon, Somerville, NJ) that does not elicit an immunologic response (Kellar 2001, Kellar 2005, Fitzpatrick 2010). Implantation of this 3DFC immediately after MI or in an ischemic CHF model, 3 weeks after permanent occlusion of the left coronary artery, results in formation of a microvascular bed and the consequent increase in myocardial blood flow to the infarcted tissue (Thai 2009, Lancaster 2010). The embedded fibroblasts are an important component of the bioengineered scaffold because dermal fibroblasts have been demonstrated to play a role in microvascular organization in vitro through paracrine-mediated effects or other factors (Camelliti 2005, Camelliti 2006, Liu 2008). Yet, implanting the 3DFC alone in CHF did not improve cardiac function (Thai 2009, Lancster 2010).

In the present study, we explored the potential of the microvascular bed induced by the 3DFC to support an overlaying population of cardiomyocytes seeded on the 3DFC. We demonstrate that rat neonatal cardiomyocytes (NCM) can be successfully co-cultured with human fibroblasts in a biodegradable scaffold and that they form an electromechanically organized syncytium capable of improving the left ventricular (LV) function of a chronically infarcted heart.

Materials and methods

The 3DFC

The 3DFC is a cryopreserved bioabsorbable scaffold populated with human neonatal fibroblasts (Kellar 2001, Kellar 2005, Thai, 2009, Lancaster 2010). The fibroblasts have been tested for cell morphology, karology, isoenzymes, and

tumorigenicity and are free from viruses, retroviruses, endotoxins, and mycoplasma. The 3DFC was provided by Theregen Inc (San Francisco, CA) frozen (–75 ± 10C) in 5 x 7.5 cm pieces with an average thickness of 200 μm. The 3DFC is thawed in phosphate buffered saline (34C–37C) and handled gently to limit cellular damage. The 3DFC does not generate an immune response (Kellar 2001, Kellar 2005, Fitzpatrick 2010, Thai 2009, Lancaster 2010) (investigators' brochure ITT-101, Theregen).

Cardiomyocyte Isolation, Seeding and Culture

Cardiomyocytes were isolated from 1 to 2 day-old neonatal Sprague-Dawley (Harlan, Indianapolis, IN) rat hearts. Briefly, the hearts were excised, the atria were removed, and the ventricles were minced into 0.5 to 1mm portions and digested in a pancreatin/collagenase solution. After each enzymatic digest, cardiomyocytes were collected, combined, and re-suspended in Dulbecco Modified Eagle's medium (DMEM) with 10% fetal bovine serum (FBS). Lastly, the suspension was differentially plated in Ham's F-12 with 100 mg/ml bovine serum albumin. The 3DFC was thawed, cut into 1.5-cm diameter sections, and seeded with NCM at densities ranging from 0.6×10^6 to 2.7×10^6 cells/cm^2 using methods developed in our laboratory. The NCM and NCM-3DFC were cultured in 10% FBS in DMEM-LG (Gibco- Invitrogen, Carlsbad, CA), maintained at 37C and 5% CO_2. Patches were constructed as described for in vitro and in vivo evaluation. The NCM-3DFC patches for in vivo evaluation were seeded, cultured, and implanted onto the rat heart 3 weeks after left coronary artery ligation within 18 hours of seeding. Patches prepared for in vitro evaluation were seeded and cultured 1 to 10 days.

Quantitative Measurements of Cardiomyocytes and Fibroblasts

Serial stained tissue samples were reacted with specific markers for cardiomyocytes (troponin) and fibroblasts (vimentin). Immunohistochemically reacted glass slides were digitally scanned (whole- slide scanning) using an Aperio scanner (Aperio, Vista, CA), with subsequent FACTS (Feature Analysis on Consecutive Tissue Sections). Whole-slide scanning allowed for an objective digital quantitative analysis of the entire tissue sections to ensure against investigator bias. The parameters for a generic image analysis algorithm for quantifying cells were independently adjusted for counting cardiomyocytes and fibroblasts. This was used for the objective analysis. The algorithm-based FACTS process performs image-to-image registration on prepared tissue sections on each glass slide. The FACTS process was used to align the serial sections to ensure that corresponding areas were analyzed in each stained slide to provide a fair sample comparison.

Filed Stimulation and Pacing

NCM-seeded 3DFC patches were transferred to a thermos-regulated culture well (Bipolar Temperature Controller; Medical Systems, Greenvale, NY) containing culture medium maintained at 371C. The NCM-3DFC were paced (S44; Grass Instruments, Quincy, MA) by field stimulation (~7 V) through 99.7% pure silver wires placed into the culture well on opposing sides of the NCM-3DFC. The pacing rate varied from 60 to 270 ± 30 beats/min for 10 seconds.

Cell-to-Cell Communication

Functional gap junction formation was examined in 3DFC, NCM-3DFC, and halothane-treated NCM-3DFC patches at 6 days. Three dyes were injected simultaneously: [2-(4-nitro-2,1,3-benzoxadiol- 7-

yl)aminoethyl]trimethylammonium (NBD-TMA [provided by Dr. Steve Wright, University of Arizona, Tucson, AZ] 24; mol wt 280, net charge 1þ, 10 mmol/liter), Alexa 350 (mol wt 326, net charge 1–, 10 mmol/liter), and rhodamine dextran (0.1 mg/ml; both Molecular Probes; Invitrogen, Carlsbad, CA).

Microelectrode tips were created from 1.0-mm filament glass (A-M Systems, Sequim, WA) on a Sutter Instruments puller (Novato, CA), their tips filled by capillary action with the dye mixture and backfilled with 3 mol/liter KCl. The microelectrodes were lowered onto a cell field in the preparation until contact with a cell surface was achieved and cytoplasm access was gained. The dyes were slowly and continuously injected by a slight capacitance overcompensation of the amplifier (SEC- 05LX; NPI Electronics, Tamm, Germany). Images were captured at different times during the next 5 to 20 minutes. Halothane, a known gap junction inhibitor, was added to the superfusate (final concentration, ~8 mmol/liter) to temporarily decrease intercellular dye diffusion and further confirm the transjunctional nature of this phenomenon (Ek-Vitorin 2005, He 2000, Turner 1994).

Multielectrode Array Electrical Mapping

The NCM-3DFC was electrophysiologically mapped in real-time using a 10-electrode custom-designed multielectrode array (Ad-Tech Medical Instrument Corp, Racine, WI) and a 1-kHz low-pass filter. Action potentials were collected using a BIOPAC MP150 (BIOPAC Systems Inc, Goleta, CA) data acquisition system with MCE100C signal conditioning modules. The MCE module has multiple gain settings from 10 to 1,000 and an on- board configurable signal filter. Up to 16 channels of data were acquired simultaneously at a 5-kHz sampling rate. Notch filters were configured in the data acquisition system for removing the

60 Hz noise and its higher harmonics. Data recordings were collected in 10-second intervals. Seeded patches were evaluated in vitro at 1 to 8 days in culture for spontaneous field potential amplitude, duration, conduction velocities, propagation patterns, and mono- phasic action potentials. The NCM-3DFC was maintained at 37C in standard culture medium.

Coronary Artery Ligation Experimental CHF

All animals in this study received humane care in compliance with the “Principles of Laboratory Animal Care” and the “Guide for the Care and Use of Laboratory Animals.” The rat coronary artery ligation model is standard in our laboratory (Gaballa 1995, Raya 1989, Raya 1997). In brief, Sprague- Dawley rats were anesthetized with ketamine and acepromazine and underwent a left thoracotomy. The heart was expressed from the thorax and a ligature placed around the proximal left coronary artery. The rats were maintained post-operatively on standard rat chow, water ad libitum, and pain medication. Only rats with an EF of $\leq$35% after permanent left coronary artery ligation at 3 weeks post-MI were enrolled in the study. Three weeks after MI, the chest was reopened, and the NCM- 3DFC was implanted with suture on the infarcted ventricle bridging to viable myocardium.

Echocardiography

Closed-chest transthoracic echocardiography was performed using a Vingmed, Vivid 7 system echo machine with EchoPac (both GE Ultrasound, Fairfield, CT) programming software with a 10-MHz multiplane transducer, with views in the parasternal short-axis and long-axis, to evaluate the anterior, lateral, anterolateral, inferior, and posterior walls. Systolic displacement of the anterior

wall and EF were obtained from 2D and M-mode measurements of myocardial wall thickness and LV dimensions (Thai 2009, Thai 2006).

Hemodynamic Measurements In Vivo

Rats were anesthetized with a 100 mg/kg intraperitoneal injection of Inactin (Sigma-Aldrich, St. Louis, MO), intubated, and placed on a rodent ventilator with a 2F solid-state micromanometer-tipped catheter with 2 pressure sensors (Millar Instruments Inc, Houston, TX) inserted through the carotid artery. One sensor was located in the LV and another in the ascending aorta. The pressure sensor was equilibrated in 37ºC saline, and LV and aortic pressures/heart rate were recorded and digitized at a rate of 1,000 Hz to calculate LV dP/dt and the time constant (Tau) of LV relaxation (Thai 2009, Gaballa 1995, Raya 1989, Raya 1997, Thai 2006). Hemodynamic measurements were obtained at the end of the study, 6 weeks post-MI (3 weeks post- implantation of 3DFC), and 21 weeks post-MI (18 weeks post-implantation).

Statistical Analysis

Data are expressed as mean ± standard error (SE). Student's t-test was used for single comparison of group vs group analysis of statistical significance ($p<0.05$).

Results

Cardiomyocyte Seeding

Cardiomyocyte seeding densities were evaluated between 0.6 and 2.7 x 10^6 cells/cm^2. Lower-density cardiomyocyte preparations (0.6 to 1.2 x 10^6 cells/cm^2) displayed spontaneous, non-synchronized contractions after 48 hours in tissue culture. At 72 hours, these contractions began synchronizing, and by 84 hours, cell contractions were fully synchronized. Higher density cardiomyocyte

preparations (1.8 to 2.7 x 10^6 cells/cm^2) displayed synchronized and spontaneous contractions of the entire scaffold after 48 hours in tissue culture.

Contractions increased in robustness from 48 hours to 5 days. At day 5, scaffolds seeded with 2.7 x 10^6 cells/cm^2 contracted in a consistent rhythmic and directional fashion. NCMs plated in 35-mm^2 plates (control) displayed contractions at 97 ± 4 beats/min, whereas NCM-3DFC was recorded at 43 ± 3 beats/min (Fig. 25 & 27) with a mean displacement of 1.3 ± 0.3 mm (Fig. 28) and a contraction velocity of 0.8 ± 0.2 mm/sec (*n* = 10; Fig. 29).

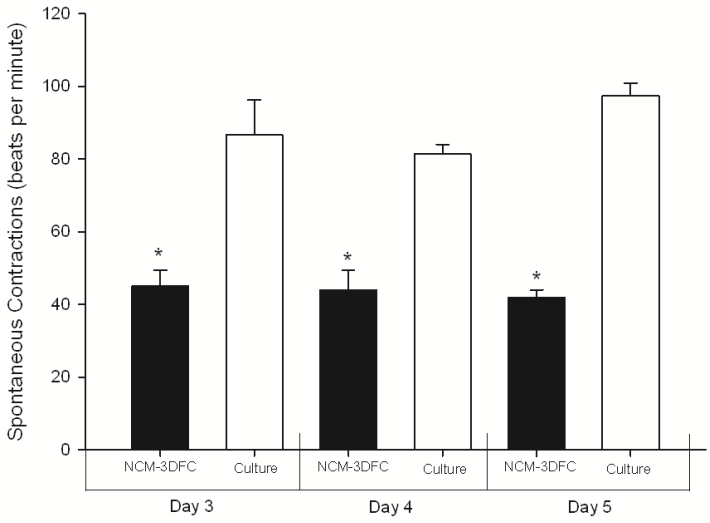

Figure 26: Rate of spontaneous contractions in NCM-3DFC and cultured neonatal cardiomyocytes. NCM-3DFC (N=4), culture (N=3). Data are mean±SE. * denotes statistical significance between seeded and culture for each day (P < 0.05).

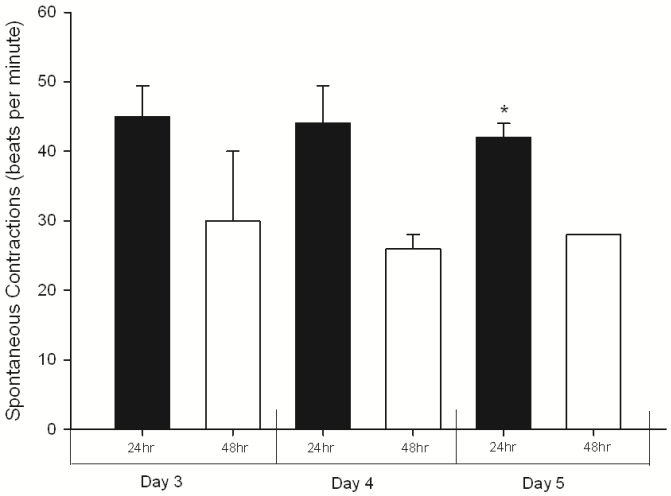

Figure 27: Rate of spontaneous contractions in NCM-3DFC with media changes every 24 or 48 hrs. 24hr (N=4), 48hr (N=2). Data are mean±SE.* denotes statistical significance between 24hr and 48hr for day 5 ($P < 0.05$).

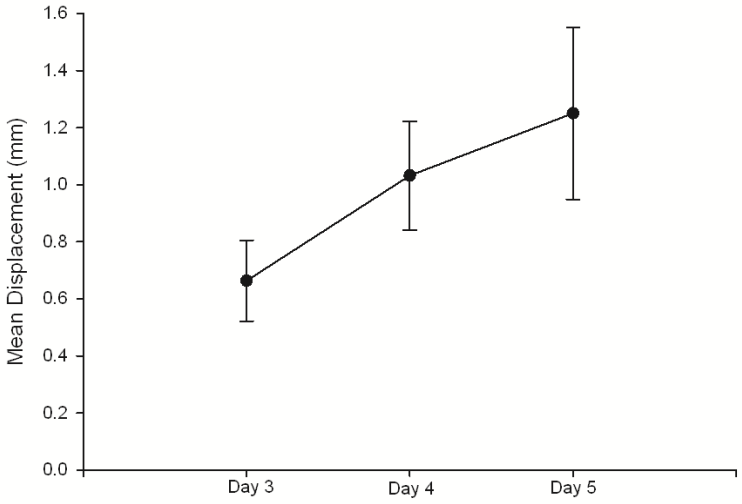

Figure 28: Mean displacement of NCM-3DFC (fed every 24 hrs) at 3, 4 and 5 days after seeding. Day 3 (N=6), day 4 (N=10), day 5 (N=9). Data are mean±SE.

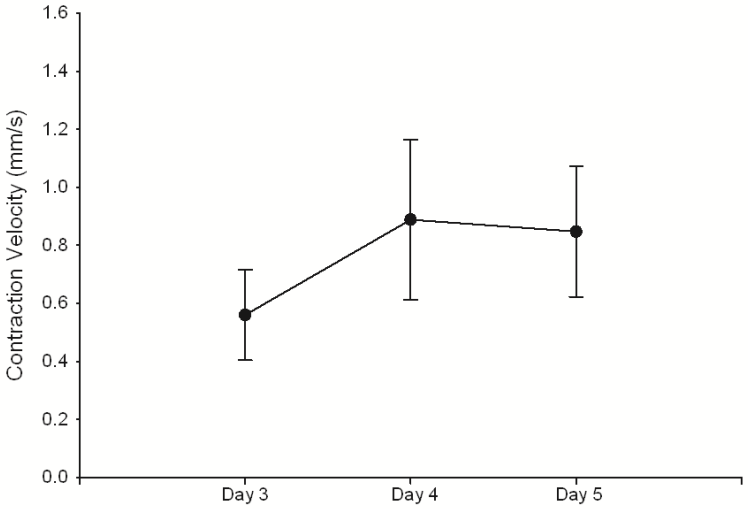

Figure 29: Contraction velocity of NCM-3DFC (fed every 24 hrs) at 3, 4, and 5 days after seeding. Day 3 (N=6), day 4 (N=9), day 5 (N=8). Data are mean±SE.

In Vitro Cellular Composition

In vitro quantification of the cellular composition of the NCM-3DFC showed a fibroblast nuclear density (n = 5) of 931 ± 72 and 974 ± 95 nuclei/mm^2 and a cardiomyocyte nuclear density (n = 4) of 5,808 ± 527 and 4,923 ± 287 nuclei/mm^2 at 2 and 8 days in culture, respectively. Thus, a 5:1 ratio of myocyte to fibroblast nuclear density and no cell loss were found between 2 and 8 days in culture.

Field Stimulation

External field stimulation was applied to the NCM-3DFC at varying culture time points (2–6 days) in temperature- controlled (37°C) wells. The NCM-3DFC contracted synchronously when paced for 20-second intervals at physiologic rates up to 270 ± 30 beats/min (Thai 1999).

Cell-to-Cell Communication

Dye injections into the fibroblasts of the 3DFC alone resulted in no detectable transjunctional diffusion (Fig. 30A). In contrast, dye diffusion readily occurred from the injected myocytes toward neighboring cells on the NCM-3DFC (Fig. 30B). Furthermore, as can be expected from the gradual organization of cell bundles, junctional connectivity increased from Day 2 through 6 days (data not shown). When the NCM-3DFCs were exposed to halothane, dye was retained in the donor cell, reaching higher concentrations but failing to diffuse to the neighboring cells despite the obvious intercellular gradient (Fig. 30C).

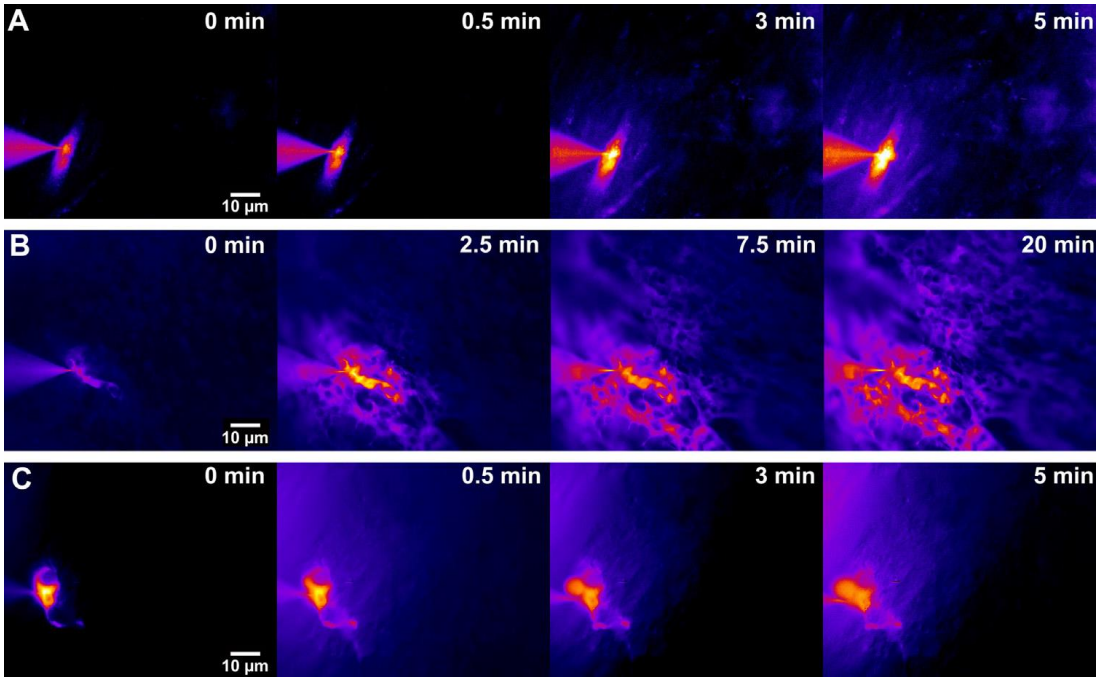

Figure 30: Time elapsed images (original magnification x40) of (A) 3-dimensional fibroblast construct (3DFC), (B) neonatal cardiomyocyte (NCM)-3DFC, and (C) NCM-3DFC treated with halothane at day 6 of culture. In all images, the dye-filled electrode is at the left, and its tip allows the location of the injected cell (donor). From this cell, dye may diffuse across gap junctions to other (recipient) cells. The dye [2-(4-nitro-2,1,3-benzoxadiol-7-yl)aminoethyl]trimethylammonium (NBD) easily occupies the cytoplasmic space, but does not penetrate the nucleus; thus, individual recipient cells can be located by the image of NBD fluorescence surrounding a central, less fluorescent area. (A) No detectable intercellular dye transfer occurs from the injected fibroblast to neighboring cells. (B) The dye injected into a single NCM spreads through established gap junctions toward neighboring cells. (C) After halothane treatment, a transient decrease on the speed of transjunctional dye diffusion was observed. In this particular image, the reflection of the highly concentrated dye in the injected cell is perceived, but only 1 recipient cell (adjacent to the injected one) can be clearly identified after 5 minutes.

Electrical Mapping

The spontaneous electrical activation of the NCM-3DFC was mapped by electrically recording constructs at varying times in tissue culture. The NCM-3DFC yielded maximum and minimum transverse conduction voltage amplitude

of 42 µV and –75 µV, respectively. A consistent sequence of transverse activation was seen beat-to-beat (Fig. 31).

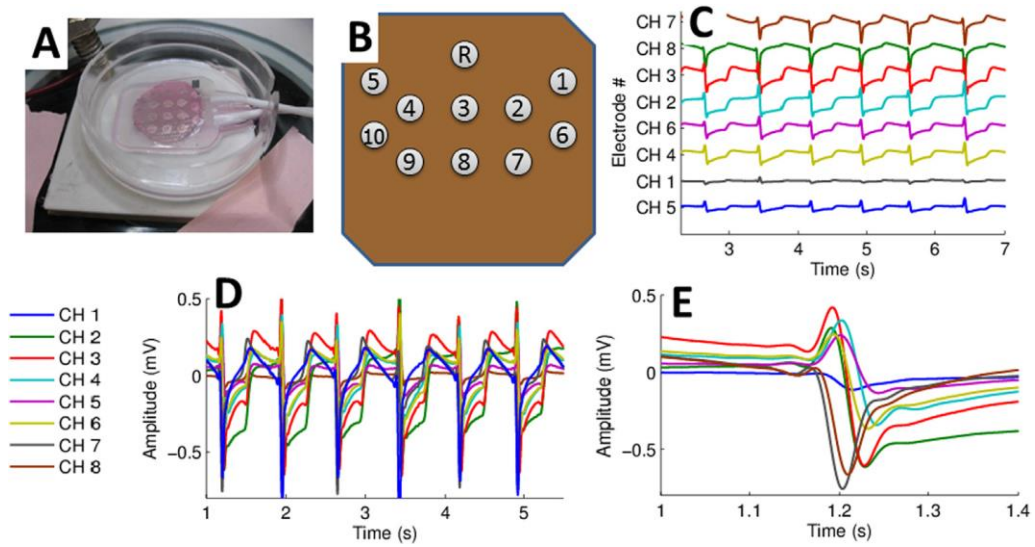

Figure 31: (A) Electrical activation mapping was performed on the neonatal cardiomyocyte (NCM)-3-dimensional fibroblast construct (3DFC) in tissue culture 5 days after co-culturing using a custom designed multielectrode array with 18 recording sites spaced 500 mm apart. (B) Recordings were performed from 10 electrodes; each recording site was numbered sequentially as channel 1–10. (C) The electrical activation of the patch shows consistent beat-to-beat activation, as shown in 7-second interval displaying the peak transverse conduction voltage for each individual channel. The amplitude is shown (D) with all channels superimposed in a beat-to-beat sequence and (E) during a single activation. The amplitude was recorded as (D) 0.03 to 0.42 and (E) -0.13 to -0.75 mV.

Hemodynamics and Echocardiography

At 3 weeks after implantation, the NCM-3DFC increased (*p* o 0.05) EF from 31% ± 2% to 39% ± 1% (Fig. 32), cardiac index from 0.46 ± 0.05 to 0.61 ± 0.06 ml/(g min), dP/dt(+) from 4,651 ± 250.4 to 5,806.2 ± 192.1 mm Hg/ sec, dP/dt(–) from 2,852.9 ± 147.7 to 3,516.9 ± 229.5 mm Hg/sec, and peak developed pressure (PDP) from 112.2 ± 7.6 to 146.4 ± 5.4 mm Hg (Table 6), while decreasing (*p* < 0.05) LV end diastolic pressure from 24 ± 2 to 15 ± 3 mm Hg and Tau from 24.9

± 1.2 to 20.9 ± 1.1 msec (Table 6). At 18 weeks post-implantation, the NCM-3DFC improved LV function by increasing ($p < 0.05$) EF from 21.8% ± 2.8% to 33.6% ± 4.1% (Fig. 32), MAP from 84.3 ± 1.7 to 101 ± 2.9 mm Hg, dP/dt(+) from 4047.7 ± 216.6 to 4713.0 ± 118.4 mm Hg/sec, dP/dt(–) from 2,172.3 ± 130.2 to 2,915.3 ± 218.6 mm Hg/sec, and PDP from 98.3 ± 9 to 137.3 ± 5 mm Hg (Table 4). Importantly, the rats maintained normal sinus rhythm throughout the entire study, and the echocardiography revealed the previously infarcted area contracted in sync with the rest of the heart, with no arrhythmias and no evidence of dyssynchrony.

Tissue Histopathology

As shown in Figure 33, implantation of the NCM-3DFC is well tolerated, and within 3 weeks of implantation, the synthetic Vicryl components have degraded and are not visible. As shown by echocardiography and hemodynamic values, implantation of the NCM-3DFC results in improvements of cardiac function. This may be partly due to the effective integration of the transplanted myocytes, or alternatively, enhanced survival/migration/function of endogenous myocardium under the implant. In either case, an increased presence of myocytes in or around the infarcted area was observed (Fig. 33).

Discussion

The present report demonstrates NCMs can be seeded and co-cultured onto the 3DFC, resulting in cardiac patches that in vitro contract spontaneously in a rhythmic, synchronous manner in culture and are cable of being electrically paced when subject to electrical field stimulation. We confirmed the existence of functional gap junctions by cell-to-cell diffusion of permeant dye across the patch (Fig. 30B) and were further validated by transient gap junction inhibition with

halothane,(Ek Vitorin, He 2000, Turner 1994) effectively blocking dye passage (Fig. 30C). Furthermore, electrical mapping of the NCM-3DFC with a multielectrode array system demonstrated consistent beat-to- beat electrical activation and cellular coupling (Fig. 31). Quantitative evaluation of cellular composition showed no loss of cells during tissue culture between 2 and 8 days. These findings support the 3DFC as a suitable construct to support cardiomyocytes and permit structural organization of the seeded cardiomyocytes in a manner allowing electromechanical synchrony and thus the potential to track in sinus rhythm in vivo after implantation.

When implanted into rats with CHF and EFs below 35%, the NCM-3DFC improved ($p < 0.05$) LV function 3 weeks after implantation by increasing EF, cardiac index, dP/dt(+), dP/dt(–), and PDP, while lowering EDP and LV relaxation (Table 6). In addition, long-term improvements were also observed 18 weeks after implantation by increasing EF, MAP, dP/dt(+), dP/dt(–), and PDP (Table 4 & Fig. 32). Implantations of the NCM-3DFC occurred 18 hours after culture to permit cardiomyocyte adhesion onto the 3DFC yet before the onset of spontaneous contractions and subsequent cellular organization, potentially allowing the underlying native myocardium to dictate organization in vivo. This may have contributed to the observation that all rats that received the NCM-3DFC maintained sinus rhythm with no observed arrhythmias. Echocardiographic data showed no LV dyssynchrony, supporting the observation that the patch does not alter local LV electrical- mechanical function (Fig. 33). Furthermore, these findings demonstrate sustained functional improvements, not only over the short-term but long-term.

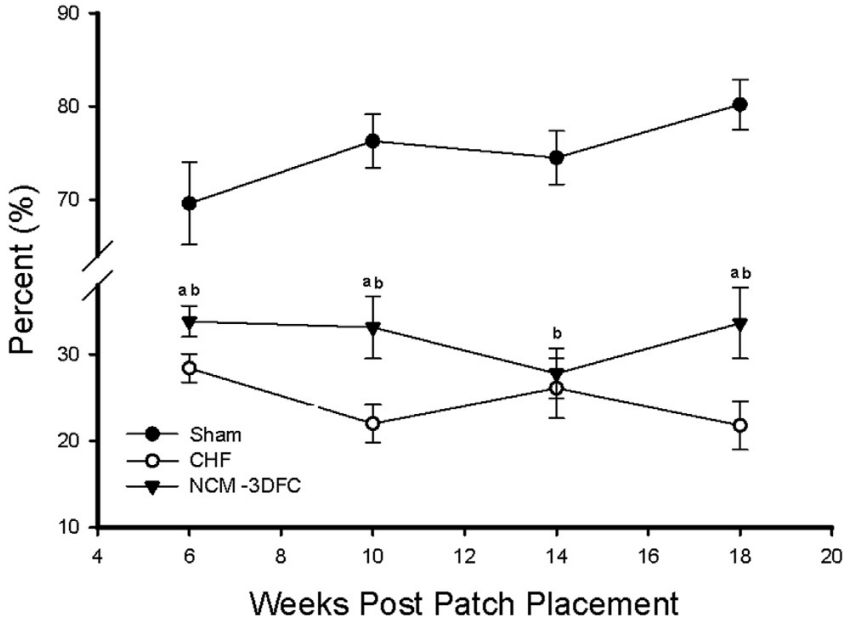

Figure 32: Echocardiography evaluation of EF in rats with CHF at 6, 10, 14, and 18 weeks after patch implantation. Implantation of the neonatal cardiomyocyte (NCM) 3-dimensional fibroblast construct (3DFC) improves EF at 6 (p = 0.037), 10 (p = 0.015), and 18 (p = 0.046) weeks compared with CHF. Data are mean + standard error; a (as reported above) and b (p = 0.001 for all groups) denote statistical significance of CHF vs NCM+3DFC and sham vs CHF respectively. Sham, n = 8 for all groups; CHF, n = 20 at 6 weeks, n = 7 at 10 weeks, n = 6 at 14 weeks, n = 5 at 18 weeks; and NCM-3DFC, n =26 at 6 weeks, n = 10 at 10 weeks, n = 9 at 14 weeks, n =5 at 18 weeks.

Table 6: Three-week endpoint hemodynamics for rats treated with NCM-3DFC

	MAP	SYS	EDP	CI	dP/dt (+)	dP/dt (-)	Tau	PDP
	mmHg	*mmHg*	*mmHg*	*(ml/(minXg))*	*mmHg/s*	*mmHg/s*	*ms*	*mmHg*
Sham	129+4	128+4	5+1	0.52+0.04	7146+285	6368+468	15+1	171+5
CHF	103+4β	124+5	27+2β	0.45+0.05β	4651+250β	2853+148β	25+1β	112+8β
NCM+3DFC	100+5	126+4	15+3α	0.61+0.06α	5806+192α	3517+230α	21+1α	146+5α

Table 6: Hemodynamic values three weeks after NCM-3DFC implantation in rats with CHF. Data are mean ± SE. α, p<0.05 CHF vs. NCM+3DFC and β, p<0.05 Sham vs. CHF. Implantation of the NCM-3DFC improved (p<0.05) EDP, CI, dP/dt, Tau and PDP as compared to untreated CHF rats. Sham, N = 7-20; CHF, N = 6-12; NCM-3DFC, N = 7-13. MAP, mean arterial pressure; SYS, systolic pressure; EDP, end diastolic pressure; CI, cardiac index; PDP, peak developed pressure; CHF, chronic heart failure; NCM+3DFC, neonatal cardiomyocyte 3 dimensional fibroblast construct.

Table 7: Eighteen week hemodynamics for rats treated with NCM-3DFC.

	MAP	SYS	EDP	CI	dP/dt (+)	dP/dt (-)	Tau	PDP
	mmHg	*mmHg*	*mmHg*	*(ml/(minXg))*	*mmHg/s*	*mmHg/s*	*ms*	*mmHg*
Sham	119±2	119±2	8±1	0.35±0.03	7355±400	6103±287	16±1	178±6
CHF	84±2β	105±7β	28±3β	0.32±0.03	4048±217β	2172±130β	29±1β	98±9β
NCM+3DFC	101±3α	111±6	17±7	0.33±0.06	4713±118α	2915±219α	25±2	137±5α

Table 7: Hemodynamic values 18 weeks after NCM-3DFC implantation in rats with CHF. Data are mean ± SE. α, $p<0.05$ CHF vs. NCM+3DFC and β, $p<0.05$ Sham vs. CHF. Implantation of the NCM-3DFC improved ($p<0.05$) MAP, dP/dt, and PDP as compared to untreated CHF rats. Sham, N= 8; CHF, N=3-6, NCM+3DFC, N=2-3. MAP, mean arterial pressure; SYS, systolic pressure; EDP, end diastolic pressure; CI, cardiac index; PDP, peak developed pressure; CHF, chronic heart failure; NCM+3DFC, neonatal cardiomyocyte 3 dimensional fibroblast construct.

Although the mechanism of action in cell-based therapies have not been fully elucidated, it should be postulated that many contributory roles are at play that may include transplanted cell survival and paracrine-mediated effects that result in the observed reported functional benefits. Histologic evaluation at 3 and 18 weeks after implantations showed an increase in viable myocardium underneath the patch (Fig. 33). This population of cells may be in part from the transplanted NCMs, endogenous cardiomyocyte migration, or enhancement of the native viable myocardium. Our previous work has shown that once implanted, the dermal fibroblasts embedded in the 3DFC secrete angiogenic cytokines, establishing microvascular support and increased blood flow (Lancaster 2010). The angiogenic cytokines may be supplementing and facilitating the survival of the transplanted cardiomyocytes.

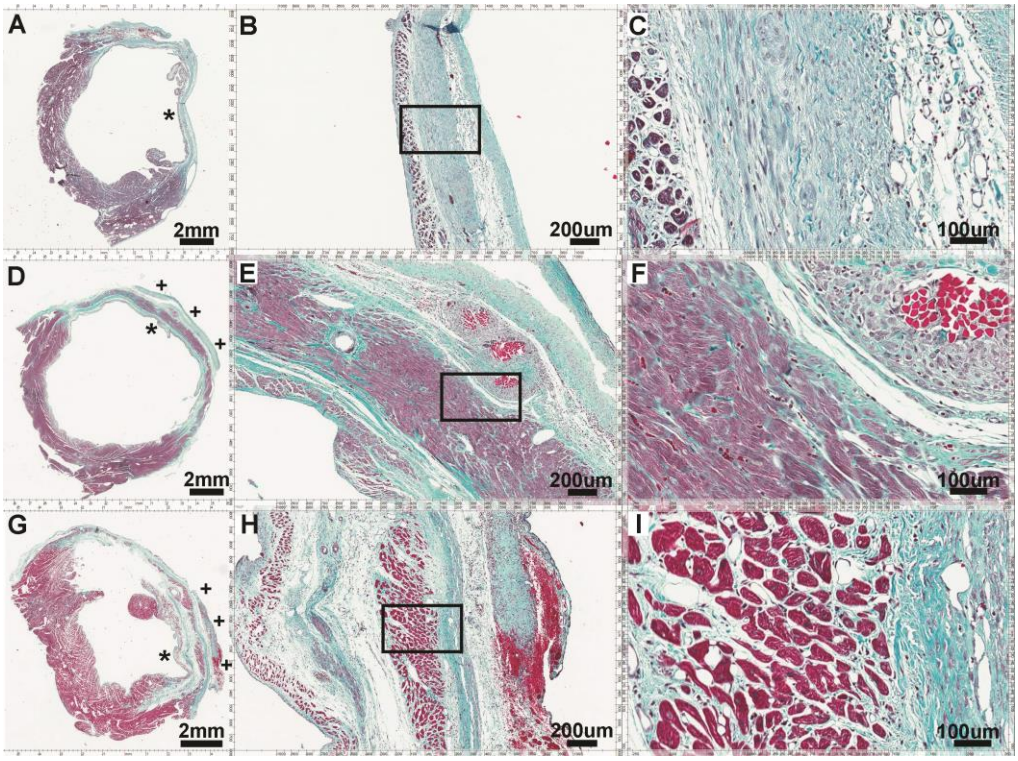

Figure 33: Trichrome-stained left ventricular cross sections of (A–C) 6-week CHF control receiving an infarct but no treatment, (D–F) CHF þ neonatal cardiomyocyte (NCM)–3-dimensional fibroblast construct (3DFC) 6 weeks after coronary artery ligation (3 weeks after implant), and (G–I) CHF þ NCM-3DFC 21 weeks after coronary artery ligation (18 weeks after implant). Hearts were excised, and right ventricles were removed and cut in 5-mm transverse sections along the midpoint of the ventricle. Healthy myocardium is represented as red-purple, collagen/scar as blue, and red blood cells as small red dots. The * (A, D, and G) and box insets (B, E, H) represent area of corresponding higher magnification. The þ in panel D and G highlights the location of the NCM-3DFC implant. Implantation of a cardiomyocyte patch results in increased LV wall thickness (D, E, G, H vs A and B) and preservation and/or generation of myocardium (D–F and G–I). The synthetic Vicryl (Ethicon, Somerville, NJ) components of the patch are degradable and not detectable after 3 weeks in vivo. (E and F) Remnants of the suture used for implantation of the NCM-3DFC can be seen as the bright red clusters.

These findings are exciting and support further evaluation of tissue-engineered scaffolds for therapeutic use to treat CHF, but limitations remain that must be overcome. Additional studies will have to be done developing a patch with a clinically relevant cell type. These cells need to be isolated with ease and in robust enough numbers to permit constructing patches. In addition, the concept of allogeneic vs autologous approaches needs to be addressed.

Induced Pluripotent Stem Cell Derived Cardiomyocyte Tissue Engineered Patch Improves Systolic Function, Diastolic Function, and Electro-mechanical Coupling in Rats with Heart Failure

Introduction

Chronic heart failure is the leading cause of morbidity and mortality worldwide with over 600,000 new cases annually in the United States alone (Heidenreich 2005). The incidence and prevalence of CHF is growing, placing an ever-growing need for development of new treatments. Current CHF therapeutic paradigms rely heavily on drug/device management with the goal to prolong life, prevent further cardiac functional deterioration and to improve quality of life. Only with late stage CHF are mechanical assist devices and heart transplantation considered; both are limited by cost, surgical burden and the latter by donor supply (less than 2,500 heart transplants are performed in the US annually) (US Department of Health and Human Services 2014). Simply put, there is a need for the development of novel therapeutics to treat early stage CHF patients with an emphasis on restoring cardiac function potentially through regenerative approaches.

Regenerative medicine has the potential to alter the current paradigm by restoring long-term cardiac function while also improving the quality and length of life in patients with CHF. Of specific interest are stem cells, and to date, a number of cells have already undergone clinical testing (Fisher 2015). While most of these clinical studies have shown to be safe and well tolerated by patients, there has been limited efficacy that can be improved upon. This lack of success may be due in part because the injected cells do not survive transplantation or persist long enough to generate a functional benefit, which may be due to: 1) lack of matrix/structural support, 2) limited nutrient/blood supply and/or 3) loss of cells because of wash out through injection sites (Dow 2005, Muller-Ehmsen 2002). As a result, there is a growing emphasis on cell-based TE therapeutics for CHF, as TE approaches have the potential to provide the requisite structural and vascular precursors to enhance cell survival, integration, in addition to paracrine mechanisms to improve functional outcomes (Leor 2005, Thai 2009, Lancaster 2010, Lancaster 2014).

We have developed a TE cardiac patch comprised of a bioabsorbable polyglactin 910 knitted mesh embedded with human neonatal fibroblasts, and co-cultured with hiPSC-CMs (Fig. 34). The fibroblasts secrete angiogenic growth factors that increase microvascular formation and myocardial blood flow in the infarcted heart (Kellar 2001, Kellar 2005, Fitzpatrick 2010, Thai 2009, Lancaster 2010). The bioabsorbable mesh, paired with fibronectin and collagen extracellular matrix deposits from the fibroblasts provides structural support for hiPSC-CM attachment (Lancaster 2014). In addition, the mesh provides a robust and resilient mechanical structure permitting handling and manipulation, as needed during surgical implantation.

It is important to emphasize that to-date therapeutic approaches to treat systolic dysfunction have been extensively studied yet there is a paucity of data on the effective treatment for diastolic dysfunction. Traditionally, cell-based studies use improvement in LV systolic function as the primary endpoint. However, diastolic dysfunction post-myocardial infarction, independent of changes in systolic function, carries a poor prognosis for patients and unfortunately our available armamentarium to treat diastolic dysfunction is very limited (Heidenreich 2013, Bussoni 2013). Therefore, delineating the potential effectiveness of cell-based therapy on improving diastolic dysfunction is important.

In the present study, we expand upon our previous work developing a multi-cell type TE preparation (Thai 2009, Lancaster 2010, Lancaster 2014) by utilizing a clinically relevant hiPSC-CM cell preparation. In a rat model of ischemic CHF we assess functional improvements of this TE hiPSC-CM patch on parameters of both systolic and diastolic function as well as electrical integration in the infarcted heart. These data demonstrate the potential for clinical application of hiPSC-CMs in a TE preparation to treat patients with CHF.

Materials and methods

Induced Pluripotent Stem Cell Derived Cardiomyocytes

We used commercial-grade hiPSC-CMs (iCell cardiomyocytes) from Cellular Dynamics International (CDI), Madison, WI. These hiPSC-CMs possess a stable and expected cardiac gene expression profile over prolonged culture (Babiarz 2012), appropriate protein expression and sub-cellular localization, (Kattman

2011), electrophysiology (Ma 2011), Ca^{2+} handling (Sirenko 2012, Cerignoli 2012), contractility (Puppala 2012), and GPCR biology consistent with human cardiomyocytes (Ivanchenko 2012). Furthermore, iCell Cardiomyocytes respond with the expected pathophysiology to chemical challenge from (but not limited to) ion channel blockade, receptor signaling, intracellular pathways, and global responses such as hypertrophy (Babiarz 2012, Kattman 2011, Ma 2011, Sirenko 2012, Cerignoli 2012, Puppala 2012, Ivanchenko 2012, Zhi 2012, Guo 2011, Guo 2013, Cohen 2011).

hiPSC-CM Patch

The hiPSC-CM patch was constructed using previously described methods and seeded with hiPSC-CMs ranging from $2x10^5$ to $2x10^6$ cells/cm^2 (Lancaster 2014). The hiPSC-CM patches were cultured using medium provided by CDI. All tissue culture was performed at 37°C and 5% CO_2. The hiPSC-CM patches for in-vivo application were cultured and implanted onto the rat heart within 48 hrs of generation. The hiPSC-CM patch was implanted 3 weeks after MI; the chest was re-opened and the hiPSC-CMs patch was implanted by suturing onto the infarcted LV bridging viable-to-viable myocardium, covering scar (Thai 2009, Lancaster 2010, Lancaster 2014).

Field Stimulation

The hiPSC-CM patches for *in-vitro* evaluation were cultured as previously described (9). Field stimulation testing was performed between 2 and 6 days of culture. The hiPSC-CM patches were paced (SD9 Grass Stimulator, Quincy MA) with field stimulation (~2V) placed on opposing sides of the hiPSC-CM patch. Pacing was performed up to 120 beats per minute for 10 seconds in duration.

Myocardial Infarction / Chronic Heart Failure

All animal studies were performed in accordance with and under the institutional guidelines established by the Association for Assessment and Accreditation of Laboratory Animal Care (AAALAC) using adult male Sprague-Dawley rats (Harlan Laboratories). A myocardial infarction was created by the left coronary artery ligation model that is well established in our laboratory (Thai 2009, Lancaster 2010, Lancaster 2014). At 3 weeks after ligation, rats have stable CHF with elevated LV-EDPs, dilated LVs, with ventricular remodeling, decreased LV dP/dt, decreased cardiac output and decreased survival (Thai 2009, Lancaster 2010, Lancaster 2014). At this time rats were assigned a treatment group and studied terminally 6 weeks after ligation Three weeks post infarction, animals with stable CHF have elevated LV-EDPs, dilated LVs, with ventricular remodeling, decreased LV dP/dt, decreased cardiac output and decreased survival (Lancaster 2010, Lancaster 2014).

Echocardiography

Rats were lightly anesthetized with 1-1.5% isoflurane in 100% oxygen gas and positioned supine on a warming pad. Transthoracic echocardiography was performed with a dedicated rodent echocardiography system (Vevo2100 with 13-25MHz linear array transducer) at 3 and 6 weeks post-infarction with views through the parasternal short and long axis as well as two-chamber apical views to evaluate the anterior, lateral, antero-lateral, inferior and posterior walls. Ejection fraction and LV chamber size were obtained from 2D and M-mode measurements of myocardial wall thickness at the midpapillary muscle level in the parasternal short axis view (Dow 2005, Muller-Ehmsen 2002, Leor 2005). Diastolic function was evaluated through assessment of mitral valve inflow

patterns (E and A waves) by pulsed echo-doppler in the parasternal long axis and two-chamber apical views, and Tissue Doppler Imaging for quantification of early and late regional myocardial relaxation (e' and a') at the midpapillary level of the anterior wall on the parasternal short axis view. Measurements were made by a blinded observer over 3 cardiac cycles and the mean value obtained. Rats 3 weeks post MI with an EF of 20-70% were randomly assigned a treatment group of either CHF control (no patch) or CHF hiPSC-CM patch, Sham operated animals were entered as comparison.

Hemodynamic Measurements

Rats were anesthetized with Inactin (Sigma) (100 mg/kg IP injection), placed on a specially equipped operating table with a heating pad, intubated, and placed on a rodent ventilator with a 2F solid state micromanometer tipped catheter (Millar Instruments, Inc. Houston, TX) inserted via the carotid artery, into the ascending aorta and then into the LV. The pressure sensor was equilibrated in 37ºC saline, LV and aortic pressures/heart rate recorded, digitized at a rate of 1000 Hz to calculate LV dP/dt and the time constant (Tau) of LV relaxation (Thai 2009, Lancaster 2010, Lancaster 2014). Hemodynamic data were obtained at the end of study; 6 weeks post MI (3 weeks after hiPSC-CM patch implantation).

Electrophysiology Mapping

Bipolar recordings across the LV epicardium were taken to investigate the possibility of dyssynchronous or aberrant electrical activity due to implantation of the hiPSC-CM patch. Activation mapping during paced rhythm was performed to verify normal tissue response in hiPSC-CM patch treated hearts. Waveforms were collected using a 7F quadrupolar deflectable BioSense Webster catheter through a standard biopotential amplifier (Biopac MCE100C) at 2 kHz sampling

rate and saved to hard drive using MATLAB software (Weigand 2016). Electrograms were collected from 15 locations on the LV over a region approximately 10 mm x 15 mm. The peri-infarct region and septum provided reference points such that the area of interest was consistent and reproducible across rats. Whole heart electrical pacing from healthy tissue near the apex of the LV was performed using a function generator (Agilent 33220A). Hearts were paced at twice diastolic threshold at a cycle length of 180 ms. Specific MATLAB software developed in the laboratory was used to filter and plot waveforms (local representation), and each position was analyzed for activation time to generate the corresponding maps for spatial representation. Activation time was defined by max |dV/dt| relative to pacing stimulus during ventricular pacing and relative to beginning of R wave during sinus rhythm.

Real Time PCR Evaluation of Gene Expression

Following the 6 week end-point hemodynamic studies, hearts were excised and LVs flash frozen in liquid nitrogen for quantitative real-time polymerase chain reaction (qRT-PCR) gene expression of connexin 43 (Cx43), beta myosin heavy chain (βMYH7), angiopoietin-1 (ANG-1), vascular endothelial growth factor (VEGF) and insulin-like growth factor-1 (IGF-1). Tissue samples were homogenized using an Omni THQ rotor-stator homogenizer with hard tissue tips at 19K RPM (Omni International, Kennesaw, GA) in 10 mL of TRIzol reagent (Life Technologies, Grand Island, NY). After homogenization, lysate was immediately utilized for RNA extraction or stored at -80°C for long-term storage. RNA isolation and purification was performed with TRIzol Plus RNA purification kit (Life Technologies). DNA digestion was performed using the RNAse-free DNAse Set, (Qiagen, Valencia, CA). Eluted RNA was assessed for quality control

measures with an Agilent Bioanalyzer (Agilent Technologies, Santa Clara, CA) using the RNA 6000 Nano kits (both Agilent Technologies, Santa Clara, CA). RNA samples with RIN score greater than or equal to 7.0 were considered acceptable for cDNA synthesis. cDNA synthesis was performed with the SuperScript III First-Strand Synthesis System (Life Technologies) as per manufacturer's suggested protocol, including RNAse H digestion after strand synthesis was completed. GAPDH endogenous control Taqman assay (Life Technologies) was used for control assays. Taqman reactions were performed in triplicate using Taqman Fast Advance Master Mix and Taqman probe sets. All qRT-PCR reactions were run on an ABI 7900HT, using the SDS 2.4 software (Life Technologies). For all markers both human and rat specific primers were utilized. Gene expression was reported as standard deviation in the cT measurements of 0.5 or less, and final relative fold changes in gene expression (Pfaffl 2001).

Statistical Analysis

Cardiac construct culture densities were tested between $2x10^5$ to $2x10^6$ cells/cm^2 with hiPSC-CMs. All constructs displayed spontaneous and synchronous contractions after 48hrs in culture. Contractions were initially observed on a cellular level, developing in robustness and across the full thickness of the construct from 48-96hrs. The hiPSC-CMs seeded patches beat spontaneously after 48hrs at 36±5 beats per minute (bpm).

Results

Cardiomyocyte Seeding

Cardiac construct culture densities were tested between 0.6 to 1.2 x 10^6 cells/cm^2 with hiPSC-CMs. All constructs displayed spontaneous and synchronous contractions after 48hrs in culture. Contractions were initially observed on a cellular level, developing in robustness and across the full thickness of the construct from 48-96hrs.

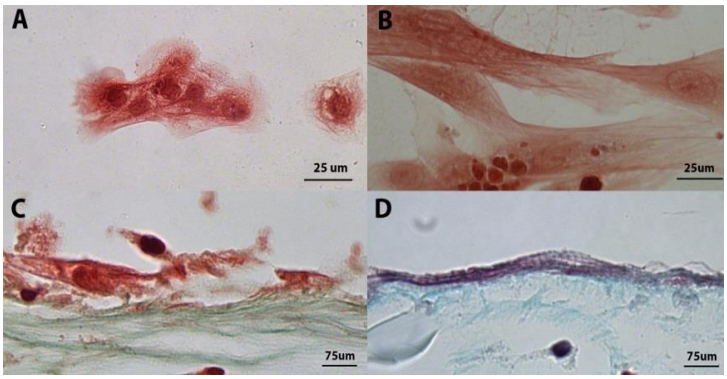

Figure 34: The fibroblast embedded polyglactin mesh provides structural support for hiPSC-CM co-seeding and culture. Trichrome stained hiPSC-CMs at two (A) versus six (B) days in standard tissue culture as compared to two (C) and six (D) days of *in vitro* fibroblast patch culture. At both two and six days in culture, all cells stain positive (red/purple) for muscle. When seeded on the fibroblast embedded polyglactin mesh, the hiPSC-CMs adhere (C) and by six days (D) the hiPSC-CMs have organized and developed into an intact layer and develop striations as compared to standard tissue culture suggesting enhanced myofibril architecture.

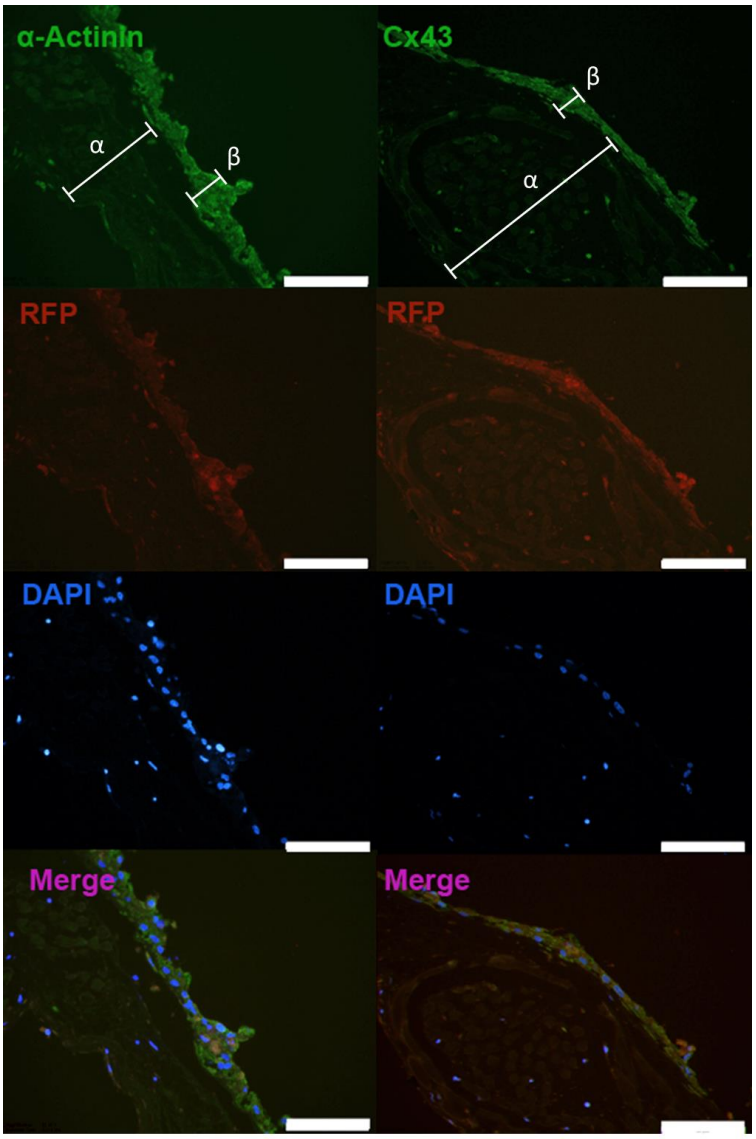

Figure 35: Human iPSC-CM patches demonstrate postive expression of α-actinin and Cx43 at 6 days of *in-vitro* culture. The α-actinin and Cx43 were perfomed on separate hiPSC-CM patches. The biodegradable VICRYL mesh provides suitable pore space for embedded fiobroblasts to attach and establish an extracellular matrix rich of collagen and fibronectin as denoted by bar α. The cardiomyocytes remain localized on the surface of the patch (bar β) as confirmed by positive α-actinin and Cx43 staining intrinsic RFP expression within the mycocytes layer (β). Postive DAPI staining shows distribution of both fibroblasts and cardiomyocytes throughout the thickness of the patches. During implantation the myocyte layer (β) is placed epicardially over the infarcted region.

Field Stimulation

External Field stimulation was applied to hiPSC-CM patches in culture as previously reported at varying time points (2-6 days) in culture (Lancaster 2014). Patches were maintained at 37°C and paced at 10 second intervals at rates up to 120 beats per minute. All patches maintained synchronous contractions and underwent 7±2 second post pacing recovery before contracting at intrinsic, pre-paced rates.

Hemodynamics and Echocardiography

At 3 weeks after patch placement (6 weeks post ligation) CHF rats had significant ($P<0.05$) changes in systolic and diastolic function was defined by increases in LV EDP, and decreases in LV +/-dP/dt, tau, and peak developed pressure compared to Sham rats. In CHF rats the hiPSC-CM patch decreased ($P<0.05$) LV EDP from 22±2 to 12±1 mmHg, Tau from 31±2 to 22±1 MS with no changes in heart rate, LV systolic pressure, +/- LV dP/dt or peak developed pressure (Table 8).

Transthoracic echocardiography documented significant ($P<0.05$) changes in EF, e', E/e' and e'/a' compared to in CHF compared to Sham rats. In CHF rats the hiPSC-CM patch decreased ($P<0.05$) E/e' from 48±5 to 36±3 and increased ($P<0.05$), e'/a' 1.1±0.08 to 1.5±0.08 versus CHF with trending improvements in EF from 44±5 to 50±4% and e' from 20±2 to 24±2 (Table 9). The hemodynamic and echocardiographic data document that the hiPSC-CM patch improves both LV systolic and diastolic function after implantation.

Table 8: Hemodynamics CHF rats treated with patch seeded with hiPSCs

Groups	HR (BPM)	LV sys P (mmHg)	LV EDP (mmHg)	LV(+)dP/dt (mmHg/sec)	LV (-)dP/dt (mmHg/sec)	Tau (ms)	PDP (mmHg)
Sham	306±9*****	139±3	7±1*****	7638±198*****	7344±269*****	18±1*****	195±5*
CHF	278±5†	130±6	22±2†	5829±356†	4095±345†	31±2†	186±6†
hiPSC-CM	290±7	129±3†	12±1*****	6514±302	5271±385†	22±1*****	163±5*****

Table 8: Data are mean ± SE where ***** denotes significance ($p<0.05$) vs CHF, † denotes significance ($p<0.05$) vs Sham. Implantation of the human iPSC-CM patch results in statistical improvements ($p<0.05$) in Sys, EDP, Tau, as compared to CHF and 3DFC only controls. Sham, N=12; CHF, N=8-21, N=20-24 per group. Abbreviations: CHF, chronic heart failure; iPSC-CMs, induced pluripotent stem cell derived cardiomyocytes; Sys BP, systolic pressure; EDP, end diastolic pressure; Tau, time constant of relaxation constant; +LV dP/dt, change in LV pressure over change in time.

Table 9: Echocardiographic parameters in CHF rats treated with patch seeded with hiPSC-CMs

Groups	EF (%)	e' (mm/s)	E/e'	e'/a'
Sham	76±2	28±1	28±1	1.6±0.08
CHF	44±5†	20±2†	48±5†	1.1±0.08†
hiPSC-CM	50±4†	24±2	36±3†*****	1.5±0.08*****

Table 9: Data are mean±SE where ***** denotes significance ($p<0.05$) vs CHF, and † denotes significance ($p<0.05$) vs Sham. Implantation of the hiPS-CM patch results in statistical improvements ($p<0.05$) in E/E' and e'/a' as compared to CHF controls. Sham, N=12; CHF, N=8-21, hiSPC-CM, N=20-24 per group. Abbreviations: CHF, Chronic heart failure; hiPSC-CM, human induced pluripotent stem cell derived cardiomyocytes, EF, ejection fraction; e', early LV relaxation velocity; a', late peak LV velocity; E/e', ratio of early peak flow velocity to early peak LV velocity; e'/a', ratio of early to late peak LV velocities.

Electrophysiologic Mapping

Electrophysiology studies show electro-mechanical coupling between the patch and the native myocardium with synchronous electrical activation throughout the patch verified by 1) comparing bipolar electrograms reflecting local tissue activation over the scarred/patch-treated area with the surface ECG and analogous measurements taken in non-treated LVs 2) increased voltage amplitudes in previously infarcted tissue and, 3) activation mapping showing normal sequential propagation of the electrical excitation wave across the patch (Fig. 36).

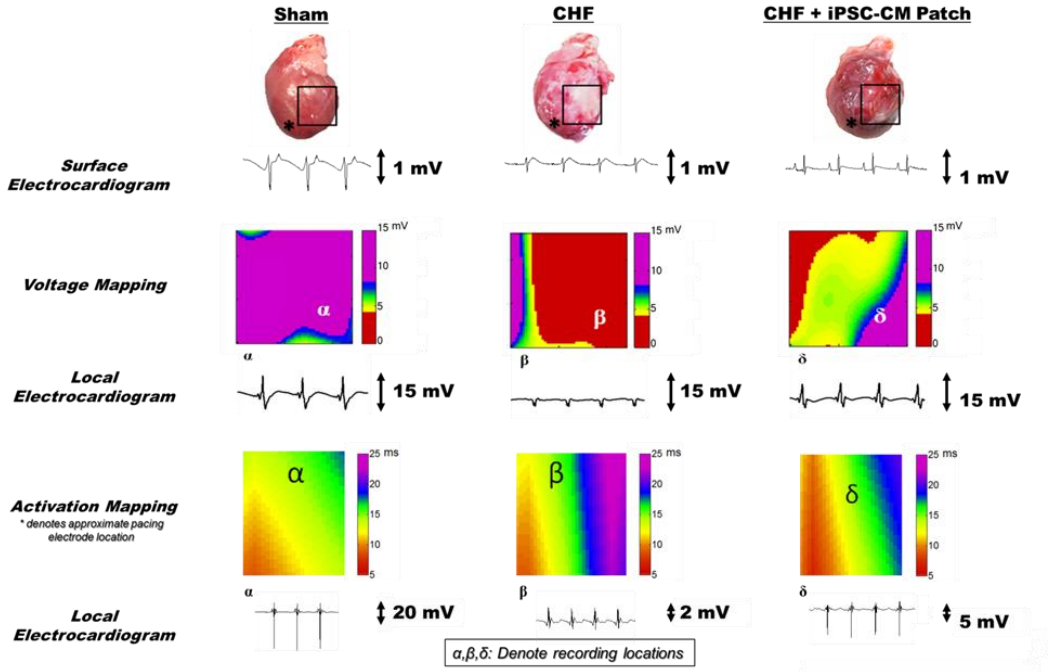

Figure 36: Summary of electrophysiology measurements across experimental groups. Data include a representative surface electrocardiogram (ECG), local ECG, LV voltage map, and LV activation map collected from each group. Normal Sinus Rhythm is depicted for the surface ECG traces, which are plotted with the same scaling, indicated on the right. Local electrogram tracings, in millivolts, are depicted with the corresponding scaling indicated to the right of each tracing. Each mapping has a corresponding local electrogram. The approximate epicardial location of each local electrogram is indicated by a Greek letter on both the voltage and activation maps. A black box indicates the approximate voltage and activation mapped region on each excised representative heart. The asterisk(*) indicates the approximate pacing electrode location on the epicardium for activation mapping only. Voltage magnitudes, in millivolts, and activation times, in milliseconds, are transformed using the colormap on the right of each map and interpolated into a two-dimensional array.

Expression of Cytokines

Rats treated with the hiPSC-CM patch showed significant (P<0.05) fold expression of 3.3 (Cx43), 3.63 (ANG-1), 3.8 (VEGF), 6.4 (βMYH7) and 22.9 (IGF-1) (Table 10). Compared to CHF rats, there was no significant change in relative fold expression with the patch alone in CHF rats as compared with controls (data not shown). The hiPSC-CM patch showed significant increase in relative fold expression of ANG-1 by 2 fold and VEGF expression by 3.6-fold compared to CHF control rats. All PCR analysis was performed in triplicate (technical replicates) and the cDNA was generated from RNA that was pooled from all hearts in that group. We had different Ns for biological replicates: Sham, N=8; CHF, N=3; hiPSC-CM treated CHF, N=17.

Table 10: Relative fold expression of mRNA

Groups	VEGF	ANG-1	Cx43	β-MHC	IGF-1
Sham	1.0±0.2	0.9±0	1.2±0.4	1.8±0.1	8.9±2.7
CHF	0.6±0.2	0.5±0.3	2.0±0.2	1.7±0.4	5.9±0.5
hiPSC-CM	3.8±0.2*****	3.6±0.4*****	3.3±0.4*****	6.4±0.2*****	22.9±0.4*****

Table 10: Data are relative change in fold expression compared to Sham and represent mRNA expression 6 weeks post infarction, 3 weeks post patch implantation. Data are mean±SE where ***** denotes significance (P < 0.001) vs CHF. Abbreviations: CHF, chronic heart failure; #DFC, 3-dimentional fibroblast construct; iPSC, induced pluripotent stem cell.

Left Ventricular Pathology

Six weeks post infarct, the untreated LV displays ventricular remodeling consistent with a large infarct. The Masson's Trichome staining permits denotation between infarcted and un-infarcted myocardium. Consistent with our previous work with rat neonatal cardiomyocytes, treatment with hiPSC-CM patches results in increased anterior wall thickness and what appears to be

increased myocyte density in the previously infarct region as compared to untreated tissue (Fig. 37, Lancaster 2014). In addition, there is no indication of hyper-acute or acute rejection as observed in histological sections.

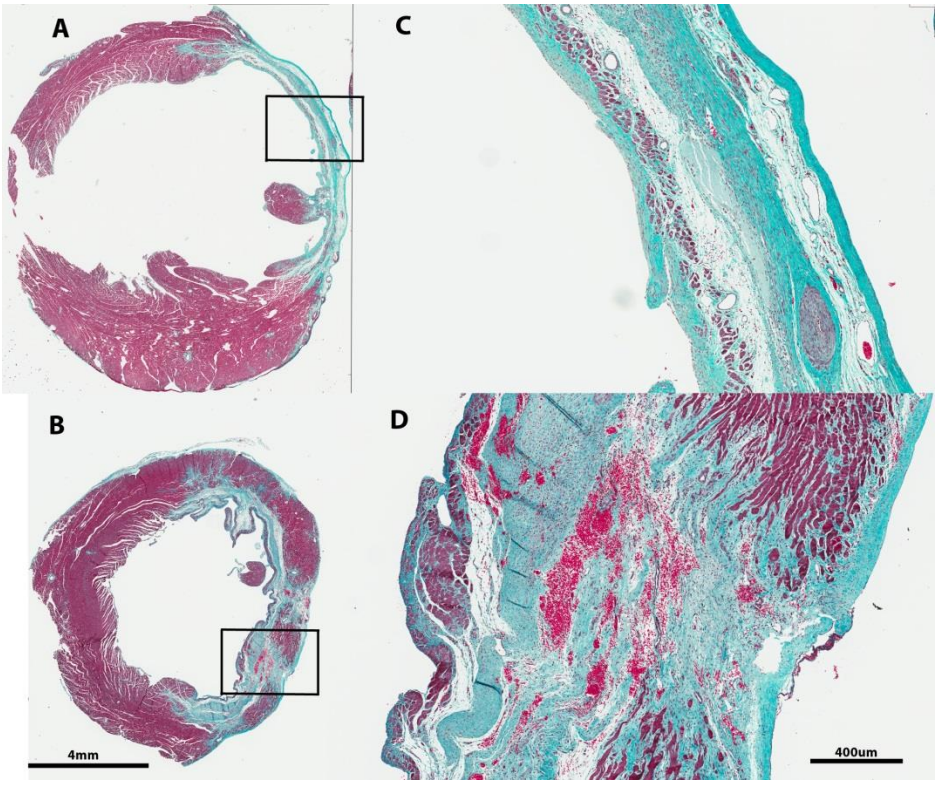

Figure 37: Trichrome-stained left ventricular cross sections (A&B) of 6wk CHF control receiving an infarct but no treatment, (D&E) CHF + human induced pluripotent stem cell derived cardiomyocytes (iPSC-CM) patch 6 weeks after coronary artery ligation (3 weeks after implantation). Hearts were excised, right ventricles removed and cut into 5um transverse sections along the midpoint of the ventricle. Healthy myocardium is represented as red-purple, collagen/scar as blue, and red blood cells as small red dots. Box insets represent area of higher magnification. Implantation of the human iPSC-CM patch results in increased LV wall thickness (D) and preservation and/or generation of myocardium (D).

Discussion

This study outlines the potential of using a multicellular (human neonatal dermal fibroblasts and hiPSC-CMs) TE cardiac patch to treat CHF. This combination of

cells grown into a bioabsorbable polyglactin 910 knitted matrix improves LV function in rats with CHF resulting in a decreased ($P<0.05$) LV EDP (45%), Tau (29%), E/e' (23%) and increased ($P<0.05$), e'/a' (36%) with a trend toward improvements in EF (14%) and e' (20%). Furthermore, rats maintained normal sinus rhythm after patch implantation with synchronized conduction including electro-mechanical coupling between the patch and the native myocardium, restoration of electrical amplitude and activation sequences across the infarcted myocardium and no evidence of arrhythmia induction or dyssynchrony. Furthermore, we saw no evidence of a hyper-acute or acute rejection in the xenograft implants in immunocompetent rats.

To date a handful of TE preparations have been reported in the literature (Kawamura 2012, Kawamura 2013, Guyette 2016, Wassenarr 2016, Costa 2016, Schmuck 2014). While there is much enthusiasm for this emerging filed, clinical applicability may be limited by approaches that are overly fragile making implantation challenging. Utilization of bioabsorbable or other meshes during the engineering process may help overcome limitations associated with fragility. In our patch, the bioabsorbable polygalactin mesh offers a site for fibroblast attachment, proliferation and promotes extracellular matrix deposition providing a favorable milieu for hiPSC-CMs integration and enhanced myofibril architecture (Fig. 34, Herron 2016). In addition, the mesh provides tensile strength and resilience making the hiPSC-CM patch easily handled and implanted. The patch mesh offers structural support for the implanted syncytium of cells to remain in direct contact with the injured tissue before dissolving. This approach can be seen as favorable to direct injection modalities where disperse, isolated and focal

cellular deposits occur which likely experience rapid wash out and loss of cells (Dow 2005, Muller-Ehmsen 2002, Lancaster 2014).

To date, the mechanism(s) of action of cell-based therapy to treat CHF remain unknown. While the initial emphasis of mechanisms focused primarily on exogenous cell retention, recent studies suggest functional benefits may be primarily from growth factor, cytokine, and/or exosomes, which stimulate and promote endogenous regeneration (Herron 2016, Chong 2014, Ong 2015). The specific growth factor/cytokine stimulation pattern however may vary from cell type to cell type and requires additional study. While a number of mechanisms may contribute to the reported functional benefits of the hiPSC-CM patch, we have shown in previous work that the fibroblast patch releases numerous growth factors and cytokines, which elicit a robust endogenous angiogenic response (Lancaster 2010). In the present study we found that the hiPSC-CM patch increased ($P<0.05$) mRNA expression of VEGF, Ang1, Cx43, MYH7 and IGF-1 in the previously infarcted hearts (Table 10). Increased pro-angiogenic cytokines, ANG-1 and VEGF builds on our previous work showing that the human neonatal fibroblasts embedded within the patch secrete angiogenic growth factors responsible for increases in myocardial blood flow in the previously infarcted heart (Thai 2009, Lancaster 2010). Furthermore, increased expression of gap junction proteins (Cx43), which allow for cell-to-cell propagation of intercellular signaling, is consistent with previously reported findings validated through single cell dye injections with rat neonatal cardiomyocyte seeded patches (Lancaster 2014). Increased MYH7 expression suggests thick filament prevalence and contractile protein development *in-vivo* while increased IGF-1 expression levels may help facilitate healing and regeneration of insulted myocardium (Leor 2005,

Troncoso 2014, Torella 2004). Together the increased expression of IGF-1, ANG-1 and VEGF may enhance tissue compliance as seen in improvements in Tau, and increased LV myocyte concentration/density. We hypothesize that the mechanism(s) of action of our hiPSC-CM patch are multifactorial but are due in large part to specific cytokine activation from both the fibroblasts and hiPSC-CMs. The result is: 1) increase myocardial blood flow and 2) support myocyte presence in the previously infarcted region which together result in overall improvement in LV function which occurs with one administration of the hiPSC-CM patch on the infarcted heart. Furthermore, combination cell therapy as with the described hiPSC-CM patch, where multiple cell types are given together, may synergistically improve functional outcomes as opposed to only one cell type given alone (Patel 2016).

Human iPSC-CMs offer great potential opportunity for development of cell-based therapies. These cells can be generated in high quantities at exacting specifications with non-integrating episomal or viral vectors thus void of any exogenous genetic materials and, if need be, from donors with known human leukocyte antigens. While both tumorigenecity and immunogenicity are of concern with hiPSC derived therapies, neither was observed in this study yet warrant additional investigation. Overall safety may rely heavily on the age of the cell donor and purity of the cardiomyocytes generated from iPSCs as teratoma formation may be a result of inadequate purity of the differentiated cell (Okano 2013, Kang 2016).

Clinically, patients with CHF have both LV systolic and diastolic dysfunction and while investigators have made major advances in the treatment of systolic

dysfunction, there is currently no effective treatment for diastolic dysfunction. Our data showing improvements in indices of diastolic dysfunction using echocardiography and invasive solid-state pressure recordings suggest this cell-based therapy with iPSC-CMs may have a role in treating diastolic dysfunction in the presence of ischemia induced CHF. Importantly, if we were to see similar changes in patients, i.e., a lowering of LV EDP and a shortening of Tau, we would expect that patients should feel better with less shortness of breath and improved exercise tolerance.

Feasibility of Cardiomyocyte Patch Implantation in Pre-Clinical Swine Models of Chronic Heart Failure

Introduction

Cell-based therapies have been explored in clinical trials as potential therapies for both acute MI and CHF. While clinical trials for MI and CHF have demonstrated human safety with cell therapies, limited functional improvements have been observed (*Patel 2016*). One hypothesis for these limited outcomes is that the current administration routes which consist primarily of direct myocardial injection or coronary infusion do not provide adequate structural and nutrient support to the administered therapeutic cells (Muller-Ehmsen 2002, Dow 2005).

We have overcome these limitations through the development of a three dimensional bio-engineered tissue (heart patch) comprised of a bioabsorbable mesh, human fibroblasts and human induced pluripotent stem cell derived cardiomyocytes (hiPSC-CMs) (Lancaster 2015). The heart patches beats spontaneously, demonstrates functional gap junctions and is electrically stable with synchronous contractions. Furthermore, it provides hiPSC-CM structural

support and is rapidly vascularized in vivo. Previous studies have demonstrated long-term functional benefits in both systolic and diastolic function when implanted in rat models of CHF with improvements in electrical conductance and voltage amplitudes in the previously infarcted tissue (Lancaster 2015).

These studies were performed to address: 1) the upscale and engineering of clinical sized heart patches, 2) development of large animal implantation methods, and 3) to validate pre-clinical large animal models of CHF. The swine model is the gold standard for large animal preclinical cardiovascular studies because of its similar size and coronary anatomy to the human heart. Yet varying swine breeds and technical methods have been reported for infarct generation and assessing functional outcomes which have required study validation (Dib 2005, Kawamura 2012, McCall 2012, Munz 2011, Schuleri 2008).

Materials and Methods

As part of this feasibility study we examined 3 different swine breeds to define the most suitable for future studies: 1) three domestic farm swine (Steve Thompson, Wilcox, AZ) of 4 mo of age weighting 31.3-40.9 kg, 2) four Male Gottingen mini swine (Sinclair) of 10 mo of age weighing 12.45-17.25 kg, and 3) two Yucatan mini pigs (Sinclair Bio Resources, Auxvasses, MO) of 7.1 mo of age weighing 26.3-27.3 Kg. Swine arrived approximately 20 days before study to undergo functional capacity (FCT) and quality of life (QoL) training and establish baseline values. All farm and Gottingen swine underwent MI, recovered 4wks to develop CHF and then surgically implanted with the cardiac patch and recovered for four additional weeks (Fig. 38). Longitudinal and cross sectional analysis of MRI, hemodynamics, and pressure volume loops were performed.

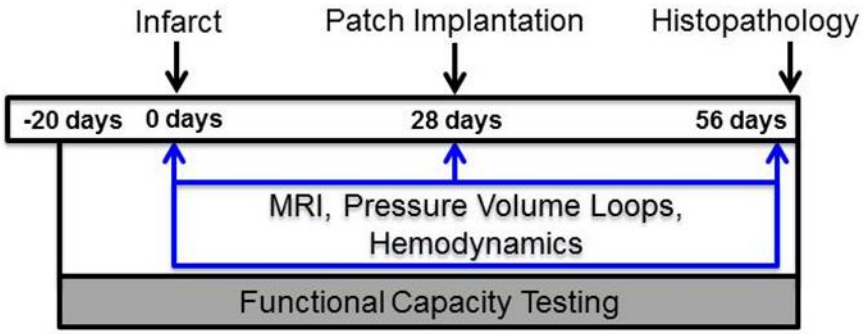

Figure 38. Swine surgical and feasibility study design. Swine undergo functional capacity testing for the entirety of the study. MRI, hemodynamics and pressure volume analysis were performed as shown.

Cardiac Patch Upscale

The hiPSC-CM patch was previously constructed with a diameter of 1.5cm for testing in a rat model of CHF and seeded with hiPSC-CMs ranging from $3x10^5$ to $2.7x10^6$ cells/cm^2 (Lancaster 2014, Lancaster 2015). Using previously described methods, we scaled-up and optimized the culture of the heart patch up to generate 6cm diameter patches (Lancaster 2014, Lancaster 2015). The hiPSC-CM patches were cultured using cell and medium provided by Cellular Dynamics International (CDI). All tissue culture was performed at 37°C and 5% CO_2. The hiPSC-CM patches were cultured and implanted onto the pig heart within 48hrs of cardiomyocyte integration. The hiPSC-CM patch was applied either, 4 weeks after MI (farm pigs and Gottingen swine) or on non-infarcted myocardium (Yucatan). The chest was re-opened and the hiPSC-CMs seeded patch was implanted by suturing onto the infarcted LV bridging viable-to-viable myocardium and covering scar (Lancaster 2010, Lancaster 2014, Lancaster 2015). The hiPSC-CMs possess a stable and expected cardiac gene expression profile over

prolonged culture (Babiarz 2012), appropriate protein expression and sub-cellular localization, (Kattman 2011), electrophysiology (Ma 2011), Ca2+ handling (Sirenko 2012, Cerignoli 2012), contractility (Puppala 2012), and GPCR biology consistent with human cardiomyocytes (Ivanchenko 2012). Furthermore, iCell Cardiomyocytes respond with the expected pathophysiology to chemical challenge from (but not limited to) ion channel blockade, receptor signaling, intracellular pathways, and global responses such as hypertrophy (Babiarz 2012, Kattman 2011, Ma 2011, Sirenko 2012, Cerignoli 2012, Puppala 2012, Ivanchenko 2012, Zhi 2012, Guo 2011, Guo 2013, Cohen 2011).

Cardiac Catheterization and Chronic Myocardial Infarction

Under general anesthesia, an 18g angiographic needle was advanced into the femoral artery, a J-wire advanced and a 5-8f arterial sheath placed. A 6F, JL3.0 or JL3.5 guiding catheter (Medtronic, Inc., Minneapolis, MN) was advanced to the left main ostium. Left coronary angiography was performed to assess coronary anatomy. To occlude the LAD an 3mm X 3.3mm X 23mm VortX Diamond pushable embolization coil (Boston Scientific) was placed at mid or slightly distal to midline of the LAD preserving the first diagonal (Dib 2005). A repeat angiogram was performed 5 minutes post coil deployment to assess occlusion (Fig. 39). If total occlusion was not achieved repeat coil deployment and angiogram were performed. This process was repeated until total occlusion was achieved usually requiring 2-3 coils (Dib 2005). Left ventrciulograms were performed at baseline, 4wks post infarct and 8 weeks post infarct. A 6 F 90CM IMA (Medtronic, Inc., Minneapolis, MN) was advanced over the aortic arch and advanced into the LV. Twelve mls of contrast (Oxilan 300, Guerbet, LLC.

Bloomington, IN.) were hand injected and cinemagraphs captured to assess ventricular geometry and wall motion (Fig. 40).

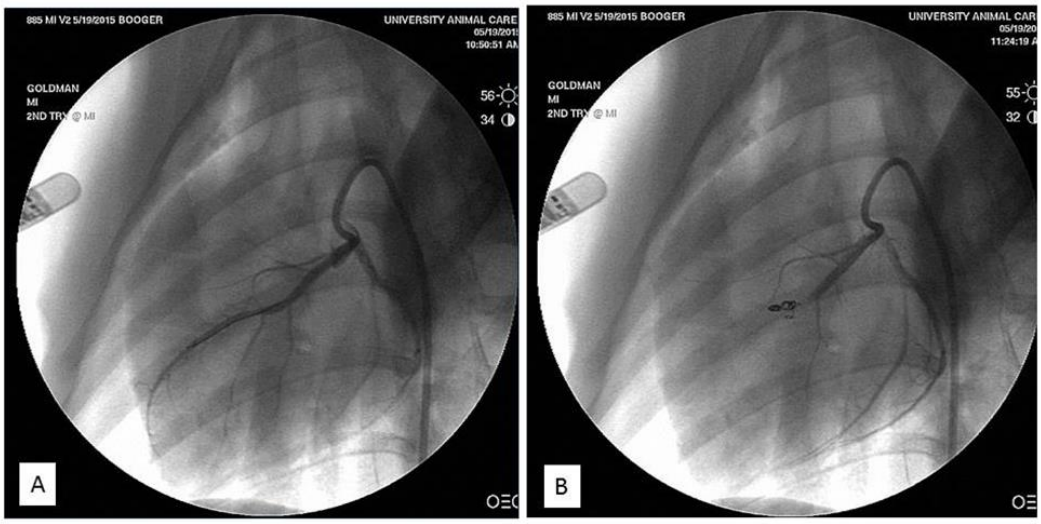

Figure 39. Under fluoroscopic guidance, the left coronary anatomy is visualized by angiography. The LAD and coronary vessel anatomy is assessed prior to coil placement (a), deployment of a 3mm X 3.3mm X 23mm VortX Diamond pushable embolizing coil placed distal of the first diagonal branch of the LAD as denoted by the arrow. After 5 minutes a repeat angiogram is performed to validate total occlusion (b). If occlusion of the vessel is not achieved, the process is repeated and additional coils deployed.

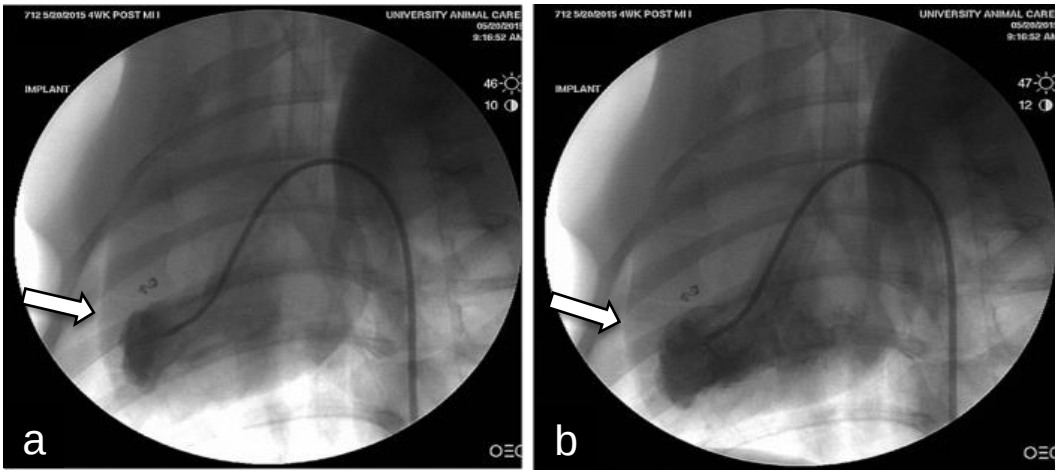

Figure 40. Left ventriculograms performed at baseline, 4wk post MI (pre and post LAD occlusion) and at the terminal point of the study to assess cardiac remodeling and LV function: systole (a) and diastole (b). Akinetic wall motion (indicated by arrows) in systole and diastole after coil deployment suggests successful infarction of the anterior wall. Yellow arrows denote location of the emobolizing coil located mid LAD.

MRI

Swine were sedated with midazolam/telazol/butorphanol/flumazenil (0.2mg/kg, 3.5mg/kg, 0.3mg/kg, 0.01mg/kg) or midazolam/ketamine (0.2mg/kg, 15mg/kg) and anesthetized with 5% Isoflurane and 2-4L oxygen via nose cone. Once anesthetic plane was reached the animal was intubated and isoflurane reduced to a maintenance level. An ear vein IV catheter was placed and IV fluids (Lactated Ringer's or similar) infused at 5-10ml/kg/hr. Respiration rate and pattern, body temperature and mucous membrane conditions were monitored during prep. Heart rate, electrocardiogram, EtCO2, PO2 and blood pressure were monitored throughout the procedure. The cardiac MRI was performed including: Localizer images including a pseudo-short axis stack, EKG-gated 2-, 3-, and 4-chamber steady-state free precession (SSFP) cine images, EKG-gated

cine short-axis stack SSFP sequence, LVOT cine SSFP image, Flow Quantification using phase contrast sequence of: Aortic Root, Mitral Valve, Pulmonary Vein, Short Tau Inversion Recovery (STIR) sequence to access myocardial edema - 2-, 3-, and 4-chamber views, in addition to dynamic perfusion images in 4-chamber and 3 representative short-axis views during Gadolinium-contrast infusion. Gadolinium-based contrast agents (0.1mmol/kg) (Dotarem, gadorate meglumine, Guerbet, LLC., Bloomington, IL. or Multihance, gadobenate dimeglumine, Bracco Diagnostics, Inc., Singen, Germany) was administered and images in 2-, 3-, 4-chamber stacks, and a short-axis stack using a phase-sensitive inversion recovery sequence (PSIR) were acquired.

Surgical Implantation of Cardiac Patch

Median sternotomies were performed on all animals under general anesthesia. Midazolam/telazol/butorphanol/flumazenil (0.2mg/kg, 3.5mg/kg, 0.3mg/kg, 0.01mg/kg) or midazolam/ketamine (0.2mg/kg, 15mg/kg) were administered for sedation, Isoflurane 1%-5% in medical air or oxygen, Propofol 1.5mg/kg IV for anesthesia, Lidocaine 2.0mg/kg; IV Bolus (repeated every 20mins) and Lidocaine 60mcg/kg/min; IV Pump (PRN) as anti-arrhythmics, Leaving the manubrium intact the ribs are retracted to expose the heart. The patch is implanted over the infarct bridging intact and viable myocardium. The patch was placed on the epicardium covering the infarcted region and bridging from viable to viable myocardium (Fig. 41). Two suture methods were tested. In initial trials, the patch was secured by tacking at 3-5 locations with shallow 5-0 or 6-0 prolene sutures. In follow-up studies continuous circumferential and 3-5 internal spot sutures were placed all with 5-0 or 6-0 prolene suture. To preserve MRI imaging integrity, the chest wall was closed using #1 Ethibond Excel at 4 to 5 intercostal

spaces to realign and close the sternum. The muscle and subcutaneous layers were closed with 1-0 to 3-0 absorbable suture and the incision sealed with tissue adhesive. Tegaderm and adhesive bandages were applied and a netted-stocking shirt fitted and affixed with co-ban and Elasticon tape. The shirt and bandage remain in place for up to 1 week.

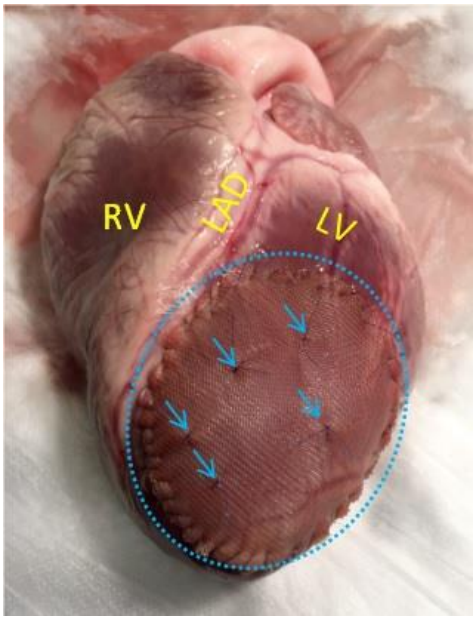

Figure 41: Surgical implant was tested on *ex-vivo* hearts prior to *in-vivo* implantation. The cardiac patch was placed on the epicardial surface of the heart and adhered to the heart using uninterrupted, running circumferential suture placement with three to five spot sutures to secure the cardiac patch.

Functional Capacity and Quality of Life

Functional capacity testing (FCT) and quality of life (QoL) assessments were performed in all swine throughout the duration of the study starting with a two week pre-study training period. During FCT animals were placed on a treadmill and exerted using a modified Bruce Protocol (Fig. 42). In brief the swine were tested over 6 minutes comprised of 30 seconds of 0.5mph, 1 minutes of 90% max exertion (as determined during training period) followed by 4 minutes 30

seconds of 75% of max exertion. Before exertion, a tail cuff monitor was placed for heart rate and sPO_2 evaluation. Baseline values were established before exertion and then every 30 seconds until completion of the 6 min exertion. Heart rate and sPO_2 evaluation was continued post exertion until the animal returned to baseline values. Quality of life assessments were performed daily through two methods: 1) video monitoring over one hour intervals and 2) using FitBark activity monitors (Fitbark Inc. Kansas City, MO) attached to the animal's collar. Animals were housed independently in neighboring pens and access to the room was restricted as to not influence the animal's activity. Animals were assessed for activity (forage and play) and rest (sleeping, laying down, inactivity), total time and percent time was used to quantify QoL during the duration of the study.

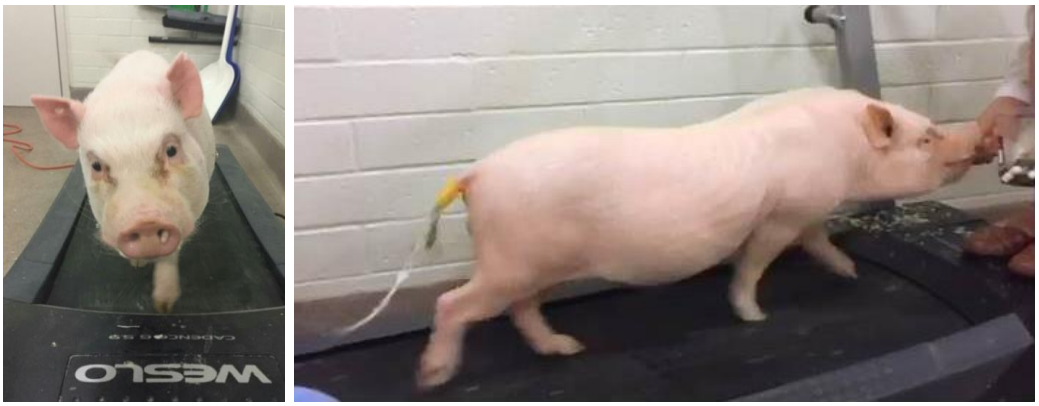

Figure 42: All mini swine were trained to perform treadmill walks to obtain data on functional capacity. Above, a Gottingen mini swine is trained to walk on a treadmill for 2 weeks to obtain functional capacity data. These data provide a surrogate for quality of life outcomes with cardiac patch treatment. A tail cuff monitor is used to assess heart rate and SPO_2 during testing.

Histological Assessments

At the time of necropsy, gross evaluation of the heart was performed after completely removing the pericardium, removing the great vessels 1.0 cm distal from the aortic/pulmonary valves, and rinsing the blood and postmortem clot out

of the atrial and ventricular chambers. The heart was then bisected in the four-chamber long axis dimension for assessment of ventricular geometry including RV and LV internal long-axis chamber lengths from the respective atrioventricular valve to the respective ventricular apex, as well as assessment of infarct size. Following longitudinal assessments, the heart was glued back into its original form before undergoing 1cm serial sectioning in the short axis plane. Short-axis ventricular geometry was then assessed including measurements of ventricular septal wall thickness, measurement of ventricular internal short-axis chamber dimension and evaluation of infarct size.

Multiple transmural sections of the LV, RV and septum were obtained in the area of patch implantation and fixed in 10% formalin. Histological sections (4-5μm) were obtained for standard H&E and Masson's Trichrome to assess tissue; cardiac patch integration, degradation of bio-absorbable materials and infarct. In addition, inflammatory infiltrates were evaluated on H&E sections and specific antibody staining for T-cell and B-cell (CD3, CD20 and CD68) mediated responses.

Results

Chronic MI

In total 6 animals underwent LAD embolization to create a MI. All six animals survived the MI procedures with normal weight and behavior post-MI. Within the Gottingen population, MRI datasets showed the following pre-MI to 4-weeks post-MI values (Fig. 43): the left ventricular (LV) EF decreased from 59 ±4% to 50 ±12% (p=0.182). LV end diastolic volume increased from 34 ±2 mL to 54 ±8 mL (p=0.003). LV end systolic volume increased from 14 ±1 mL to 28 ±9 mL

(p=0.020). Heart mass decreased from 55 ±9 g to 52 ±2 g (p=0.559). Thrombolysis in Myocardial Infarction (TIMI) grade flow was visually determined from LAD angiography at pre and 4-weeks post-MI: TIMI 3.0 ±0.0 decreased to TIMI 1.5 ±0.6

MRI

Magnetic resonance imaging of the heart was successfully completed in all swine at baseline, post MI and at the terminal part of the study. Swine clearly undergo, maladaptive remodeling (increased chamber dimension and thinning of the anterior LV wall) following MI and a decrease in EF (Figure 43 & Table 11). Stainless steel chest closure wires used for securing the sternum following median sternotomy proved problematic with loss of image as can be seen in the 8 week post MI echo below (Fig. 43). As a result, polypropylene closure suture was used, for remaining studies that preserved image acquisition.

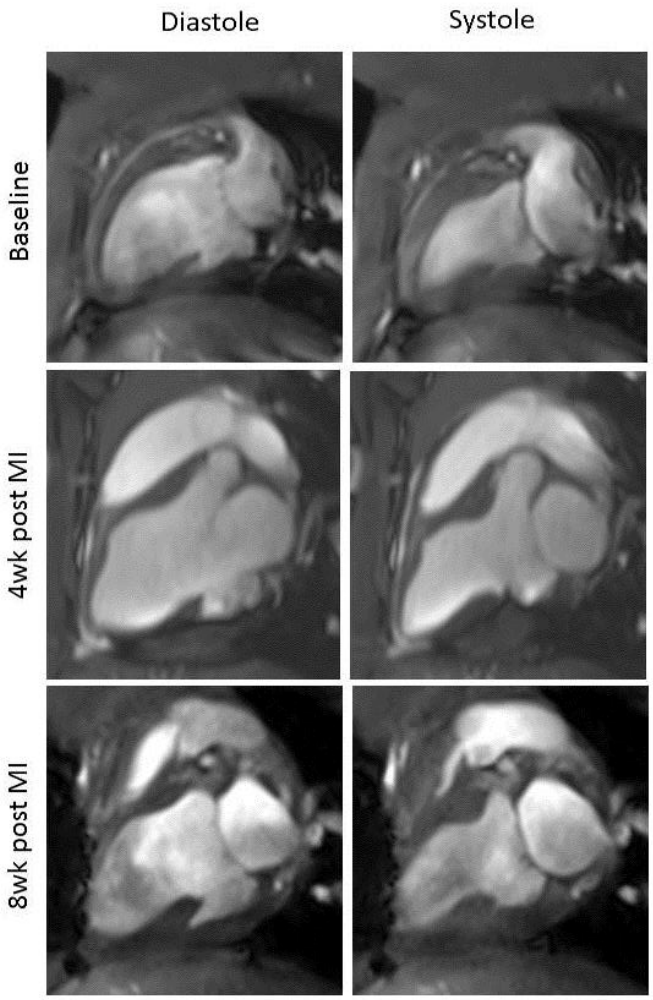

Figure 43: MRI images at baseline, 4 weeks post infarct and 8 weeks post infarct (4 weeks post treatment). The yellow arrows indicate the anterior wall the area of the infarct. An artifact is apparent in the 8 weeks post infarct image at the distal anterior wall and apex due to steel sternal wires used to close the sternum. Due this, later studies used polypropylene suture to prevent MRI artifact.

Table 11. Magnetic Resonance Imaging (MRI) for LV chamber dimensions, cardiac output, LV mass in mini-swine and TIMI flow.

	EDV (ml)	ESV (ml)	EF (%)	Mass Index (g/m2)	TIMI
Baseline	34±2	14±1	59±4	55±9	3.0±0
4wk post MI	54±8	28±9	50±12	52±2	1.5±0.6*

Table 11: Abbreviations: EDV, end diastolic volume; ESV, end systolic volume; SV, stroke volume; EF, ejection fraction; CO, cardiac output; CI, cardiac index; mass index, LV mass indexed to body surface area; TIMI, Thrombolysis in Myocardial Infarction blood flow. Data are mean±SE, N=4), * denotes P<0.05

Cardiac Patch Implantation

After the terminal study, a median sternotomy was performed to assess the integration of the cardiac patch to the heart. While chest adhesions were common in all animals, they could be effectively cleared exposing the heart. The heart patch treated areas were easily identifiable (Fig. 44). While the early spot suture of the cardiac patch proved successful, un-interrupted running circumferential and 3-5 internal spot sutures proved to be a superior implantation method and ultimately did not increase surgical implantation time.

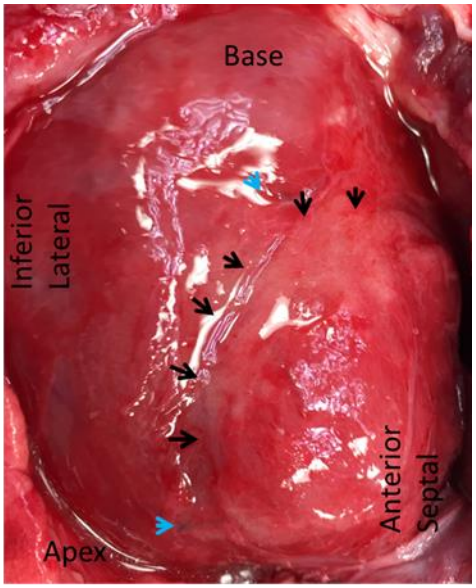

Figure 44: End of study pathology was performed on each animal. Prior to explanting the heart, the heart was assessed in an effort to denote the region treated by cardiac patch. The patch area is outlined on the epicardial surface, as indicated by black arrows. Blue arrows show suture attachments.

Histology

Histological assessments were performed on all a hearts. Infarcts were semi transmural to transmural infarcts were observed with infarct covering the LV, septum and in some occurrences the RV (Fig. 45).

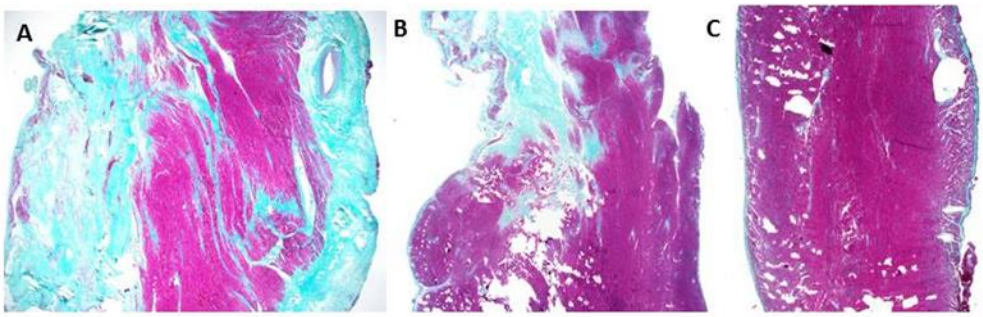

Figure 45: Masson's trichrome stain was performed on all heart sections to assess presence of infarct. Above tissue represents an infarcted un treated control. LV (A), septum (B) and right ventricular (C) samples were obtained for evaluation. Reproducible semi-transmural to transmural infarcts were observed covering the LV and septum and sometimes expanding to the RV.

The area where the cardiac patch was placed could be reliably identified upon gross examination of the heart at the time of necropsy (Fig. 46). Histopathologic examination of sections obtained from the anterior wall of the left and right ventricles and interventricular septum from each animal confirmed the presence of an old, healed transmural myocardial infarct involving the area-at-risk in the distal LAD perfusion territory where the distal LAD had been coil-embolized (Fig. 46A-B). This demonstrated that our desired outcome from LAD obstruction in the model was achieved successfully. Not surprisingly, spotty chronic ischemic changes were also encountered in the myocardium located at the interface between the infarcted zone and the adjacent viable myocardium. In each case, dense epicardial fibrous adhesions (Fig. 46A-B) were accompanied by spotty areas of non-necrotizing granulomatous inflammation, characterized by a dense histiocytic and foreign body-type giant cell response (Fig. 46C-D). Interestingly, these granulomas were invariably associated with and surrounded by dense lymphocytic inflammatory response (Fig. 46 E&F). Granulomas often contained residual fragments of foreign material consistent with degenerating

bioabsorbable mesh (Fig. 46 E&F). Preliminary immunohistochemical studies show that the infiltrate is composed of a mixture of CD20-positive B-cells and CD3-positive T-cells, surrounding a CD68-positive histiocytic foreign body-type granulomatous response to the cardiac patch. This pattern of inflammation is characteristic of host responses to foreign material, directed specifically against the cellular components of cardiac patch, and is not characteristic of an immunologic “rejection-type” response. With the exception of epicardial fibrous adhesions, these histopathologic findings were not observed in animals that did not receive the cardiac patch (Fig. 46).

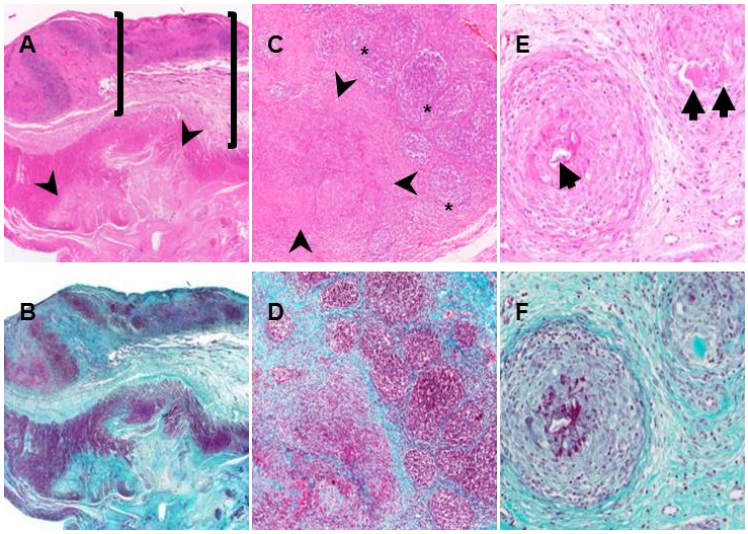

Figure 46: Transmural myocardial infarct involving the area-at-risk (A-B, arrowheads); Evidence of the cardiac patch placement is reliably observed along with dense epicardial fibrous adhesions (A-B, brackets); the fibrous adhesions are accompanied by patchy areas of non-necrotizing granulomatous inflammation, characterized by a dense histiocytic and foreign body-type giant cell response (C-D, arrowheads); the granulomas are associated with and surrounded by a peculiar, dense lymphocytic inflammatory response (C-D, asterisks); Granulomas often contain residual fragments of degenerating bioabsorbable mesh (10E-F, arrows). (A-B, 20x; C-D, 100x; E-F, 400x; A,C,E: hematoxylin & eosin stain; B,D,F: Masson trichrome stain).

Functional Capacity and Quality of Life

Swine were exposed and trained to effectively participate and complete treadmill tests in about 4 weeks. After one week the swine would engage the treadmill walking, within two weeks, maximal exertion levels could be assessed. Average maximum walking rates were assessed at 2.2±0.1mph. Each swine possesses a different level of enthusiasm for treadmill walking which appear to coincide with dominance. The more dominate the animal the more inclined to the subject was to engage the treadmill and easier to train. Lower dominance animals were timid required much more attention and time to be effectively trained for testing.

Early attempts at video monitoring and manually recording the swine proved burdensome and resulted in limited data acquisition of only 1-2 hrs over a 24hr period. Adoption of FitBark resulted in continuous 24hr recordings with fidelity and sensitivity permitting suitable for quantification of QoL assessments over the duration of the study (Fig. 47 & Fig. 48). Non-infarcted swine treated with a cardiac patch showed similar levels of activity pre and post implantation. Pre and post-surgery, swine spent 52% and 54% resting, 43% and 43% playing and 5% and 3 % playing as compared to 66%, 33%, and 1% time respectively in the three days following surgical implantation.

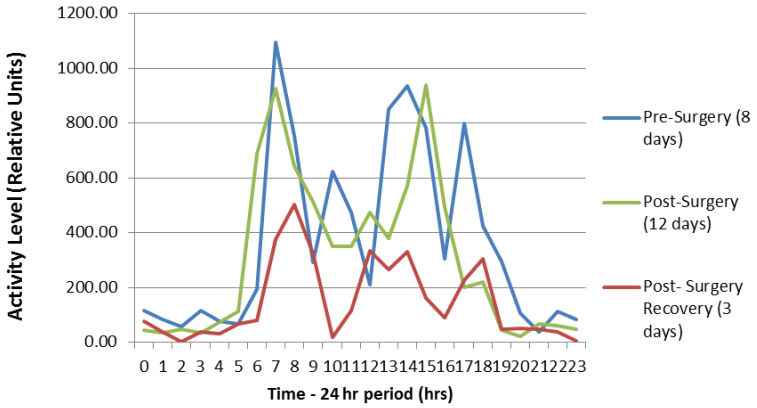

Figure 47: Passive QoL assessment of swine was performed using a FitBark collar mounted activity monitoring device continuously, 24hrs a day, during the course of study. All groups show increased activity during feeding times (~7am and 2pm) and reduced activity during the night 1900hrs to 0500hrs. There is no appreciable difference in swine before surgery and following three days of recovery. Animals immediately after surgery to three days demonstrate reduced activity levels. Data are represented as an average of activities over a 24hr period for 1) eight days pre surgery (blue line), 2) three days following median sternotomy and patch implantation (red line), and 12 days following post-surgery recovery (green line).

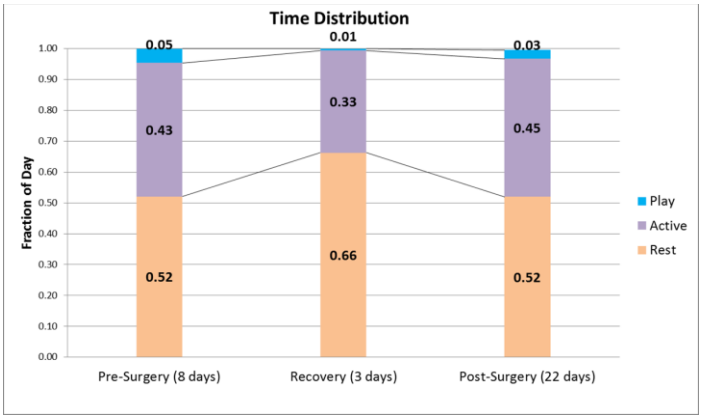

Figure 48: Using FitBark, percent time of activity was performed as part of QoL analysis. Data are represented as an average of activities over a 24hr period for 1) eight days pre surgery, 2) three days following median sternotomy and patch implantation (recovery), and 12 days following post-surgery recovery. Animals showed an 80% reduction in play time, 23% reduction in active time, and 27% increase time at rest. Three days after the recovery period animals returned to normal.

Discussion

Large animal pre-clinical testing is crucial step for determining feasibly and validation for new therapeutics. In this study three varying swine breeds were assessed to find the optimal breed for future large animal efficacy studies. While initial proof of concept work such as cardiac catheterization, MRI, and pressure volume analyses, QoL and FCT was performed in farm pigs they proved not sufficient to advance into more advanced studies; the most notable limitation of farm pigs is increased body size and mass as the animal ages. Upon completion of preliminary proof of concept and validation in the farm swine, Gottingen mini swine were assessed as a potential candidate for future studies. The techniques established with the farm pigs were easily translatable to the Gottingen. While the cost of the Gottingen is significantly more than farm swine, after one year of age they are considered fully grown and thus, if maintained on a strict diet, do not increase in size or mass. Limited availability of 12mo Gottingen and distribution issues with the Gottingen present issues for their use in future studies. As a result, secondary validation studies were repeated in Yucatan mini swine. This was done to validate the techniques learned with the Gottingen and test temperament in the event Gottingen mini swine were not available for future studies. Despite the Yucatan mini swine weighing 10-14kg more than the Gottingen, our observation was that they performed similarly and either breed could be considered for future efficacy or good laboratory practice (GLP) studies.

To advance the cardiac patch towards a human therapeutic, it was important to demonstrate the patch could be successfully upscale from 1.5cm diameter to a clinical sized, 6cm diameter patch. After upscale validation, feasibility of handling

and implantation was performed farm pigs, Gottingen's, and Yucatan. Two cardiothoracic surgeons were recruited to perform the implants. While the cardiac patch could be handled and effectively implanted onto the heart handling characteristics differed between the small and large constructs which was overcome with modifications to culture cardiac patch culture technique, surgeon training and adjusting implantation methods. While initial swine implantation tests adopted from the rodent model using spot sutures was successful, adoption of continuous un-interrupted circumferential and spot sutures was superior resulting improved implanting outcomes. In addition, all implants were performed on the beating heart without issue.

Cardiac catheterization was successfully completed in all animals. While varying catheters were tested for LV, LAD, and circumflex access, in our hands, the 90CM IMA performed the best for access to the LV and as a conduit to advance an impedance catheter. Additionally the JL 3.0/3.5 work well for accessing the LAD. Embolizing coils proved suitable for occluding the LAD and commonly took 2-3 coils to effectively occlude the vessel of interest. Interestingly, at repeat angiograms 4 weeks after occlusion, recanalization with TIMI I flow occurred. Alternatively, ischemia reperfusion using a balloon catheter could be considered for future studies. The potential advantage of using the ischemia reperfusion model is we will know the precise amount of time of the ischemic event before re-perfusion.

Transthoracic echocardiography was initially tested as an imaging modality in the swine and could easily be performed prior to surgical intervention while the animal was under general anesthesia. However due to the swines' anatomical anatomy, good imaging windows were not easily obtained. Cardiac MRI proved a

superior imaging modality in the swine. All swine were effectively imaged as described. The only issues that presented were 1) sternum closure wires used after median sternotomies resulted in artifact limiting the imaging window of the treated area which was corrected with use of #4 polypropylene and 2) the larger farm pigs which developed a larger muscle to fat ratio resulted in reduced imaging resolution. The other advantage of MRI is that we are working with Dr. Ryan Avery in Radiology to obtain MRI studies of diastolic function. The preliminary data show that we can obtain adequate MRI images to evaluate diastolic function. This is important because our data with the hiPSC-CMs seeded patch in CHF rats' shows improvement in diastolic function after patch implantation.

All swine evaluation had good temperaments and with dedication by the technical staff, easily trained to perform FCT as required. Three days were given to all animal after median sternotomies to recover before re-starting FCT testing. All swine tolerated wearing a collar and limited abrasions / chaffing were observed. Of note, all animals were housed in the same room yet in independent pens to limit social issues and disruption of the FitBark activity monitors.

Using histopathological techniques we were able to validate infarct and patch treated areas. In addition, it is important to state that to-date we and other investigators have seen no evidence of an immune response in mice, rats, dogs, or mini swine treated with the two cell types that compose the cardiac patch.

Summary and Conclusion

Summary

It is with great enthusiasm that I share this work. Retrospectively it is interesting to connect the dots of hypotheses between those that were validated and those that were not. Numerous challenges presented during this body of work from conception, through proof of concept studies and into large animal testing. It is my hope that this body of work, at the very least, provides others with information that will assist mankind with the development of TE solutions for CHF.

Conclusion

Develop a multicellular TE cardiac construct providing structural and nutrient support to engrafted cardiomyocytes capable of surgical implantation to effectively treat CHF.

Numerous challenges were overcome to generate the first generation heart patches. Cell seeding was optimized that permitted high efficiency seeding. Although we did not appreciate it at the time, this is highly important when scaling to iPSC derived cells were cost of the materials is so high. In addition, cell density studies were performed which were crucial in understanding the cell loads capable achieving. Furthermore we established cardiomyocyte to fibroblast ratios. These proof of concept studies were completed using rat neonatal cardiomyocytes. While rat neonatal cardiomyocytes were not scalable towards clinical adoption, they did provided a suitable and reliable cell source to perform the initial experiments. Observing contracting heart patches provided great enthusiasm for the research lab, especially when no microscopic

enhancement was required. The laboratory was a busy place in those early studies as enthusiasm spread. Furthermore, we were able to demonstrate the heart patches responded to external electrical stimulus which suggested to us that the patches would take ques from the native heart. Great attention and conversation was had over the potential to develop arrhythmias upon implant onto the heart.

Test feasibility, efficacy and mechanisms of action of a TE cardiac construct in a rat model of CHF

Once heart patch cultures were optimized for cell dose and culture conditions and could be effectively re-produced, feasibility studies were started to assess the therapeutic potential. Early debates were had about when after generation should the heart patches be implanted as there was some concern over arrhythmia formation. Cultures established with limited cellular contraction initially but increased over time. The hypothesis was that early implant may help direct these developing cells to adopt the contractile rates and ques from the native heart. This hypothesis was based on the finding that the heart patches could be electrically paced. As such, implants were conducted soon after incorporation of the neonatal cardiomyocytes but at a time to permit effective integration. While numerous functional studies had been performed in the lab to test varying compounds as therapeutics for CHF, none of them generated the functional recovery observed with the heart patch. In addition, it is important to note that long term functional benefits were observed. This was in contrast to comparable studies were cells were injected into the heart generated only short term functional benefits. With the long term functional data, it was suggestive that this

technology could have impact as a therapeutic to treat CHF clinically. Discussions on clinically relevant cell population candidates and performing large animal feasibility studies developed. Fortunately, during this study we were awarded a grant from Cellular Dynamic International which provided access to iPSC derived cardiomyocytes. Cultures were re-optimized with the hiPSC-CMs and secondary functional studies were performed. While long-term functional were not completed, we did observe comparable functional recovers to the neonatal cardiomyocytes short term.

The previous concerns about arrhythmias were unfounded with both the neonatal cardiomyocytes and the hiPSC-CMs. No increased mortality or adverse events were observed yet warrant additional study. Also of interest was under histological assessment it did not appear that a rejection mediated immune response was generated against the implants whether allogenic or xenograft in nature. While the current literature suggests that immune responses will be eminent and require immunosuppression, no laboratory has truly studied the immune response generated to iPSC-CM therapy in the heart. This is a short coming for the field as these data would help provide clarity on developing the ideal treatment strategy. In addition, it is important to comment that the mechanism of action of these studies remains unclear. Most likely multiple mechanisms are taking place simultaneously. Future studies will look at cellular persistence and growth factor and paracrine mediated signaling.

Confirm a large animal swine model of chronic heart failure for feasibility testing of a TE cardiac construct as a necessary prerequisite to initiating a clinical trial

As early studies demonstrated functional recovery in rats with CHF attention was given to proceed into large animal studies. In general large animal studies are expensive and time consuming yet valuable from a technology development standpoint. Protocols for infarction, pressure volume loop analysis, MRI, echocardiography and hemodynamics were developed. Furthermore, quantifiable methods to evaluate functional capacity and quality of life were developed. Upscaling the heart patches was successfully achieved using established techniques, seeding densities and cell ratios. Minimally invasive robotic surgeries were tested initially after we demonstrated they could be effectively performed in human cadaver studies however the anatomical nature of the swine made then not feasible in our initial studies. Of note this may have been due in part to the advanced age of the robotic system that was available. Long term robotic approaches would be ideal from a patient perspective and warrant future examination but are not necessary at this time. The greatest challenges came from educating the surgeon on how to handle the heart patch and how to effectively implant it on the heart. It was found that handling characteristics between the rat sized and swine size patches manifest and made challenging of the large patches more challenging. Secondary to handling, securing the heart patch to the heart required attention. Circumferential continuous suture was found to be idea and could be easily performed on the beating heart implanted through a median sternotomy. Functional and quality of life studies were developed as these may be valuable indicators of positive

outcomes that would be favorably viewed by the FDA during IND review. While time consuming, treadmill walking was achieved and methods of assessing functional capacity have been developed when large powered efficacy studies are performed. Quality of life assessments were easily performed through the adoption of FitBark collar monitors. While these are intended for dogs to grade between active, play and rest they performed well on the swine denoting enough specificity to pick up on subtitles such as estrous. Additional immune response analysis suggests that the patch does not generate a rejection mediated response. Future studies are planned to evaluate this finding.

References

Aavula BR, Ali MA, Bednarczyk D, Wright SH, Mash EA. Synthesis and fluorescence of n,n,n-trimethyl-2-[methyl(7-nitrobenzo[c][1,2,5]oxadiazol-4-yl)amino]ethanaminium iodide, a ph-insensitive reporter of organic cation transport. *Synthetic Communications*. 2006;36:701-705.

Abdel-Latif A, Bolli R, Tleyjeh IM, Montori VM, Perin EC, Hornung CA, Zuba-Surma EK, Al-Mallah M, Dawn B. Adult bone marrow–derived cells for cardiac repair a systematic review and meta-analysis. *Archives of Internal Medicine.* 2007;167:989-997.

Achilli TM, J. Meyer, and J. R. Morgan. Advances in the formation, use and understanding of multi-cellular spheroids. *Opinion on Biological Therapy*. 2012;12(10):1347–1360.

Assmus B, Honold J, Schachinger V, Britten MB, Fischer-Rasaokat U, Lehmann R, Teupe C, PistoriusK, Martin H, Abolmaali ND, Tonn T, Dimmeler S, Zeiher A. Transcoronary transplantation of progenitor cells after myocardial infarction. *New England Journal of Medicine*. 2006;355:1222–1232.

Balsam LB, Wagers AJ, Christensen JL, Kofidis T, Weissman IL, Robbins RC. Haematopoietic stem cells adopt mature haematopoietic fates in ischaemic myocardium. *Nature*. 2004;428:668–673.

Babiarz JE, Ravon M, Sridhar S, Ravindran P, Swanson B, Bitter H, Weiser T, Chiao E, Certa U, Kolaja KL. Determination of the human cardiomyocyte mRNA and miRNA differentiation network by fine-scale profiling. *Stem Cells Development*. 2012;21:1956-1965.

Bearzi C, Rota M, Hosoda T, Tillmanns J, Nascimbene A, De Angelis A, Yasuzawa-Amano S, Trofimova I, Siggins RW, LeCapitaine N, Cascapera S , Beltrami AP, D'Alessandro DA, Zias E, Quaini F, Urbanek K, Michler RE, Bolli R, Kajstura J, Leri A, Anversa P. Human cardiac stem cells. *Proceedings of the National Academy of Sciences of the Unites States of America.* 2007;104(35):14068-14073.

Beltrami AP, Barlucchi L, Torella D, Baker M, Limana F, Chimenti S, et al. Adult cardiac stem cells are multipotent and support myocardial regeneration. *Cell*. 2003;114(6):763–776.

Bergmann O, Bhardwaj RD, Bernard S, Zdunek S, Barnabé-Heider F, Walsh S, Zupicich J, Alkass K, Buchholz BA, Druid H, Jovinge S, Frisén J. Evidence for cardiomyocyte renewal in humans. *Science*. 2009;324(5923):98-102.

Berlo JH, Kanisicak O, Maillet M, Vagnozzi RJ, Karch J, Lin SC, Middleton RC, Marbán E, Molkentin JD. c-kit+ cells minimally contribute cardiomyocytes to the heart. *Nature*. 2014;509(7500):337-341.

Bodo ES, Michael B, Tobias Z, Thomas B, Christina S, Christine A, Rüdiger VS, Gesine K, Peter W, Hans-Wilhelm M, Matthias K. Regeneration of human infarcted heart muscle by intracoronary autologous bone marrow cell transplantation in chronic coronary artery disease: The IACT study. *Journal of American College of Cardiology*. 2005;46:1651–1658.

Bussoni MF, Guirado GN, Roscani MG, Polegato BF, Matsubara LS, Bazan SG, Matsubara BB. Diastolic function is associated with quality of life and exercise capacity in stable heart failure patients with reduced ejection fraction. *Brazilian Journal of Medical Biological Research*. 2013;46(9):803-808.

Doss MX, Koehler CI, Gissel C, Hescheler J, Sachinidis A. Embryonic stem cells: a promising tool for cell replacement therapy. *Journal of Cellular and Molecular Medicine*. 2004;8(4):465–473.

Byrne JA, Pedersen DA, Clepper LL, Nelson M, Sanger WG, Gokhale S, Wolf DP, Mitalipov SM. Producing primate embryonic stem cells by somatic cell nuclear transfer. *Nature*. 2007;450:497–502.

Caberra JA, Cabrera JA, Ziemba EA, Colbert R, Kelly RF, Kuskowski M, Arriaga EA, Sluiter W. Duncker DJ, Ward HB, McFalls EO. Uncoupling protein-2 expression and effects on mitochondrial membrane potential and oxidant stress in heart tissue. *Translational Research.* 2012;159(5):383–390.

Callegar A, Bollini S, Iop L, Chiavegato A, Torregrossa G, Pozzobon M, Gerosa G, De Coppi P, Elvassore N, Sartore S. Neovascularization induced by porous collagen scaffold implanted on intact and cryoinjured rat hearts. *Biomaterials.* 2007;28:5449-5461.

Camelliti P, Borg T, Kohl P. Structural and functional characterization of cardiac fibroblasts. *Cardiovascular Research*. 2005;65:40-51.

Camelliti P, Green C, Kohl P. Structural and functional coupling of cardiac myocytes and fibroblasts. *Advanced Cardiology.* 2006;42:132-49.

Cantz T, Bleidissel M, Stehling M, Schöler HR. In vitro differentiation of reprogrammed murine somatic cells into hepatic precursor cells. *Biological Chemistry*. 2008;389:889–896.

Cellular Dynamics User Manuals 2015.
http://cellulardynamics.com/resources/support/user-documentation

Cerignoli F, Charlot D, Whittaker R, Ingermanson R, Gehalot P, Savchenko A, Gallacher DJ, Towart R, Price JH, McDonough PM, Mercola M. High throughput measurement of Ca2+ dynamics for drug risk assessment in human stem cell-derived cardiomyocytes by kinetic image cytometry. *Journal of Pharmacology and Toxicology Methods*. 2012;66:246-256.

Chachques JC, Traninini J, Lago N, Masoli O, Barisani J, Cortes-Morichetti M, Schussler O, Carpentier. Myocardial assistance by grafting a new bioartificial-upgraded myocardium (MAGNUM Clinical Trial): One year follow-up. *Cell Transplant.* 2007;16:927–934.

Chien KR. Stem cells: Lost in translation. *Nature.* 2004;428:607-608.

Chong JJ, Murry CE. Cardiac regeneration using pluripotent stem cells- progression to large animal models. *Stem Cell Research*. 2014;(3 Pt B):654-65.

Choudhery MS, Badowski M, Muise A, Harris DT. Utility of cryopreserved umbilical cord tissue for regenerative medicine. *Current Stem Cell Research Therapies*. 2013;8(5):370-380.

Cohen JD, Babiarz JE, Abrams RM, Guo L, Kameoka S, Chiao E, Taunton J, Kolaja KL. Use of human stem cell derived cardiomyocytes to examine sunitinib mediated cardiotoxicity and electrophysiological alterations. *Toxicology Applied Pharmacology*. 2011;257:74-83.

Cohen S, Leor J. Rebuilding broken hearts. *Scientific American*. 2004;291:45–51.

Costa KD. Decellularized Scaffold Hydrogel Materials for MI Treatment Could "The Matrix" Really Be the Future? *Journal of American College of Cardiology*. 2016;67(9):1087-1090.

Cowan CA, Atienza J, Melton DA, Eggan K. Nuclear reprogramming of somatic cells after fusion with human embryonic stem cells. *Science*. 2005;309:1369–1373.

Dib N, Dietrich EB, Campbell A, Gahremanpour A, McGarry M, Opie SR. A percutaneous swine model of myocardial infarction. *Journal of Pharmacological and Toxicological Methods*. 2006;53:256-263.

Dvir TA, Kedem E, Ruvinov, Levy O, Freeman I, Landa N, Holbova R, Feinberg MS, Dror S, Etzion Y, Leor J, Cohen S. Prevascularization of cardiac patch on the omentum improves its therapeutic outcome. *Proceedings of the National Academy of Sciences of the Unites States of Americ*a. 2009;106:14990–14995.

Dow J, Simkhovich B, Kedes L, Kloner R. Wash-out of transplanted cells from the heart: a potential new hurdle for cell transplantation therapy. *Cardiovascular Research*. 2005;67(2):301-307.

Ek-Vitorín JF, Burt JM. Quantification of gap junction selectivity. *American Journal of Physiology and Cell Physiology*. 2005;289:C1535-1546.

Feng B, Ng JH, Heng JC, Ng HH. Molecules that promote or enhance reprogramming of somatic cells to induced pluripotent stem cells. *Cell Stem Cell*. 2009;4:301–312.

Fisher SA, Doree C, Mathur A, Martin-Rendon E. Meta-Analysis of Cell Therapy Trials for Patients with Heart Failure - An Update. *Circulation Research*. 2015; 116:1361-1377.

Fitzpatrick JR 3rd, Frederick JR, McCormick RC, Harris DA, Kim AY, Muenzer JR, Gambogi AJ, Liu JP, Paulson EC, Woo YJ. Tissue-engineered pro-angiogenic fibroblast scaffold improves myocardial perfusion and function and limits ventricular remodeling after infarction. *Journal of Thoracic and Cardiovascular Surgery.* 2010;140:667-676.

Frangogiannis NG. The immune system and the remodeling infarcted heart: cell biological insights and therapeutic opportunities. *Journal of Cardiovascular Pharmacology*. 2014;63:185–195.

French AJ, Adams CA, Anderson LS, Kitchen JR, Hughes MR, Wood SH. Development of human cloned blastocysts following somatic cell nuclear transfer (SCNT) with adult fibroblasts. *Stem Cells*. 2008;26:485–483

Fukuda S, Kaga S, Sasaki H, Zhan L, Zhu L, Otani H, Kalfin R, Das DK, Maulik N. Angiogenic signal triggered by ischemic stress induces myocardial repair in rat during chronic infarction. *Journal of Molecular and Cellular Cardiology*. 2004;4:547–559.

Fujimoto KL, Tobita K, Merryman D, Guan J, Momoi N, Stolz DB, Sacks MS, Keller BR, Wagner WR. An elastic, biodegradable cardiac patch induces contractile smooth muscle and improves cardiac remodeling and function in subacute myocardial infarction. *Journal of American College of Cardiology*. 2007;49:2292–2300.

Gaballa MA, Goldman S. Ventricular remodeling in heart failure. *Journal of Cardiac Failure*. 2002;6:S476–485.

Gaballa MA, Raya TE, Goldman S. Large artery remodeling after myocardial infarction. *American Journal of Physiology*. 1995;268:H2092–2103.

Gaballa MA, Sunkomat JN, Thai H, Morkin E, Ewy G, Goldman S. Grafting an acellular 3-dimensional collagen scaffold onto a non-transmural infarcted myocardium induces neo-angiogenesis and reduces cardiac remodeling. *Journal of Heart and Lung Transplantation*. 2006;25(8):946-954.

Gao D, Critser JK. Mechanisms of cryoinjury in living cells. *Institute for Laboratory Animal Research Journal*. 2000;41(4):187–196.

Gattazzo F, Urciuolo A, Bonaldo P. Extracellular matrix: a dynamic microenvironment for stem cell niche. *Biochimica et Biophysica Acta*. 2014;1840(8)2506–2519.

Garber K. RIKEN suspends first clinical trial involving induced pluripotent stem cells. *Nature Biotechnology*. 2015;33:890-891.

Gaudette GR, Cohen IS. Cardiac regeneration material can improve the passive properties of myocardium, but cell therapy must do more. *Circulation.* 2006;114:2575–2577.

Gnecchi M, He H, Liang OD, Melo LG, Morello F, Mu H, Noiseux N, Zhang L, Pratt RE, Ingwall JS, Dzau VJ. Paracrine action accounts for marked protection of ischemic heart by Akt-modified mesenchymal stem cells. *Nature Medicine*. 2005;11(4):367–368.

Goldman S, Raya TE. Rat infarct model of myocardial infarction and heart failure. *Journal of Cardiac Failure*. 1995;1:169–177.

Guo L, Abrams RM, Babiarz JE, Cohen JD, Kameoka S, Sanders MJ, Chiao E, Kolaja KL. Estimating the risk of drug-induced proarrhythmia using human induced pluripotent stem cell-derived cardiomyocytes. *Toxicology Science*. 2011:123(1):281-289.

Guo L, Coyle L, Abrams R, Kemper R, Chiao ET, Kolaja KL. Refining the human iPSC-cardiomyocyte arrhythmic risk (hCAR) assessment model. *Toxicology Science*. 2013;136(2):581-94.

Gunter J, Wolint P, Bopp A, Steiger J, Cambria E, Hoerstrup SP, Emmert MY. Microstissues in cardiovascular medicine: regenerative potential based on a 3D microenvironment. *Stem Cells International*. 2016;201:Article ID 9098523, http://dx.doi.org/10.1155/2016/9098523

Guyette JP, Charest J, Mills RW, Jank B, Moser PT, Gilpin S, Gershlak JR, Okamoto T, Gonzalez G, Milan DJ, Gaudette GR, Ott HC. Bioengineering human myocardium on native extracellular matrix. *Circulation Research.* 2016;118:56-72.

Ivashchenko CY, Pipes GC, Lozinskaya IM, Lin Z, Xiaoping X, Needle S, Grygielko ET, Hu E, Toomey JR, Lepore JJ, Willette RN. Human-induced pluripotent stem cell-derived cardiomyocytes exhibit temporal changes in phenotype. *American Journal Physiological Heart Circulatory Physiology*. 2013;305:H913-H922.

He, DS, Burt JM. Mechanism and selectivity of the effects of halothane on gap junction channel function. *Circulation Research.* 2000;86:E104-109.

He Q, Trindade PT, Stumm M, Li J, Zammaretti P, Bettiol E, et al. Fate of undifferentiated mouse embryonic stem cells within the rat heart: role of myocardial infarction and immune suppression. *Journal of Cellular and Molecular Medicine*. 2009; 13(1):188–201.

Heidenreich PA, Albert NM, Allen LA, Bluemke DA, Butler J, Fonarow GC, Ikonomidis JS, Khavjou O, Konstam MA, Maddox TM, Nichol G, Pham M, Piña IL, Trogdon JG; American Heart Association Advocacy Coordinating Committee; Council on Arteriosclerosis, Thrombosis and Vascular Biology; Council on Cardiovascular Radiology and Intervention; Council on Clinical Cardiology; Council on Epidemiology and Prevention; Stroke Council. Forecasting the impact of heart failure in the United States: A policy statement from the American Heart Association. *Circulation Heart Failure*. 2013;6:606-619.

Heldman AW, DiFede DL, Fishman JE, Zambrano JP, Trachtenberg BH, Karantalis V, Mushtaq M, Williams AR, Suncion VY, McNiece IK, Ghersin E, Soto V, Lopera G, Miki R, Willens H, Hendel R, Mitrani R, Pattany P, Feigenbaum G, Oskouei B, Byrnes J, Lowery MH, Sierra J, Pujol MV, Delgado C, Gonzalez PJ, Rodriguez JE, Bagno LL, Rouy D, Altman P, Foo CW, da Silva J, Anderson E, Schwarz R, Mendizabal A, Hare JM. Transendocardial mesenchymal stem cells and mononuclear bone marrow cells for ischemic cardiomyopathy: the TAC-HFT randomized trial. *Journal of American Medical Association*. 2014;311(1):62–73.

Herron TJ, Da Rocha AM, Campbell KF, Ponce-Balbuena D, Cicero Willis B, Guerrero-Serna G, Liu Q, Klos M, Musa H, Zarzoso M, Bizy A, Furness J, Anumonwo J, Mironov S, Jalife J. Extracellular matrix–mediated maturation of human pluripotent stem cell–derived cardiac monolayer structure and electrophysiological function. *Circulation Arrhythmia and Electrophysiology.* 2016;9:e003638.

Hirt MN, Hansen A, Eschenhagen T. Cardiac tissue engineering: state of the art. *Circulation Research*. 2014;114(2):354-367.

Ieda M, Fu JD, Delgado-Olquin P, Vedantham V, Hayashi Y, Bruneau BG, Srivastava D. Direct reprogramming of fibroblasts into function cardiomyocytes by defined factors. *Cell*. 2010;142(3):375-386.

Hurlbut WB. Ethics and embryonic stem cell research: altered nuclear transfer as a way forward. *BioDrugs*. 2007;21:79–83.

Ibrahim AGE, Ke Cheng, and Eduardo Marbán. Exosomes as critical agents of cardiac regeneration triggered by cell therapy. *Stem Cell Reports*. 2014;2(5):606–619.

Iso Y, Spees JL, Serrano C, Bakondi B, Pochampally R, Song YH, et al. Multipotent human stromal cells improve cardiac function after myocardial infarction in mice without long-term engraftment. *Biochemical and Biophysical Research Communications*. 2007; 354(3):700–706.

Janssens S, Dubois C, Bogaert J, Theunissen K, Deroose C, Desmet W, Kalantzi M, Herbots L, Sinnaeve P, Dens J, Maertens J, Rademakers F, Dymarkowski S, Gheysens O, Van Cleemput J, Bormans G, Nuyts J, Belmans A, Mortelmans L, Boogaerts M, Van de Werf F. Autologous bone marrow-derived stem-cell transfer in patients with ST-segment elevation myocardial infarction; double blind, randomized controlled trial. *Lancet.* 2006;367:113-121.

Jhund PS, McMurray JV. Heart failure after myocardial infarction. A lost battle in the war on heart failure? *Circulation*. 2008;118:2019-2021.

Jiao A, Trosper NE, Yang HS, Kim J, Tsui JH, Frankel SD, Murry CE, Kim DH. Thermoresponsive nanofabricated substratum for the engineering of three-dimensional tissues with layer-by-layer architectural control. *American Chemical Society Nano*. 2014;8(5):4430-4439.

Kajstura J, Rota M, Whang B, Cascapera S, Hosoda T, Bearzi C, Nurzynska D, Kasahara H, Zias E, Bonafé M, Nadal-Ginard B, Torella D, Nascimbene A, Quaini F, Urbanek K, Leri A, Anversa P. Bone marrow cells differentiate in cardiac cell lineages after infarction independently of cell fusion, *Circulation Research.* 2005;96:127-137.

Karantalis V, DiFede DL, Gerstenblith G, Pham S, Symes J, Zambrano JP, Fishman J, Pattany P, McNiece I, Conte J, Schulman S, Wu K, Shah A, Breton E, Davis-Sproul J, Schwarz R, Feigenbaum G, Mushtaq M, Suncion VY, Lardo AC, Borrello I, Mendizabal A, Karas TZ, Byrnes J, Lowery M, Heldman AW, Hare JM. Autologous mesenchymal stem cells produce concordant improvements in regional function, tissue perfusion, and fibrotic burden when administered to patients undergoing coronary artery bypass grafting: The Prospective Randomized Study of Mesenchymal Stem Cell Therapy in Patients Undergoing Cardiac Surgery (PROMETHEUS) trial. *Circulation Research*. 2014;114(8):1302–1310.

Kattman SJ, Koonce CH, Swanson BJ, Anson BD. Stem cells and their derivatives: a renaissance in cardiovascular translational research. *Journal of Cardiovascular Translational Research*. 2011;4:66-472.

Kang E, Wang X, Tippner-Hedges R, Ma H, Folmes CDL, Gutierrez NM, Lee Y, Van Dyken C, Ahmed R, Li Y, Koski A, Hayama T, Luo S, Harding CO, Amato P, Jensen J, Battaglia D, Lee D, Wu D, Terzic A, Wolf DP, Huang T, Mitalipov S. Age-related accumulation of somatic mitochondrial DNA mutations in adult-derived human iPSCs. *Cell Stem Cell.* 01.09.2015.

Kawamura M, Miyagawa S, Fukushima S, Saito A, Miki K, Ito E, Sougawa N, Kawamura T, Daimon T, Shimizu T, Okano T, Toda K, Sawa Y. Enhanced survival of transplanted human induced pluripotent stem cell-derived cardiomyocytes by the combination of cell sheets with the pedicled omental flap technique in a porcine heart. *Circulation*. 2013;128(11Suppl1):S87-94.

Kawamura M, Miyagawa S, Miki K, Saito A, Fukushima S, Higuchi T, Kawamura T, Kuratani T, Daimon T, Shimizu T, Okano T, Sawa Y. Feasibility, safety, and therapeutic efficacy of human induced pluripotent stem cell-derived cardiomyocyte sheets in a porcine ischemic cardiomyopathy model. *Circulation*. 2012;126:S29-S37.

Kellar RS, Lancaster JJ, Goldman S, McAllister TN, L'Heureux N. Cardiovascular Tissue Engineering. In: P. Ducheyne KE, Healy, D.W. Hutmacher, D.W. Grainger, C.J. Kirkpatrick (eds.). *Comprehensive Biomaterials.* 2011;5:361-376, Elsevier.

Kellar RS, Landeen LK, Shepherd BR, Naughton GK, Ratcliffe A, Williams SK. Scaffold-based 3- D human fibroblast culture provides a structural matrix that support angiogenesis in infarcted heart tissue. *Circulation*. 2001;104:2063–2068.

Kellar RS, Shepherd BR, Larson DF, Naughton GK, Williams SK. A cardiac patch constructed from human fibroblasts attenuates a reduction in cardiac function following acute infarct. *Tissue Engineering*. 2005;11(11–12):1678–1687.

Kern A, Liu K, Mansbridge J. Modification of fibroblast gamma-interferon responses by extracellular matrix. *Invitatory Dermatology*. 2001;17:112–118.

Kim K, A Doi, B Wen, K Ng, R Zhao, P Cahan, J Kim, MJ Aryee, H Ji, L Ehrlich, A Yabuuchi, A Takeuchi, KC Cunniff, H Hongguang, S Mckinney-Freeman, O Naveiras, TJ Yoon, RA Irizarry, N Jung, J Seita, J Hanna, P Murakami, R Jaenisch, R Weissleder, SH Orkin, IL Weissman, AP Feinberg, and GQ Daley. Epigenetic memory in induced pluripotent stem cells. *Nature*. 2010;467(7313):285-290.

Kirklin JK, Naftel DC, Kormos RL, Stevenson LW, Pagani FD, Miller MA, Baldwin JT, Young JB. Fifth INTERMACS annual report: risk factor analysis from more than 6000 mechanical circulatory support patients. *Journal of Heart and Lung Transplantation*. 2013:32:141–156.

Lailiang Ou, Wenzhong Li, Yue Zhang, Weiwei Wang, Jun Liu, Heiko Sorg, Dario Furlani, Ralf Gäbel,Peter Mark, Christian Klopsch, Liang Wang, Karola Lützow, Andreas Lendlein, Klaus Wagner, Doris Klee,Andreas Liebold, Ren-Ke Li, Deling Kong, Gustav Steinhoff, Nan Ma. Intracardiac injection of matrigel induces stem cell recruitment and improves cardiac functions in a rat myocardial infarction model. *Journal of Cellular and Molecular Medicine*. 2011;15(6):1310–1318.

Lait PA, Hei DJ, Raval AN, Kamp TJ. Induced pluripotent stem cells for post-myocardial infarction repair: Remarkable opportunities and challenges. *Circulation Research.* 2014;114:1328-1345.

Lancaster JJ, Juneman E, Hagerty T, Do R, Hicks M, Meltzer K, Standley P, Gaballa M, Kellar R, Goldman S, Thai H. Viable fibroblast matrix patch induces angiogenesis and increases myocardial blood flow in heart failure after myocardial infarction. *Tissue Engineering Part A.* 2010;16:3065-3073.

Lancaster JJ, Juneman E, Arnce SA, Johnson NM, Qin Y, Witte R, Thai H, Kellar RS, Ek Vitorin J, Burt J, Gaballa MA, Bahl JJ, Goldman S. An electrically coupled tissue-engineered cardiomyocyte scaffold improves cardiac function in rats with chronic heart failure. *Journal of Heart and Lung Transplantation*. 2014;33(4):438-445.

Lancaster JJ, Juneman E, Sanchez P, Weigand K, Moukabary T, LaHood N, Bahl J, Goldman S. Induced pluripotent stem cell derived cardiomyocte scaffold improvers electro-mechanical coupling and left ventricular function in rats with heart failure. *Journal of Cardiac Failure*. 2015;21(8S):208,pS92.

Landa N. Miller l, Feinberg MS, Micha S. MD; Holbova R, Shachar M, Freeman I, Cohen S, Leor J. Effect of injectable alginate implant on cardiac remodeling and function after recent and old infarcts in rat. *Circulation.* 2008;117(11):1388-1396.

Lei L, Zhou R, Zheng W, Christensen L, Weiss R, Tomanek R. Bradycardia induces angiogenesis, increases coronary reserve, and preserves function of the postinfarcted heart. *Circulation*. 2004;110(7):796–802.

Leor J, Aboulafia-Etzion S, Dar A, Shapiro L, Barbash IM, Battler A, Granot Y, Cohen S. Bioengineered cardiac grafts: a new approach to repair the infarcted myocardium? *Circulation*. 2000;102 (suppl III):56-61.

Leor J, Amsalem JY, Cohen S. Cells, Scaffolds, and molecules for myocardial tissue engineering. *Pharmacology and Therapeutics*. 2005;105:151-163.

Libby P: inflammation in atherosclerosis. *Nature.* 2002;420:868

Libby P. Mechanisms of acute coronary syndromes and their implications for therapy. *New England Journal of Medicine*. 2013;368:2004-2013.

Lipinski MJ, Biondi-Zoccai GGL, MD Abbate A, Khianey R, Sheiban I, Bartunek J, Vanderheyden M, Kim HS, Kang HJ, Strauer BE, Vetrovec GW. Impact of Intracoronary Cell Therapy on Left Ventricular Function in the Setting of Acute Myocardial Infarction. A Collaborative Systematic Review and Meta-Analysis of Controlled Clinical Trials. *Journal of American Medical Association.* 2007;50:1761-1767.

Liu H, Chen B, Lilly B. Fibroblast potentiate blood vessel formation partially through secreted factor TIMP-1. *Angiogenesis*. 2008;11:223-234.

Lunde K, Solheim S, Aakhus S et al., for the ASTAMI Investigators. Intracoronary injection of mononuclear bone marrow cells in acute myocardial infarction. *New England Journal of Medicine.* 2006;1199-1209.

Ma J, Guo L, Fiene SJ, Anson BD, Thomson JA, Kamp TJ, Kolaja KL, Swanson BJ, January CT. High purity human-induced pluripotent stem cell-derived cardiomyocytes: electrophysiological properties of action potentials and ionic currents. *American Journal of Physiology Heart Circulation Physiology*. 2011;301(5):H2006-H2017.

Ma J, Wang Q, Fei T, Han J J-D, Chen Y-G. MCP-1 meidates TGF-B-induced angiogenesis by stimulating vascular smooth muscle cell migration. *Blood*, 2007;1:987-994.

Ma XH, Shi Y, Hou Y, Liu Y, Zhang L, Fan WX, Ge D, Liu TQ, Cui ZF. Slow-freezing cryopreservation of neural stem cell spheres with different diameters. *Cryobiology*. 2010; 60(2):184–191.

Madden LR, Mortisen DJ, Sussman EM, Dupras S, Fugate JA, Cuy JL, Hauch KD, Laflamme MA, Murry CE, Ratner BD. Proangiogenic Scaffold as Functional Templates for Cardiac Tissue Engineering. *Proceedings of the National Academy of Sciences of the United States of America*. 2010;107:15211-15216.

Makkar RR, Smith RR, Cheng K, Malliaras K, Thomson LE, Berman D, Czer LS, Marbán L, Mendizabal A, Johnston PV, Russell SD, Schuleri KH, Lardo AC, Gerstenblith G, Marbán E. Intracoronary cardiosphere-derived cells for heart regeneration after myocardial infarction (CADUCEUS): a prospective, randomized phase 1 trail. *Lancet*. 2012;379(9819):895–904.

Mangi AA, Noiseux N, Kong D, He H, Rezvani M, Ingwall JS, Dzau VJ. Mesenchymal stem cells modified with Akt prevent remodeling and restore performance of infarcted hearts. *National Medicine*. 2003;9(9):1195–1201.

Mann, DL. Mechanisms and models in heart failure: a combinational approach. *Circulation*. 1999;100:999-1008.

Mansour S, Vanderheyden M, De Bruyne B, Vande-kerckhove B, Delrue L, Van Haute I, Heyndrickx G, Carlier S, Rodriguez-Granillo G, Wijns W, Bartunek J. Intracoronary delivery of hematopoietic bone marrow stem cells and luminal loss of the infarct-related artery in patients with recent myocardial infarction. *Journal of American College of Cardiology*. 2006;47:1727–1730.

McCall F, Kartik S Telukuntla, Vasileios Karantalis, Viky Y Suncion, Alan W Heldman, Muzammil Mushtaq, Adam R Williams & Joshua M Hare. Myocardial infarction and intramyocardial injection models in swine. *Nature Protocols*. 2012;7(8):1479-1496.

Meissner A, Jaenisch R. Generation of nuclear transfer-derived pluripotent ES cells from cloned Cdx2-deficient blastocysts. *Nature*. 2006;439:212–215.

Menasché P, Alfieri O, Janssens S, McKenna W, Reichenspurner H, Trinquart L, Vilquin J-T, Marolleau J-P, Seymour B, Larghero J, Lake S, Chatellier G, Solomon S, Desnos M, Hagège AA. The Myoblast Autologous Grafting in Ischemic Cardiomyopathy (MAGIC) Trial First Randomized Placebo-Controlled Study of Myoblast Transplantation. *Circulation*. 2008;117:1189-1200.

Mozaffarian D, Benjamin EJ, Go AS, Arnett DK, Blaha MJ, Cushman M, de Ferranti S, Després JP, Fullerton HJ, Howard VJ, Huffman MD, Judd SE, Kissela BM, Lackland DT, Lichtman JH, Lisabeth LD, Liu S, Mackey RH, Matchar DB, McGuire DK, Mohler ER 3rd, Moy CS, Muntner P, Mussolino ME, Nasir K, Neumar RW, Nichol G, Palaniappan L, Pandey DK, Reeves MJ, Rodriguez CJ, Sorlie PD, Stein J, Towfighi A, Turan TN, Virani SS, Willey JZ, Woo D, Yeh RW, Turner MB; American Heart Association Statistics Committee and Stroke Statistics Subcommittee. Heart disease and stroke statistics--2015 update: a report from the American Heart Association. *Circulation*. 2015;131(4):e29-322.

Mukherjee N, Chen Z, Sambanis A, Song Y. Effects of cryopreservation on cell viability and insulin secretion in a model tissue-engineered pancreatic substitute (TEPS). *Cell Transplantation*. 2005;14(7):449–456.

Müller-Ehmsen J, Whittaker P, Kloner RA, Dow JS, Sakoda T, Long TI, Laird PW, Kedes L. Survival and development of neonatal rat cardiomyocytes transplanted into adult myocardium. *Journal of Molecular Cellular Cardiology*. 2002;34(2):107–116.

Murry CE, Field LJ, Menasché P. Cell-based cardiac repair reflections at the 10-year point. *Circulation*. 2005;112(20):3174–3183.

Murry CE, Soonpaa MH, Reinecke H, Nakajima H, Nakajima HO, Rubart M, Pasumarthi KB, Virag JI, Bartelmez SH, Poppa V, Bradford G, Dowell JD, Williams DA, Field LJ. Haematopoietic stem cells do not transdifferentiate into cardiac myocytes in myocardial infarcts. *Nature*. 2004;428(6983):664-668.

Murry CE, Wiseman RW, Schwartz SM, Hauschka SD. Skeletal myoblast transplantation for repair of myocardial necrosis. Journal of Clinical Investigation. 1996; 98(11):2512–2523.

Mussolino ME, Nasir K, Neumar RW, Nichol G, Palaniappan L, Pandey DK, Reeves MJ, Rodriguez CJ, Sorlie PD, Stein J, Towfighi A, Turan TN, Virani SS, Willey JZ, Woo D, Yeh RW, Turner MB; American Heart Association Statistics Committee and Stroke Statistics Subcommittee. Heart disease and stroke statistics – 2015 update: a report from the American Heart Association. *Circulation*. 2015;131(4):e29-322.

Munz MR, Faria MA, Monteiro JR, Aguas AP, Amorim MJ. Surgical porcine myocardial infarction model through permanent coronary occlusion. *Computational Medicine*. 2011;61(5):445-452.

Okano H, Nakamura M, Yoshida K, Okada Y, Tsuji O, Nori S, Ikeda E, Yamanaka S, Miura K. Steps Toward Safe Cell Therapy Using Induced Pluripotent Stem Cells. *Circulation Research*. 2013;112:523-533.

Okita K, Nagata N, Yamanaka S. Immunogenicity of induced pluripotent stem cells. *Circulation Research*. 2011;109:720-721.

Ong SG, Huber BC, Lee WH, Kodo K, Ebert AD, Ma Y, Nguyen PK, Diecke S, Chen WY, Wu JC. Microfluidic Single-cell analysis of transplanted human induced pluripotent stem cell-derived cardiomyocytes after acute myocardial infarction. *Circulation.* 2015;132:762-771.

Orlic D, Kajstura J, Chimenti S, Jakoniuk I, Anderson SM, Li B, Pickel J, McKay R, Nadal-Ginard B, Bodine DM, Leri A, Anversa P. Bone marrow cells regenerate infarcted myocardium. *Nature*. 2001;410(6829):701-705.

Ott HC, Matthiesen TS, Goh SK, Black LD, Kren SM, Netoff TI, Taylor DA. Perfusion-decellullarization matrix: using nature's platform to engineer a bioartifical heart. *Nature Medicine*. 2008;14(2):213-221.

Oz MC, Konertz WF, Kleber FX, Mohr FW, Gummert JF, Ostermeyer J, Lass M, Raman J, Acker MA, Smedira N. Global surgical experience with the Acron cardiac support devise. *Journal of Thoracic Cardiovascular Surgery*. 2003;126:983–991.

Page RL, Ambady S, Holmes WF, et al. Induction of stem cell gene expression in adult human fibroblasts without transgenes. *Cloning Stem Cells*. 2009;11:1–10.

Passier R, van Laake LW, Mummery CL. Stem-cell-based therapy and lessons from the heart. *Nature*. 2008;453(7193):322–329.

Pantilat SZ, Steimle AE. Palliative care with heart failure. *Journal of the American Medical Association*. 2004;291: 2476–2482.

Park H, Larson BL, Guillemette MD, Jain SR, Hua C, Engelmayr GC, Freed LE. The significance of pore microarchitecture in a multi-layered elastomeric scaffold for contractile cardiac muscle constructs *Biomaterials*. 2011;32:1856–1864.

Patel AN, Henry TD, Quyyumi AA, Schaer GL, Anderson RD, Toma C, East C, Remmers AE, Goodrich J, Desai AS, Recker D, DeMaria A, for the ixCELL-DCM Investigators. Ixmyelocel-T for patients with ischaemic heart failure: a prospective randomised double-blind trial. *Lancet.* 2016;pii:S0140-6736(16):30137-30144.

Patel AN, Sherman W. Cardiac stem cell therapy from bench to bedside. *Cell Transplant*ation. 2007;16:875–878.

Pennock GD, Raya TE, Bahl JJ, Goldman S, Morkin E. Combination treatment with captopril and the thyroid hormone analog 3,5-diiodothyroproprionic acid (DITPA): A new approach to improving left ventricular performance in heart failure. *Circulation*. 1993;88:1289–1298.

Perin EC, Dohmann HF, Borojevic R, Silva SA, Sousa AL, Mesquita CT, Rossi MI, Carvalho AC, Dutra HS, Dohmann HJ, Silva GV, Belém L, Vivacqua R, Rangel FO, Esporcatte R, Geng YJ, Vaughn WK, Assad JA, Mesquita ET, Willerson JT. Transendocardial, autologous bone marrow cell transplantation for severe, chronic ischemic heart failure. *Circulation*. 2003; 107(18):2294–2302.

Perin EC, Willerson JT, Pepine CJ, Henry TD, Ellis SG, Zhao DX, Silva GV, Lai D, Thomas JD, Kronenberg MW, Martin AD, Anderson RD, Traverse JH, Penn MS, Anwaruddin S, Hatzopoulos AK, Gee AP, Taylor DA, Cogle CR, Smith D, Westbrook L, Chen J, Handberg E, Olson RE, Geither C, Bowman S, Francescon J, Baraniuk S, Piller LB, Simpson LM, Loghin C, Aguilar D, Richman S, Zierold C, Bettencourt J, Sayre SL, Vojvodic RW, Skarlatos SI, Gordon DJ, Ebert RF, Kwak M, Moyé LA, Simari RD; Cardiovascular Cell Therapy Research Network (CCTRN). Effect of transendocardial delivery of autologous bone marrow mononuclear cells on functional capacity, left ventricular function, and perfusion in chronic heart failure: the FOCUS-CCTRN trial. Journal of the American Medical Association. 2012;307(16):1717–1726.

Pfaffl MW. A new mathematical model for relative quantification in real-time RT-PCR. *Nucleic Acids Res*. 2001;29(9):e45.

Prigione A, Hossini AM, Lichtner B, Serin A, Fauler B, Megges M, Lurz R, Lehrach H, Makrantonaki E, Zouboulis CC, Adjaye J. Mitochondrial-associated cell death mechanisms are reset to an embryonic-like state in aged donor-derived iPS cells harboring chromosomal aberrations. *PLOS One*. 2011;6(11):e27352.

Puppala D, Collis LP, Sun SZ, Bonato V, Chen X, Anson B, Pletcher M, Fermini B, Engle SJ. Comparative gene expression profiling in human-induced pluripotent stem cell--derived cardiocytes and human and cynomolgus heart tissue. *Toxicology Science*. 2013;131:292-301.

Radisic MH, Park H, Chen F, Salazar-Lazzaro JE, Wang Y, Dennis R, Langer R, Freed LE, Vunjak-Novakovic G. Biomimetic approach to cardiac tissue engineering: oxygen carriers and channeled scaffolds. *Tissue Engineering*. 2006;12:2077–2091.

Raya TE, Gaballa M, Anderson P, Goldman S. Left ventricular function and remodeling after myocardial infarction in aging rats. *American Journal of Physiology*. 1997;273(6 Pt 2):H2652–H2658.

Raya TE, Gay RG, Aguirre M, Goldman S. The importance of venodilatation in the prevention of left ventricular dilatation after chronic large myocardial infarction in rats: a comparison of captopril and hydralazine. *Circulation Research.* 1989;64:330-338.

Raynaud CM, Yacoub MH. Clinical trials of Bone marrow derived cells for ischemic heart failure. Time to move on? TIME, SWISS-AMI, CELLWAVE, POSEIDON, and C-CURE. *Global Cardiology Science and Practice*. 2013;(3):207-211.

Reardon S. Mutated mitochondria could hold back stem-cell therapies. *Nature*. 2016.

Reinhardt CP, Dalberg S, Tries MA, Marcel R, Leppo JA. Stable labeled micorspheres to measure perfusion: validation of a neutron activation assay technique. *American Journal of Physiology*. 2001;280:H108–H116.

Reis LA, Chiu LLY, Feric N, Fu L, Radisic M. Biomaterials in myocardial tissue engineering. *Journal of Tissue Engineering and Regenerative Medicine*. 2016;10:11–28.

Reis LA, Chiu LL, Liang Y, Hyunh K, Momen A, Radisic M. A peptide-modified chitosan-collagen hydrogel for cardiac cell culture and delivery. *Acta Biomaterialia*. 2012;8:1022–1036.

Riolobos L1, Hirata RK, Turtle CJ, Wang PR, Gornalusse GG, Zavajlevski M, Riddell SR, Russell DW. HLA engineering of human pluripotent stem cells. *Molecular Theories*. 2013;21:1232-1241.

Sanganalmath SK, Bolli R. Heart Failure Compendium. Cell therapy for heart failure. *Circulation*. 2013;113:810-834.

Shimizu T, Yamato M, Kikuchi A, Okano T. Cell sheet engineering for myocardial tissue reconstruction. *Biomaterials*. 2003;24(13):2309-2316.

Schachinger V, Assmus B, Britten MB, Honold J, Lehmann R, Teupe C, Abolmaali ND, Vogl TJ, Hofmann WK, Martin H, Dimmeler S, Zeiher AM. Transplantation of progenitor cells and regeneration enhancement in acute myocardial infarction Final one-year results of the TOPCARE-AMI Trial. *Journal of American College of Cardiology. 2004*;44:1690-1699.

Schächinger V, Erbs S, Elsasser A. Intracoronary bone marrow-derived progenitor cells in acute myocardial infarction: A randomized, double-blind, placebo controlled multicenter trial (REPAIR- AMI). *New England Journal of Medicine*. 2006;355:1210–1221.

Schächinger V, Erbs S, Elsässer A, Haberbosch W, Hambrecht R, Hölschermann H, Yu J, Corti R, Mathey DG, Hamm CW, Süselbeck T, Werner N, Haase J, Neuzner J,

Germing A, Mark B, Assmus B, Tonn T, Dimmeler S, and Zeiher AM for the REPAIR-AMI Investigators. Improved clinical outcome after intracoronary administration of bone-marrow-derived progenitor cells in acute myocardial infarction: final 1-year results of the REPAIR-AMI trial. *Europena Heart Journal*. 2006;27:2775-2783.

Schuleri KH[1], Boyle AJ, Centola M, Amado LC, Evers R, Zimmet JM, Evers KS, Ostbye KM, Scorpio DG, Hare JM, Lardo AC. The adult Göttingen minipig as a model for chronic heart failure after myocardial infarction: focus on cardiovascular imaging and regenerative therapies. *Comparative Medicine*. 2008;58(6):568-579.

Schmuck EG, Mulligan JD, Ertel RL, Kouris NA, Ogle BM, Raval AN, Saupe KW. Cardiac fibroblast-derived 3D extracellular matrix seeded with mesenchymal stem cells as a novel device to transfer cells to the ischemic myocardium. *Cardiovascular Engineering Technologies*. 2014;5(1):119-131.

Sekine H, Shimizu T, Hobo K, Sekiya S, Yang J, Yamato M, Kurosawa H, Kobayashi E, Okano T. Endothelial cell coculture within tissue-engineered cardiomyocyte sheet enhances neovascularization. *Circulation*. 2008;118[suppl 1]:S145-152.

Sirenko O, Crittenden C, Callamaras N, Hesley J, Chen YW, Funes C, Rusyn I, Anson B, Cromwell EF. Multiparameter in Vitro Assessment of Compound Effects on Cardiomyocyte Physiology Using iPSC Cells. *Journal of Biomolecular Screening*. 2013;18:39-53.

Smith RR, Barile L, Cho HC, Leppo MK, Hare JM, Messina E, Giacomello A, Abraham MR, Marbán E. Regenerative potential of cardiosphere derived cells expanded from percutaneous endomyocardial biopsy specimens. *Circulation*. 2007;115(7):896-908.

Smits AM, van Vliet P, Hassink RJ, Goumans MJ, Doevendans PA. The role of stem cells in cardiac regeneration. *Journal of Cellular and Molecular Medicine*. 2005;9(1):25–36.

Song K, Nam YJ, Luo X, Tan W, Huang GN, Acharya A, Smith CL, Tallquist MD, Neilson EG, Hill JA, Bassel-Budy R, Olson E. Heart repair by reprogramming non-myocytes with cardiac transcription factors. *Nature*. 2012;485(7400):599-604.

Srivastava, D, Ivey KN. Potential of stem-cell-based therapies for heart disease. *Nature*. 2006;441:1097-99.

Stadtfeld M, Hochedlinger K. Without a trace? PiggyBac-ing to pluripotency. *Nature Methods*. 2009;6:329–330.

Stadtfeld M, Nagaya M, Utikal J, Weir G, Hochedlinger K. Induced pluripotent stem cells generated without viral integration. *Science*. 2008;322:945–949.

Strauer BE, Brehm M, Zeus T, Bartsch T, Schannwell C, Antke C, Sorg RV, Kogler G, Werner P, Muller HW, Kostering M. Regeneration of human infarcted heart muscle by intracoronary autologous bone marrow cell transplantation in chronic coronary artery disease. The IACT Study. *Journal of the American College of Cardiology.* 2005;46:1651-1658.

Taylor CJ, Peacock S, Chaudhry AN, Bradley A, Bolton EM. Generating an iPSC Bank for HLA-Matched Tissue Transplantation Based on Known Donor and Recipient HLA Types. *Cell Stem Cell*. 2012;11(2):147-152.

Thai H, Castellano L, Juneman E, Phan H, Do R, Gaballa MA, Goldman S. Pretreatment with angiotensin receptor blockade prevents left ventricular dysfunction and blunts LV remodeling associated with acute myocardial infarction. *Circulation*. 2006;114:1933–1939.

Thai H, Juneman E, Lancaster J, Hagerty T, Do R, Castellano L, Kellar R, Williams S, Sethi G, Schmelz M, Gaballa MA, Goldman S. Implantation of a 3-dimensional fibroblast matrix improves left ventricular function and blood flow after acute myocardial infarction. *Cell Transplantation.* 2009;18(3):283-295.

Thai H, Van H, Gaballa M., Goldman S, Raya T. Effects of AT1 receptor blockade after myocardial infarct on myocardial fibrosis, stiffness, and contractility. *American Journal of Physiology*. 1999:276**:**H873-880.

Takahashi K, Tanabe K, Ohnuki M, Narita M, Ichisaka T, Tomoda K, Yamanaka S. Induction of pluripotent stem cells from adult human fibroblasts by defined factors. *Cell*. 2007;131:861-872.

Tileman L, Ishikawa K, Weber T, Hajjar RJ. Gene therapy for heart failure. *Circulation Research*. 2012;110(5):777-793.

Torella D, Rota M, Murzynska d, Musso E, Monsen A, Shiraishi I, Zias E, Walsh K, Rosenzweig A, Sussman MA, Urbanek K, Nadal-Ginard B, Kajstura J, Anversa P, Leri A. Cardiac stem cell and myocyte aging, heart failure, and insulin like growth factor-1 overexpression. *Circulation Research*. 2004; 94:514-524.

Traverse JH, Henry TD, Pepine CJ, Willerson JT, Zhao DX, Ellis SG, Forder JR, Anderson RD, Hatzopoulos AK, Penn MS, Perin EC, Chambers J, Baran KW,Raveendran G, Lambert C, Lerman A, Simon DI, Vaughan DE, Lai D, Gee AP, Taylor DA, Cogle CR, Thomas JD, Olson RE, Bowman S, Francescon J, Geither C, Handberg E, Kappenman C, Westbrook L, Piller LB, Simpson LM, Baraniuk S, Loghin C, Aguilar D, Richman S, Zierold C, Spoon DB, Bettencourt J, Sayre SL, Vojvodic RW, Skarlatos SI, Gordon DJ, Ebert RF, Kwak M, Moyé LA, Simari RD; Cardiovascular Cell Therapy Research Network (CCTRN). Effect of the use and timing of bone marrow mononuclear cell delivery on left ventricular function after acute myocardial infarction: the TIME randomized trial. *Journal of American Medical Association*. 2012;308(22):2380-2389.

Troncoso R, Ibarra C, Vicencio JM, Jaimovich E, Lavandero S. New Insights into IGF-1 Signaling in the Heart. *Trends in Endocrinology & Metabolism.* 2014;25(3):128-137.

Turner LA, Vodanovic S, Bosnjak ZJ. Interaction of anesthetics and catecholamines on conduction in the canine His-Purkinje system. *Advanced Pharmacology.* 1994;31:167-184.

US Department of Health and Human Services
http://optn.transplant.hrsa.gov/latestData/rptData.asp

Wagers AJ, Sherwood RI, Christensen JL, Weissman IL. Little evidence for developmental plasticity of adult hematopoietic stem cells. *Science*. 2002;297:2256–2259.

Wall ST, Walker JC, Healy K, Ratcliffe MB, Guccione J. Theoretical impact of the injection of material into the myocardium: A finite element model simulation. *Circulation*. 2006;114:2627–2635.

Wang WE, X. Chen, S. R. Houser, and C. Zeng. Potential of cardiac stem/progenitor cells and induced pluripotent stem in ischaemic heart disease. *Clinical Science*. 2013;125(7):319–327.

Wassenarr JW, Gaetani R, Garcia JJ, Braden RL, Luo CG, Huang D, DeMaria AN, Omens JH, Christman KL. Evidence for Mechanisms Underlying the Functional Benefits of a Myocardial Matrix Hydrogel for Post-MI Treatment. *Journal of American College of Cardiology*. 2016;67(9):1074-1086.

Weigand K, Witte R, Moukabary T, Chinyere I, Lancaster JJ, Pierce MK, 1 Goldman S, Juneman E, In-vivo Electrophysiological Study of Induced Ventricular Tachycardia in Intact Rat Model of Chronic Ischemic Heart Failure. *IEEE Transactions on Biomedical Engineering*. 2016 – In Press.

Williams AR, Hatzistergos KE, Addicott B, McCall F, Carvalho D, Suncion V, Morales AR, Da Silva J, Sussman MA, Heldman AW, Hare JM. Enhanced effect of combining human cardiac stem cells and bone marrow mesenchymal stem cells to reduce infarct size and to restore cardiac function after myocardial infarction. *Circulation*. 2013;127(2):213-223.

Wilson SR, Mudge GH, Stewart GC, Givertz MM. Evaluation for ventricular assist device: selectin the appropriate candidate. *Circulation*. 2009;119:2225-2232.

Wollert KC, Meyer GP, Lotz J, Rings-Lichtenberg S, Lippolt P, Breidenbach C, Fichtner S, Korte T, Horing B, Messinger D, Arseniev L, Ganser A, Drexler H. Intracoronary autologous bone-marrow cell transfer after myocardial infarction: the BOOST randomized controlled clinical trial. *Lancet.* 2004;364:141-148.

Yoon YS, Wecker A, Heyd L, Park JS, Tkebuchava T, Kusano K, Hanley A, Scadova H, Qin G, Cha DH, Johnson KL, Aikawa R, Asahara T, Losordo DW. Clonally expanded novel multipotent stem cells from human bone marrow regenerate myocardium after myocardial infarction *Journal of Clinical Investigation.* 2005;115:326-338.

Yu J, Chau KF, Vodyanik MA, Jiang J, Jiang Y. Efficient feeder-free episomal reprogramming with small molecules. *PLOS One*. 2011;6(3):e17557.

Zammaretti P, Jaconi M. Cardiac tissue engineering: regeneration of the wounded heart. *Current Opinions in Biotechnology*. 2004;15:430-434.

Zeng L, Hu Q, Wang X, Mansoor A, Lee J, Feygin J, et al. Bioenergetic and functional consequences of bone marrow-derived multipotent progenitor cell transplantation in hearts with postinfarction left ventricular remodeling. *Circulation*. 2007;115(14):1866–1875.

Zhao Y, Feric NT, Thavandiran N, Nunes SS, Radisic M. The role of tissue engineering and biomaterials in cardiac regenerative medicine. *Canadian Journal of Cardiology*. 2014 ;30(11):1307-1322.

Zhi D, Irvin MR, Gu CC, Stoddard AJ, Lorier R, Matter A, Rao DC, Srinivasasainagendra V, Tiwari HK, Turner A, Broeckel U, Arnett DK. Whole-exome sequencing and an iPSC-derived cardiomyocyte model provides a powerful platform for gene discovery in left ventricular hypertrophy. *Frontiers in Genetics*. 2012;28(3):92.

Zimmermann WH, Schneiderbanger K, Schubert P, Didié M, Münzel F, Heubach JF, Kostin S, Neuhuber WL, Eschenhagen T. Tissue engineering of a differentiated cardiac muscle construct. *Circulation Research*. 2002;90:223–230.

Zimmermann WH, Melnychenko I, Wasmeier G, Didié M, Naito H, Nixdorff U, Hess A, Budinsky L, Brune K, Michaelis B, Dhein S, Schwoerer A, Ehmke H, Eschenhagen T.. Engineered Heart Tissue Grafts Improve Systolic and Diastolic Function in Infarcted Rat Hearts. *Nature Medicine*. 2006;12:452-458.